PERFORMANCE ANALYSIS AND SIMULATION OF AN AUTONOMOUS UNDERWATER VEHICLE EQUIPPED WITH THE COLLECTIVE AND CYCLIC PITCH PROPELLER

By

MINH QUANG TRAN, B.Eng (Aerospace Engineering)

National Centre for Maritime Engineering and Hydrodynamics

Australian Maritime College

College of Sciences and Engineering

Submitted in fulfilment of the requirements for the degree of Doctor of Philosophy

University of Tasmania

December 2017

To my family, my love, and my PhD supervisors.

Declaration of Originality

This thesis contains no material which has been accepted for a degree or diploma by the University or any other institution, except by way of background information and duly acknowledged in the thesis, and to the best of my knowledge and belief no material previously published or written by another person except where due acknowledgement is made in the text of the thesis, nor does the thesis contain any material that infringes copyright.

Minh Quang Tran

December 2017

Statement of Authority of Access

Minh Quang Tran

December 2017

Statement of Co-Authorship

The following people and institutions contributed to the publication of work undertaken as part of this thesis:

- Minh Quang Tran, University of Tasmania (Candidate)
- Dr Hung Nguyen, University of Tasmania (Author 1)
- Associate Professor Jonathan Binns, University of Tasmania (Author 2)
- Associate Professor Shuhong Chai, University of Tasmania (Author 3)
- Assistant Professor Alexander Forrest, University of California Davis (Author 4)

Authors details and their roles:

Conference Papers

Paper 1 (Part of Chapter 1). A Study of new propulsion system for an Autonomous Underwater Vehicle, *9th Graduate Research Conference at the University of Tasmania*, Hobart, Australia, 2015.

Candidate was the primary author and with author 1, author 2, author 3, and author 4 contributed to the ideas and presentation.

Paper 2 (Part of Chapter 6). Performance Prediction of Autonomous Underwater Vehicle with Different Propulsion System Configurations. *International Conference on Modelling and Simulation for Autonomous Systems.* Springer, 72-82.

Candidate was the primary author and with author 1, author 2, author 3, and author 4 contributed to the ideas and refinement.

Paper 3 (Part of Chapter 7). Least Squares Optimisation Algorithm Based System Identification of an Autonomous Underwater Vehicle, *Proceedings of the 3rd Vietnam Conference on Control and Automation*, Vietnam, 2015.

Candidate was the primary author and with author 1 contributed to the control algorithm. Author 2, author 3, and author 4 contributed to the ideas and refinement.

Paper 4 (Part of Chapter 7). Optimal control of an autonomous underwater vehicle equipped with the collective and cyclic pitch propeller. *Control Conference (ASCC), 2017 11th Asian.* IEEE, 354-359.

Candidate was the primary author and with author 1 contributed to the refinement and presentation. Author 2, author 3, and author 4 contributed to the ideas and refinement.

Journal Papers

Paper 5 (Part of Chapter 4). A practical approach to the dynamics modelling of an underwater vehicle propeller in all four quadrants of operation, *Proceedings of the Institution of Mechanical Engineers, Part M: Journal of Engineering for the Maritime Environment.* (Published).

Candidate was the primary author with the laboratory assistance from author 1 and author 2. Author 3 and author 4 contributed to the ideas and refinement.

Paper 6 (Part of Chapter 5). Experimental Study of the Collective and Cyclic Pitch Propeller, *The Journal of Marine Science and Application.* (Accepted for publication).

Candidate was the primary author with the laboratory assistance from author 1 and author 2. Author 3 and author 4 contributed to the ideas and refinement.

Paper 7. A comparison study of two propulsion system configurations for an autonomous underwater vehicle, *Ocean Engineering, An International Journal of Research and Development.* (In progress).

Candidate was the primary author and with author 1, author 2, author 3, and author 4 contributed to the ideas and refinement.

We the undersigned agree with the above stated "proportion of work undertaken" for each of the above published (or submitted) peer-reviewed manuscripts contributing to this thesis:

Signed:

…….....	……..
Primary Supervisor	Head of School
Australian Maritime College	Australian Maritime College
University of Tasmania	University of Tasmania

ABSTRACT

There is a growing need within marine sciences and engineering that requires the torpedo shaped Autonomous Underwater Vehicles (AUVs) being capable of accomplishing various complex surveillance missions, including scientific, commercial and military applications. Besides the traditional research on the control and navigation of an AUV, the propulsion system study becomes more and more essential to increase the manoeuvrability and efficiency of AUV.

The conventional propulsion system with fixed pitch propeller (FPP) and control surfaces at the aft end is the predominant propulsion type used by AUVs. This propulsion configuration has the shortcoming of insufficient low-speed manoeuvrability since the control surface manoeuvring forces are only generated when the vehicle is in motion. This is one of the fundamental limiting factors for the current torpedo shaped AUVs. The development of new propulsion system enabling both low speed and cruising speed operations could expand the typical operational envelope of an underwater vehicle and pave the way for the new applications.

This thesis focuses on the characteristic analysis of an innovative propulsion system called the Collective and Cyclic Pitch Propeller (CCPP) and the manoeuvring performance of an AUV equipped with CCPP. In the CCPP mechanism, the angles of each propeller blade can be positioned periodically during a rotation in both collective and cyclic pitch setting. CCPP has the capability to provide continuous propulsive force and manoeuvring forces simultaneously.

The primary task of the thesis was to explore the feasibility of a prototype CCPP to an underwater vehicle by numerically conducting the comparison between the AUV equipped with CCPP and FPP in standard manoeuvring tests. Initially, the Experimental Fluid Mechanics

approach was utilised to investigate the performance and derive the mathematical models of the CCPP and FPP. Two separate experimental apparatus were designed and implemented in this research for CCPP and FPP system. In the first experiment, the dynamic modelling of FPP using the four-quadrant model was proposed based on experimental data. The second experimental study involved the extensive investigation of the CCPP to establish its hydrodynamic characteristics. A series of comprehensive bollard pull and captive model tests were designed and conducted to evaluate the propulsion performance. Furthermore, the research developed a numerical simulation program called AUVSIPRO to examine the performance and manoeuvring characteristics of an AUV equipped with the CCPP as well as conventional configuration FPP. The Gavia AUV was used as the research platform and its mathematical model with nonlinear hydrodynamic coefficients were defined using the theoretical approach. Standard manoeuvring tests of marine vehicles were fully presented in the simulation program to analyse the manoeuvrability. In addition, the results from the experiments and simulation were utilised in the comparison study between the CCPP and conventional configuration applied to AUV. Finally, the controller design for an AUV equipped with a CCPP was conducted. The two-stage system identification method was proposed to develop the linear system model, which was applicable for the control design. The optimal state feedback algorithm was presented as the control strategy.

The propulsion systems for AUV have been subject to an increased focus with respect performance and manoeuvrability. This research is an exploration into the feasibility and viability of CCPP propulsion system for a torpedo shaped AUV and contributes to the areas related to the development of propulsion system for an underwater vehicle.

ACKNOWLEDGEMENTS

I would like to express my special appreciation and thanks to my primary supervisor, Dr. Hung Duc Nguyen, for his relentless support and encouragement during the past three years.

I also would like to acknowledge my co-supervisors, Associate Professor Jonathan Binns, Associate Professor Shuhong Chai at the Australian Maritime College, University of Tasmania; and Assistant Professor Alexander Forrest at the University of California Davis, who provided me with their supportive and valuable guidance throughout the course of my research project.

I am grateful to the members of the technician team at the Australian Maritime College, University of Tasmania for their assistance on the accomplishment of the experiments in the Towing Tank.

I also would like to thank the University of Tasmania for the financial support from the Tasmania Graduate Research Scholarship.

My deepest appreciation is to my parents, my family, my love and all of my friends for their endless dedication and encouragement.

Minh Quang Tran
Tasmania, Australia
December 2017

"Shoot for the moon. Even if you miss it you will land among the stars."

TABLE OF CONTENTS

LIST OF FIGURES

Chapter 1

Chapter 2

Chapter 3

Chapter 4

Chapter 5

Chapter 6

Chapter 7

LIST OF TABLES

NOMENCLATURE

A_O	Frontal area
B	Buoyancy Force
CB	Centre of Buoyancy
CG	Centre of Gravity
C_T	Thrust coefficient in four-quadrant model
C_Q	Torque coefficient in four-quadrant model
d	Diameter
F	Total force
J	Advance coefficient
I_x	Mass moment of inertia about the x axis
I_y	Mass moment of inertia about the y axis
I_z	Mass moment of inertia about the z axis
K	Moment about the x axis or rolling moment
K_T	Thrust coefficient
K_Q	Torque coefficient
l	Length of the vehicle
M	Moment about the y axis or the pitching moment
m	mass of the vehicle
N	Moment about the z axis or the yawing moment
n	Rotational speed
p	Angular velocity component about the x axis

$\dot{p}$	Angular acceleration component about the x axis
Q	Torque
q	Angular velocity component about the y axis
$\dot{q}$	Angular acceleration component about the y axis
r	Angular velocity component about the z axis
$\dot{r}$	Angular acceleration component about the z axis
U	Total uncertainty in force measurement
t	Time value
u	Velocity component in direction of x axis (surge)
$\dot{u}$	Acceleration component in direction of x axis
v	Velocity component in direction of y axis (sway)
$\dot{v}$	Acceleration component in direction of y axis
W	Total weight of AUV
w	Velocity component in direction of y axis (heave)
$\dot{w}$	Acceleration component in direction of z axis
X	Force in the x axis
x	Displacement in the x axis
$\dot{x}$	Rate of change of displacement in the x axis
x_B	The location of CB in x axis
x_G	The location of CG in x axis
Y	Force in the y axis
y	Displacement in the y axis
$\dot{y}$	Rate of change of displacement in the y axis
y_B	The location of CB in y axis
y_G	The location of CG in y axis
Z	Force in the z axis

z	Displacement in the x axis
$\dot{z}$	Rate of change of displacement in the z axis
z_B	The location of CB in z axis
z_G	The location of CG in z axis
SSE	Sum of Squares due to Error
$RMSE$	Root Mean Squared Error
R^2	Coefficient of determination

Greek Symbol

ϕ	Roll angle of the AUV
$\dot{\phi}$	Roll rate
θ	Pitch angle of the AUV
$\dot{\theta}$	Pitch rate
ψ	Yaw angle of the AUV
$\dot{\psi}$	Yaw rate
β	Advance angle
δ	Control surface deflection angle
δ_{col}	CCPP collective angle
δ_{cyc}	CCPP cyclic angle
$\boldsymbol{\tau}_{RB}$	External rigid body force
$\boldsymbol{\tau}_S$	Hydrostatic force
$\boldsymbol{\tau}_H$	Hydrodynamic force
$\boldsymbol{\tau}_{prop}$	Propulsion force
ρ	Density of the surrounding fluid
g	Acceleration due to gravity

η	Efficiency
∇	Volume

ABBREVIATIONS

AMC	Australian Maritime College
ASV	Autonomous Surface Vehicle
AUV	Autonomous Underwater Vehicle
CCPP	Collective and Cyclic Pitch Propeller
CFD	Computational Fluid Dynamic
DAQ	Data Acquisition system
DOF	Degree of Freedom
EFD	Experimental Fluid Dynamic
FPP	Fixed Pitch Propeller
IMO	International Maritime Organisation
ITTC	International Towing Tank Conference
LQR	Linear Quadratic Regulator
LS	Least Square
PID	Proportional-Integrate-Derivative
ROV	Remote Operated Vehicle
SNAME	Society of Naval Architects and Marine Engineers

SI	System Identification
UAV	Unmanned Aerial Vehicle
UTAS	University of Tasmania
UUV	Unmanned Underwater Vehicle

CHAPTER 1

Introduction

Chapter 1 provides the context for the thesis, briefly discussing the field of underwater vehicle propulsion system. The motivation, scope of the research, contribution to research, outline of the thesis, and publications are presented in this chapter.

1.1 Motivation

About 70% of the Earth's surface is covered with water and its influence is crucial to all aspects. The past half-century of oceanographic research has demonstrated that the ocean and seafloor hold the keys to understanding many of the processes responsible for shaping our planet (Steele et al., 2009). The explorations of marine environment have been providing valuable knowledge to many fields of science and engineering.

With the assistance of the robotic systems and their advancements, it is possible to reach the most extreme and remote area on the Earth. Compared to manned underwater vehicles and human divers, the robotic systems are safer and more efficient. The marine robotics have experienced tremendous growth for various scientific, civilian and military applications. These applications include three main categories: inspection and surveying; search and rescue; surveillance and security. Different robotic platforms have been deployed in the study of marine science and engineering including the Unmanned Aerial Vehicle (UAV), Autonomous Surface Vessel (ASV), and Unmanned Underwater Vehicle (UUV), as shown in Figure 1.1.

Among these robotic systems, UUVs have been the focus for many researchers and are becoming more attainable for a variety of underwater missions. The UUVs represent a rapid growth with the potential widespread deployment that will have a significant impact in the future. The recent development requires the underwater vehicles being capable of accomplishing more complex and advanced missions in various challenging operational environments; for example, under ice explorations, deep-ocean floor surveys and industrial subsea infrastructure inspections (Roberts and Sutton, 2006; Roberts and Sutton, 2012).

Based on the designed tasks and modes of operations the UUVs are categorised as Remotely Operated Vehicle (ROV) and Autonomous Underwater Vehicle (AUV). The ROVs typically have open frame structure, operate in limited space with human control via a tether on the surface

ship; whereas the AUVs normally have torpedo shape and are able to manoeuvre autonomously without constant real-time control from operator. AUVs can operate freely with the missions and control strategy configured in advance. They are widely used in ocean engineering and are designed to be efficient for the long-range and large-scale survey missions. The application of AUVs in acquisition of remotely-sensed data includes benthic habitat mapping, marine geology, fisheries assessment, turbulent water columns and polar region continental shelf mapping (Lucieer and Forrest, 2016). AUVs may be divided into small AUVs and large AUVs. Small AUVs may be handled manually and operated from small boats and from shoreline. Large AUVs may weigh up to several tons and require a research vessel with a dedicated launch and recovery systems (Ludvigsen and Sørensen, 2016). The application of AUV technology has grown steadily over the last few decades, with particularly rapid growth in the last decade (Nicholson and Healey, 2008).

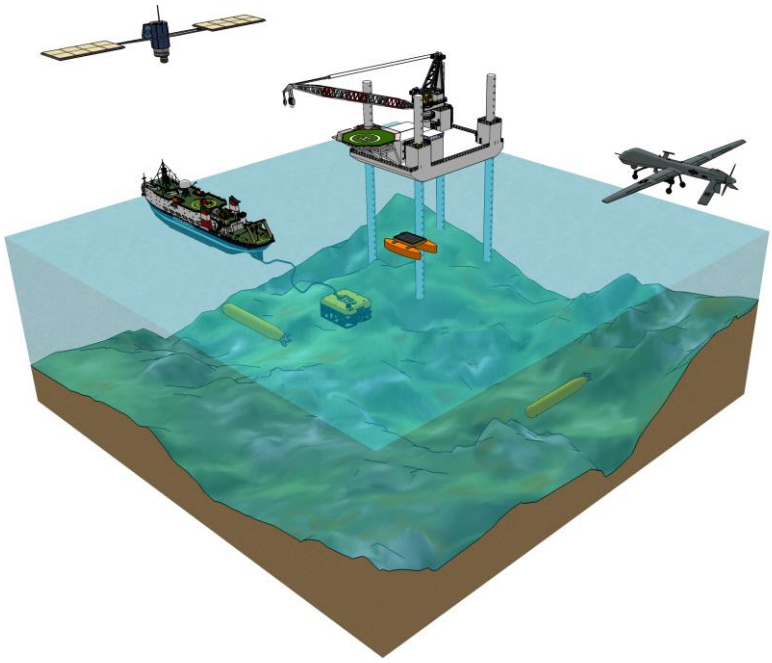

Figure 1.1. The cooperation of various systems in the study of marine science.

In the AUV development, besides the modern control system design and configuration modification, the design of advanced propulsion system is of great interest to facilitate new applications. The requirements for increased manoeuvrability and functionality have started to pose a significant impact on the research to improve the current propulsion systems. In this research context, the propulsion system is considered as the propulsor, which converts the energy from the power source into the thrust and manoeuvring forces. Depending on the tasks and missions, different propulsion systems are considered. The torpedo shaped AUV typically consists of the conventional propulsion system with the main fixed pitch propeller (FPP) providing thrust and a set of movable control surfaces generating manoeuvring forces. Originally, for this type of AUV, the main concern with regards to the operation is simply conducing the survey mission. The conventional propulsion system has been improved to facilitate this traditional mission. The manoeuvring control accuracy and the optimised efficiency provided by the propulsion system is essential for the successful completion of an AUV mission. Despite the advantages of FPP, there are some downsides to their use in AUVs. In recent applications, this type of propulsion system has been revealing the shortcoming of insufficient low-speed manoeuvrability since AUV control surface manoeuvring forces are only generated when the vehicle is moving. These control surfaces are similar to the aircraft's wings, rudders and elevators, which are effective as long as they are in motion.

Figure 1.2. Remotely Operated Vehicle (left) and Autonomous Underwater Vehicle (right). (Courtesy of Teledyne Marine).

It is obvious that the low speed manoeuvring performance is also important in AUV operations, especially in the docking and intervention missions. For example, the underwater docking for AUV is preferable since it would be very expensive and time consuming to launch and recover the AUV on board the mother ship after each mission. Docking has been identified as an enabling capability to support off-board operation of AUVs from submarines, autonomous surface vessels, other AUVs, ships, and under ice (Bellingham, 2016). The AUV must have the low speed manoeuvrability to approach the target and connect precisely to the docking platform. In the intervention application at hovering state, the AUV utilises the robotic arm or the manipulator for the sample collection in the environment that they are operating. There have been recent developments and breakthroughs in the underwater manipulator technologies for AUVs (so called autonomous manipulator) (Kim et al., 2016). The most recent effort is the Trident FP7 EU research project funded by the European Commission (Kim et al., 2016; Sanz et al., 2012). Furthermore, many underwater applications, such as marine observation and environmental assessment, require stationary observation at low speed. For a number of data collection operations, it is desirable to be able to deploy an AUV which can travel to a predetermined location, station itself in the water column at this location while recording environmental data over an extended time frame and then return to a recovery location (Briggs et al., 2010). In these missions, the AUV with conventional propulsion is inefficient due to the limitation of the control surfaces at zero or low speed operation regime. In general, there is limited access to AUVs with station keeping/hovering capabilities and this is at present the situation for AUVs with manipulator capabilities doing light intervention and sampling (Ludvigsen and Sørensen, 2016) . The current desirable characteristics of an AUV platform are cruising at medium to high speed in the survey missions, station keeping, and manoeuvring at low speed. This thesis has been motivated by the desire for an alternative propulsion system of a high manoeuvring AUV to be operated not only at cruising speed but also at low speed.

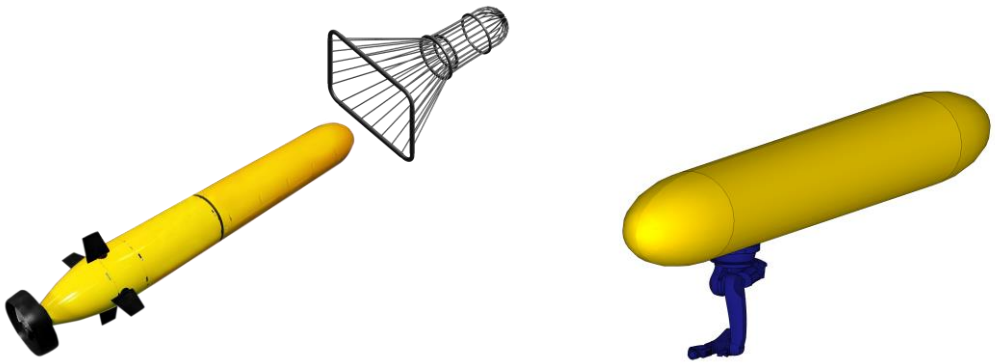

Figure 1.3. An AUV in docking mission (left) and an AUV in inspection mission (right).

The Collective and Cyclic Pitch Propeller (CCPP) to assist the low-speed operations of an AUV has been the subject of this research. The key difference between the CCPP and conventional system is the use of one integrated system instead of the FPP and control surfaces for propulsion and manoeuvring control. The CCPP has the ability to generate thrust and manoeuvring forces simultaneously. This feature of CCPP offers the unique and undistinguished capability.

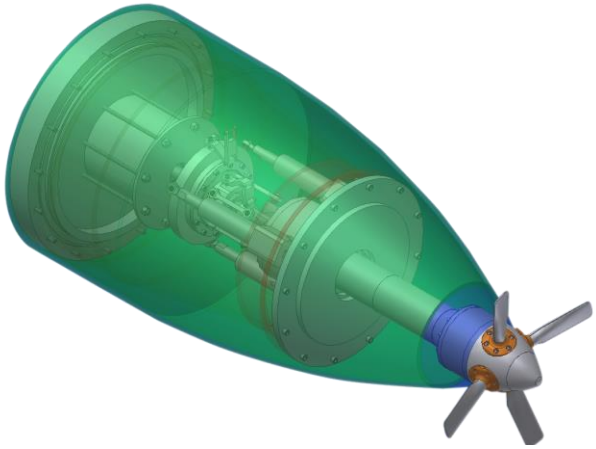

Figure 1.4. The Collective and Cyclic Pitch Propeller CCPP.

The National Centre for Maritime Engineering and Hydrodynamics at Australian Maritime College, University of Tasmania (UTAS) has been studying the CCPP system aiming to improve the AUV overall performance for complex mission tasks. CCPP has been one of the most innovative

propulsion systems designed and applied to an AUV. This is in contrast to aerial vehicle such as helicopter where the use of variable pitch systems is commonplace. Hence, there is an important need for a research into the viability of this alternative propulsion system and this is the motivation for this thesis.

1.2 Scope of the Thesis

The primary objective of the research project is to investigate the potential of the CCPP as the propulsion system of choice for a torpedo shaped AUV. In this thesis, the main research question was that: "Does the AUV equipped with CCPP have better manoeuvrability than the AUV with FPP". This thesis looked into the determination of the more applicable propulsion system for AUVs by numerically comparing the performance of an AUV equipped with CCPP to the conventional FPP. To address the research goal and answer the research question, a methodology was developed in which both experimental and numerical approaches were utilised.

Experimental approach consisted of the experimental study of the CCPP and FPP in the towing tank test. The hydrodynamic characteristics of the CCPP were difficult to model by using the theoretical and numerical approach due to the complexity in working principle. Hence, there was a need to conduct an experimental study that can measure accurately the generated forces and to construct the empirical models based on these obtained data. Two types of experiments were conducted including the bollard pull test and model captive test. The experimental procedure was based on the guideline proposed by the International Towing Tank Conference ITTC. These model tests have been widely used to predict motions and forces in marine applications. The CCPP empirical model was made non-dimensional and then scaled to the size of Gavia's FPP dimension for the comparison study. Since the CCPP was examined in the low speed operation, the scaling effect has no significant effects on its performance. The accurate modelling of

the propulsion systems were essential to calculate the AUV's response to different operational conditions and control strategies.

The use of CCPP to manoeuvre an AUV represented a challenging problem, which motivated the need for a simulation. The complexity of manoeuvres in real life makes computer simulation useful for their study (Lewis, 1988). In this thesis, the numerical approach consisted of establishing the comprehensive mathematical model of the AUV with the hydrodynamic parameters obtained from theoretical and analytical methods; constructing a numerical simulation program called AUVSIPRO based on MATLAB/Simulink™; and developing the control algorithm for AUV with CCPP. The propulsion system models and hull hydrodynamic model were incorporated in AUVSIPRO. Although validation is required, the main advantage of this approach is that it provides a good understanding of the performance of an AUV without the need for the physical model. In addition, as the development of an AUV is both costly and time consuming, the use of modelling and simulations is essential to the design process.

Figure 1.5. Gavia class AUV (Courtesy of Teledyne Marine).

At the AMC-UTAS, several AUVs have been used for the research and study. In this project, the Gavia AUV has been considered as the research platform. The CCPP has been simulated to empower the Gavia AUV based on the developed propulsion and vehicle model. Given the Gavia AUV platform with the conventional FPP propulsion system and the prototype of CCPP, it has been considered an opportunity to investigate the potential of CCPP for an AUV by conducting the comparison study.

1.3 Contribution to Research

The key contributions and achievements of this work are to provide an insight into the performance of an AUV equipped with CCPP. There had been insufficient information in the CCPP hydrodynamic characteristics and the manoeuvrability of an AUV with CCPP had not been fully examined. The dynamic modelling of an underwater vehicle FPP in four-quadrant operation was also presented. The in depth comparison results for both propulsion systems CCPP and FPP provided useful data for the researchers in selecting and designing a propulsion system for an AUV. The knowledge of the propulsion system characteristics is necessary for the operation of an AUV. An additional contribution of the research is to develop a controller for an AUV equipped with CCPP. The control problem of an AUV is very challenging since the mathematical model of AUV is characterized by high nonlinearity and strongly coupling. The novel two-stage system identification method was proposed to identify the linear mathematical model of the Gavia AUV and the optimal linear control algorithm was successfully applied to the system.

1.4 Outline of the Thesis

The thesis documents the experimental and numerical simulation studies conducted in this research project. It is divided into eight chapters as follows:

Chapter 1 provides the context for the following chapters, including the motivation, scope of the research, outline of the thesis, contribution to research, and the publications.

Chapter 2 describes the background and a comprehensive literature review of the research project. It introduces the reasons for interest in alternative propulsion system to the conventional propeller applied to an AUV. A review of the state of the art of various underwater vehicle propulsion systems are presented. The advantages and disadvantages of these propulsion systems

are discussed in term of performance characteristics. The chapter also includes a literature review regarding the previous research studies conducted on the CCPP.

Chapter 3 discusses a mathematical model for an AUV. The modelling of an AUV platform is essential to investigate the manoeuvring characteristics of an AUV equipped with a CCPP. The reference frames including the earth-fixed and body-fixed coordinates are defined. The modelling of an AUV involves the development of both kinematic and dynamic model. The analytical and theoretical method to estimate the hydrodynamic coefficients are briefly mentioned. This chapter lay the theoretical foundations of the works conducted in the following chapters.

Chapter 4 and **Chapter 5** provide an in-depth modelling of the conventional propulsion system FPP and the CCPP respectively using the experimental approach. Two separate testing techniques and setups for the FPP and CCPP testing are considered. The experiments to examine the hydrodynamic characteristics of both propulsion systems are conducted. The obtained data are analysed and discussed in detail.

Chapter 6 illustrates a detailed manoeuvring simulation of an AUV equipped with FPP and CCPP. A variety of standard manoeuvring tests for marine vehicles are considered to investigate the AUV performance.

Chapter 7 examines the control design for an AUV equipped with CCPP. The content of this chapter includes the two-stage identification method to define the linear model of Gavia AUV and the optimal control development. The depth and heading control are performed to validate the controller.

Chapter 8 presents an overview of the works conducted in the research project, summaries the main findings, emphasises the significance of the study, and provides the suggested direction for the continued investigation in light of the current works.

1.5 Publications

Parts of the thesis have been submitted and published in the following papers in the past three years during the course of the research project.

1.5.1 Presentations and Conference Papers

- Minh Tran, Hung Nguyen, Jonathan Binns, Shuhong Chai and Alex Forrest, A Study of new propulsion system for an Autonomous Underwater Vehicle, *9th Graduate Research Conference at the University of Tasmania*, Hobart, Australia, 2015.
- Minh Tran, Supun A.T. Randeni, Hung D. Nguyen, Jonathan Binns, Shuhong Chai and Alex Forrest, Least Squares Optimisation Algorithm Based System Identification of an Autonomous Underwater Vehicle, *Proceedings of the 3rd Vietnam Conference on Control and Automation*, Vietnam, 2015.
- Minh Tran, Hung Nguyen, Jonathan Binns, Shuhong Chai and Alex Forrest, AUVSIPRO–A Simulation Program for Performance Prediction of Autonomous Underwater Vehicle with Different Propulsion System Configurations. *International Conference on Modelling and Simulation for Autonomous Systems.* Springer, 72-82.
- Minh Tran, Hung Nguyen, Jonathan Binns, Shuhong Chai and Alex Forrest, Optimal control of an autonomous underwater vehicle equipped with the collective and cyclic pitch propeller. *Control Conference (ASCC), 2017 11th Asian.* IEEE, 354-359.

1.5.2 Journal Papers

- Minh Tran, Hung Nguyen, Jonathan Binns, Shuhong Chai and Alex Forrest, A practical approach to the dynamics modelling of an underwater vehicle propeller in all four quadrants of operation, *Proceedings of the Institution of Mechanical Engineers, Part M: Journal of Engineering for the Maritime Environment.* (Published).

- Minh Tran, Hung Nguyen, Jonathan Binns, Shuhong Chai and Alex Forrest, Experimental Study of the Collective and Cyclic Pitch Propeller, *The Journal of Marine Science and Application.* (Accepted for publication).
- Minh Tran, Hung Nguyen, Jonathan Binns, Shuhong Chai and Alex Forrest, A comparison study of two propulsion system configurations for an autonomous underwater vehicle, *Ocean Engineering, An International Journal of Research and Development.* (In progress).

CHAPTER 2

Literature Review

This chapter describes the background and literature review of the research project. It introduces the reasons for interest in an alternative propulsion system to the conventional propeller applied to an AUV. In this chapter, a review of the state of the art of various underwater vehicle propulsion systems are presented. The advantages and disadvantages of these propulsion systems are discussed in term of performance characteristics. The chapter concludes with the literature review of previous research conducted for CCPP propulsion system.

Part of this chapter has been published in the "*Proceeding of 9th Graduate Research Conference at the University of Tasmania*". The citation for the presentation is:

Minh Tran, Hung Nguyen, Jonathan Binns, Shuhong Chai and Alex Forrest, A Study of new propulsion system for an Autonomous Underwater Vehicle, *9th Graduate Research Conference at the University of Tasmania*, Hobart, Australia, 2015.

2.1 Introduction

AUVs play a critical role in the maritime industry to provide automated missions. AUV technology is a fast growing research area with a wide range of subsystems being developed. One of the key challenges each AUV experience, is achieving an accurate manoeuvrability. Essentially, a basic consideration for the design of swimming machines is the design of propulsors: their shape, location on the robot, mechanical properties (e.g., inertia and stiffness), and pattern of movement (Colgate and Lynch, 2004). In this chapter, the conventional propulsion system for a torpedo shaped underwater vehicle and its performance characteristics are presented. In addition, a comprehensive literature study is mentioned to describe the relevant propulsion systems with different configurations as alternative propulsion system to the conventional one. A brief description and performance analysis of these propulsion systems are conducted, discussing the advantages and disadvantages of using these systems. Finally, the CCPP configuration is briefly explained and the previous works related to the research of CCPP is reviewed.

2.2 Conventional propulsion system for an autonomous underwater vehicle and its limitations

2.2.1 Conventional propulsion system with Fixed Pitch Propeller (FPP)

In modern subsea mapping and surveying applications, AUVs are usually designed for high speed cruising so that the vehicles are able to cover the longer distance and larger range of inspection area from several meters to hundreds of meters. A majority of work related to propulsion system has been conducted on the traditional propeller-driven propulsion.

The use of a FPP at the aft end combined with control surfaces as means of propulsion are prevalent for underwater vehicles, especially for torpedo-shaped AUVs, such as HUGIN 1000 class (Hagen et al., 2003), Autosub 6000 (McPhail, 2009) and REMUS 600 class (Stokey et al., 2005). In

this conventional configuration, the FPP provides thrust for AUV while the manoeuvring of an AUV is achieved through adjustment of the control surfaces. Additionally, the ducted propellers are also utilised to increase the propulsion system efficiency of AUVs, including AUV PreToS (Chakrabarti et al., 2014) and Gavia class (Hiller et al., 2012).

Figure 2.1. REMUS class AUV. (Courtesy of Kongsberg Maritime).

2.2.2 Limitations of the conventional propulsion system

It is essential that the control surfaces be capable of generating manoeuvring forces that are sufficient in magnitude and oriented in desired control directions. However, these traditional types of propulsion system have the shortcoming of insufficient low-speed manoeuvrability because low aspect ratio control surface characteristics significantly limit their effectiveness (Huyer et al., 2010; Farnsworth et al., 2010). With the exception of thrust from the propeller, AUV control surface manoeuvring forces are only generated when the vehicle is in motion at sufficient speed. Hence, the AUV missions at zero and low speed are limited.

The control surfaces and other appendages protruding from the hull can be damaged when the vehicle travelling in a confined environment. They are also easily to be affected by the environmental disturbances and turbulence. In such a condition, the control surfaces are not able to produce enough forces and moments to counteract the influences resulted from strong ocean currents. In term of efficiency, the lack of variable pitch capability of the conventional propeller leads to AUV propulsion having relatively low efficiency at different operational conditions. For these reasons, there is an important need for research into the alternative propulsion system for

AUV, which could increase the functionality and manoeuvrability at different operational speeds and missions. The aim of the next generation of AUVs is also to be able to combine long range survey capabilities with low speed investigation of the environment encountered (Palmer, 2009). For example, with the growing acceptance of survey-class AUVs in the commercial sector, interest is growing in the use of AUVs for activities such as periodic inspection of subsea equipment installations and the use of AUVs for maintenance and repair activities (Bellingham, 2016). In addition, the underwater docking represent a major challenge in the design and improvement of current AUV propulsion.

2.3 Alternative Propulsion Systems for an Underwater Vehicle

There are already various concepts of propulsion systems, which have been designed and applied to an underwater vehicle as the solution to the downsides of a conventional FPP. These following sections describe some of the prevalent types with their specific mechanisms and unique performance capabilities. The purpose is to give an overview of the current state of research in the fields related to underwater vehicle propulsion system.

2.3.1 Thruster

To enhance the low speed manoeuvrability, the thrusters are utilised and positioned at different locations around the AUV without changing the low drag profile of the torpedo-shaped AUV. The thrusters are categorised into two main different types: through-body thrusters (tunnel thrusters) and the external thrusters. Adding thrusters enables the vehicle to travel long distances at high speeds to a desired destination and then perform tasks that require low speed manoeuvrability (Saunders and Nahon, 2002). Thruster is the standard choice in propelling low speed AUV and is widely used in turbulent environment since its generated forces and moments are generally independent of surrounding fluid. A number of these AUVs have been developed, including Typhoon (Allotta et al., 2015), Delphin2 (Philips et al., 2013), C-Scout (Saunders and

Nahon, 2002), Odyssey (Eskesen et al., 2009), and Mares (Cruz and Matos, 2008). The propeller based thrusters have been employed for low speed control due to their reliability, responsiveness and ability to generate forces throughout the operational range of the vehicle (Palmer, 2009).

Figure 2.2. Mares (Cruz and Matos, 2008) and Delphin 2 AUV (Philips et al., 2013).

However, the disadvantage of using thrusters is the reduced propulsive efficiency at high speeds. Tunnel thrusters could increase the parasitic drag of the vehicle and also take up considerable volume that could otherwise be used for energy or payload (Huyer et al., 2010). Hence, the internal architecture of the AUV using tunnel thrusters are quite complex. Moreover, the external thrusters are vulnerable to the damage and corrosion since they are subject to high influx of water. A number of thrusters installed in close proximity result in the cross-coupling interactions influencing the control characteristics considerably (Russell and Bellec, 1981).

2.3.2 Vectored Thruster

An alternative to the conventional propeller that could improve the manoeuvrability and efficiency of underwater vehicles is the vectored thruster propeller, or a steerable propeller. The vectored thrusters are a special type of the thrusters. The vectored thruster propellers applied to underwater vehicle are inspired from the azimuthing podded propulsion system for ships (Stettler, 2004). In the vectored thruster configuration, the generated force and moment are con-

trolled by actively altering the thruster direction. In spite of the mechanical complexity, the advantages of using vectored thruster propeller for propulsion system of AUV include improved manoeuvrability, and the fact that fewer fins, which may snag on underwater cables or other obstacles in a confined environment, protrude from the vehicle (von Ellenrieder and Ackermann, 2006). The vectored thruster propulsion for underwater vehicle is still under development and has not been applied in practical application.

2.3.3 Buoyancy Engine

To increase the hover capability of the conventional torpedo shaped AUV, researchers have come up with some modifications to the propulsion system by taking advantage of the balance between buoyancy and hydrodynamic forces by changing the ballast mass to drive it in water (Abraham and Yi, 2015). A review for popular buoyance engines which mainly used for the underwater gliders could be found in reference (Ullah et al., 2015). Autonomous large area surveys of ocean are currently carried out using either flight-style propeller-driven AUVs or gliders (Furlong et al., 2007). The endurance of glider is significantly longer than the traditional AUV. The power requirement for gliders are substantially low in the comparison to the propeller-driven AUVs. A detailed discussion on the current studies of the gliders could be found in the following reference (Jenkins and D'Spain, 2016).

Figure 2.3. Slocum glider. (Courtesy of Teledyne Marine).

The glider is an effective tool in measuring water column parameters. However, the accuracy in navigation and manoeuvring is limited (Ludvigsen and Sørensen, 2016). The produced thrust from buoyancy engine is not sufficient compared to other types of propulsion system resulting in the gliders instability to environmental disturbances. Hence, the gliders are not able to operate in the strong ocean currents. Moreover, due to the nature of their propulsion system gliders are restricted to seesaw flight profiles (Furlong et al., 2007).

2.3.4 Biomimetic propulsion

Researchers also look to nature as an inspiration for their design where the biomimetic propulsion system has been considered (Mazlan and Naddi, 2015). Nature preserve various means of underwater propulsion. Different species display a multitude of propulsion and manoeuvring methods appropriate for their environment (Riggs, 2010). Research on aquatic animals has increased and these animals have been mimicked to improve underwater vehicles and their locomotion mechanisms for better performance (Korkmaz et al., 2015). The most popular types of biomimetic propulsion system are the flapping foil (flexible fins) and the oscillating paddle (rigid paddles). Creatures with the large ratio of body weight to surface are normally propel themselves by flapping their wings continuously while natural species with the small ratio of body weight to area swim propelled by transferring momentum to water with the mechanism similar to jet propulsion. The swimming animals share some of similar mechanisms with flying animals but the fundamental nature of generated thrust is different. The primary goal in flying is the continuous production of steady lift, to balance the large body weight within a medium with small density. The major goal in fish swimming is to minimize drag forces within a medium a thousand times more dense than air—the generation of steady lift to support the (small) net weight is of secondary or no importance at all (Triantafyllou et al., 2004). The biomimetic propulsion is not dangerous to surrounding objects, animals and humans compared to conventional

propeller and other rotating propulsions. Biomimetic propulsion also offers some distinct advantages such as excellent manoeuvrability for steering and low-noise operation, but is considered not propulsive efficiency (Korde, 2004). Although there exist solutions on the efficiency issues, there are many challenges to overcome related to the mechanical design. The mechanism of current biomimetic propulsions are still complex and hard to control. Considerable efforts have been put into the investigation of biomimetic propulsion to decrease its power consumption and increase functionality (Read, 2001; Watts, 2009; Roper et al., 2011; Polidoro, 2003; Hubbard et al., 2014). Solving these issues will greatly facilitate the development of underwater marine robotics.

2.3.5 Preswirl Propulsor

Another concept of underwater propulsion is the preswirl propulsor. This propulsor has been designed with the intention to overcome the limitation of the conventional FPP. This novel propulsor utilises an upstream stator row, where the individual stator blade pitch angles can be varied, coupled with a downstream rotor. By sinusoidally varying the individual stator blade pitch angles around the circumference, the upstream stator row produces a significant side force (Huyer et al., 2012; Huyer et al., 2010; Farnsworth et al., 2010). The prototype of preswirl propulsor has been successfully tested but its application to an AUV has not been reported.

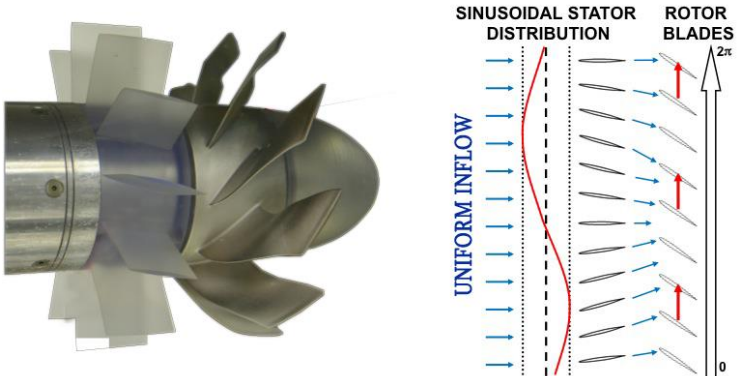

Figure 2.4. Preswirl Propulsor (Huyer et al., 2012).

2.3.6 Jet-pump or waterjet Propulsion

In the jet-pump or waterjet propulsion, the water is absorbed into the water hydraulic pump from the bow section of the AUV. After being pressurised, the water jets out of the nozzle and generates reaction thrust (Xin et al., 2013). The yaw and pitch manoeuvres are performed by either the differential thrust mechanism or the waterjet steering system.

Using jet-pumps for propulsion and steering is an alternative option to the conventional propeller-driven propulsion. Pump and jet systems are less energy efficient with respect to blade propellers and rudder steering (Alam et al., 2014). The jet-pump also offers several advantages from the point of view of the mechanical design (absence of rotating parts and transmission mechanisms), realization cost (simpler fibre-class cover), robustness with respect to transportation/deployment/recovery damages (no appendixes protruding from the cylinder), safety of occasional swimmers in proximity of the vehicle (jet-pumps are much less likely to cause harm at low speed with respect to propeller blades) (Alvarez et al., 2009). The investigations and studies of jet-pump propulsion for AUVs have been examined thoroughly in the literature (Korde, 2004; Polsenberg Thomas, 2007; Mohseni, 2006). However, the waterjet propulsion are generally not used for medium-speed and high speed applications due to the decrease in efficiency. The control accuracy of waterjet propulsion is limited in the underwater environment in which the six degree-of-freedom manoeuvrability is required.

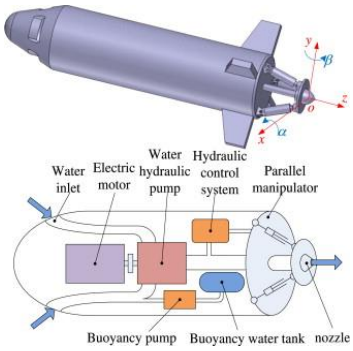

Figure 2.5. AUV water-jet propulsion system (Xin et al., 2013).

2.3.7 Hybrid Propulsors

There are a number of AUVs integrating different methods of locomotion in one system. The hybrid propulsion system have been extensively studied as a potential means for improvement of underwater vehicle performance. An excellent example of this can be seen on the Tethys-class AUV built by the Monterey Bay Aquarium Research Institute. The Tethys-class AUV has a unique ability to operate efficiently in three different operational modes with a range of actuators: traditional propeller for high speed, a moving internal mass (like a glider) for low speed, and variable buoyancy for drifting (like a float) (Hobson et al., 2012). The Guanay-II AUV uses the propulsion system comprises: a main engine, which provides the propulsion, two side thrusters, which monitor the direction of the vehicle and an internal pneumatic stainless cylinder, which allows the vehicle to dive by taking in and ejecting water (Gomáriz et al., 2015). Another hybrid AUV uses ducted propeller and rudder located at the aft for horizontal motion and internal mass shifter mechanism for vertical motion (Tran et al., 2015b) or the internal rolling mass mechanism for roll control (Hong and Chitre, 2015). The internal actuators are located inside the vehicle hull and hence are less subject to damage than the external thrusters are. However, the use of moving internal actuators are limited due to the significant requirement for the inner hull space and high power consumption from multiple systems. Additionally, it is challenging to design the control strategy for the integrated propulsion unit with different force generation methods.

2.4 Collective and Cyclic Pitch Propeller (CCPP)

Even though a variety of improvements and innovations has been made, the development of an advanced propulsion system for an AUV remains a challenging research area. It is essential to develop the alternative means of propulsion system for AUVs that could increase both efficiency and manoeuvrability. The CCPP has been developed to overcome the limitations revealed by

the current propulsion configurations and to investigate its performance characteristics in underwater working environment. The most attractive characteristic of CCPP is its capability to generate continuous thrust and manoeuvring forces simultaneously. The CCPP propulsion system has improved the underwater vehicle efficiency at cruising speed and the high degree of manoeuvrability at low speed without using the control surfaces. This section explains its basic configuration and reviews the development of the CCPP.

The CCPP, as shown in Figure 2.6, has the similar working principle to the conventional main rotor of the helicopter (Seddon and Newman, 2011) and the variable vector propeller of an underwater vehicle (Nagashima et al., 2006). The essential component of CCPP is a swashplate, which is controlled by linear actuators, as shown in Figure 2.7. The swashplate enables the adjustment of the propeller pitch angles as the shaft is rotating. There are two primary blade settings in the CCPP configuration, the collective pitch setting and the cyclic pitch setting.

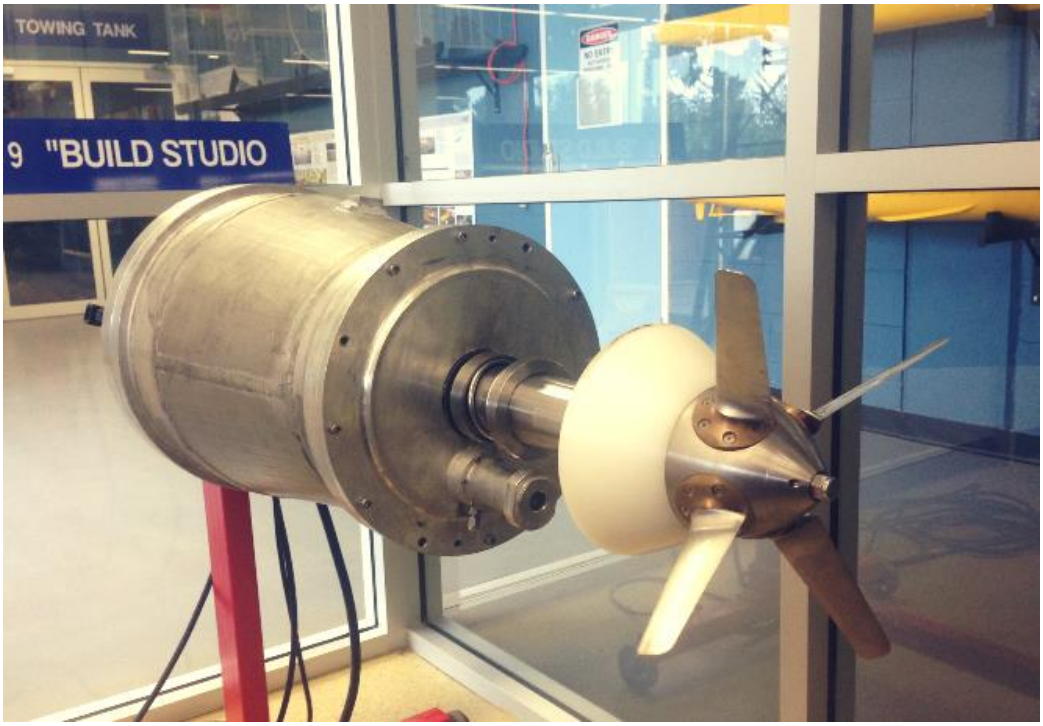

Figure 2.6. The Collective and Cyclic Pitch Propeller CCPP Prototype.

The main particulars of the examined model are given in Table 2.1.

Table 2.1. Fundamental specifications of tested propeller (Humphrey, 2005).

Symbol	Description	Value	Unit
	Scale	1:1	
Z	Number of blades	4	
	Blade section	NACA 0012	
D	Diameter	0.305	m
δ_{col}	Collective angle	-29 to 29	Degree
δ_{cyc}	Cyclic angle	-20 to 20	Degree

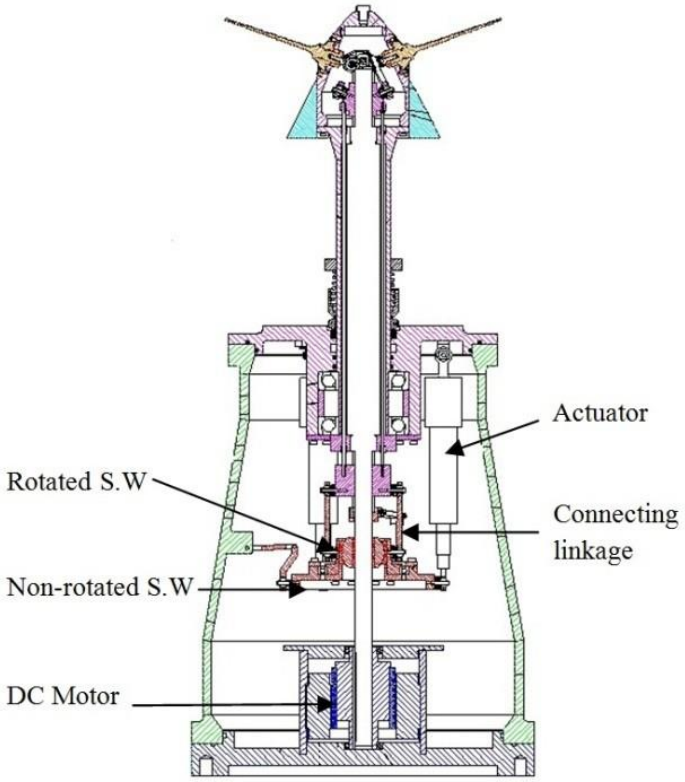

Figure 2.7. A cross section drawing of the CCPP (Humphrey, 2005).

The collective pitch setting of the CCPP is similar to Controllable Pitch Propeller (CPP) which is well-known for the advantage of full power utilisation at any circumstances, such as: accelerating and stopping; rapid manoeuvring; and dynamic positioning (Dang et al., 2012). The pitch angles of all blades could be changed simultaneously to a particular value at position 1, 2, 3 and 4 in the collective pitch setting. As shown in Figure 2.8, all the blades are increased to a defined value. This feature allows the propulsor to alter its axial thrust without changing the propeller rotational speed. The CPP has been studied for an AUV specially designed in the tunnel inspection mission (Jung et al., 2012). In these types of mission, the reverse thrust is crucial as the vehicle is operating is narrow space. In addition, the ability to change the pitch angle results in the optimised thrust from CCPP at various operating speeds. This helps the AUV reach maximum efficiency in different operations, avoid the motor to be overloaded and increase the motor duration (Tarbiat et al., 2014).

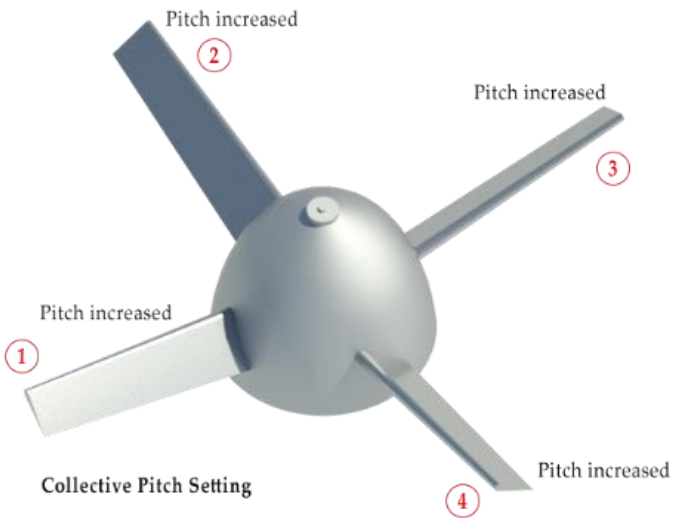

Figure 2.8. Collective Pitch Setting of CCPP.

CCPP is primarily different from the CPP in the cyclic pitch control to create the manoeuvring side forces. CCPP is a means of manoeuvring force generation that does not require the control

surface but due to the cyclic pitch setting. The angles of each propeller blade can also be positioned periodically during a rotation in the cyclic pitch setting by manipulating the orientation of swash plate. As shown in Figure 2.9, the blade pitch angle will be increased in position 2, decreased in position 4; and remained neutral in position 1 and position 3 per revolution. As the results, more lift will be created in position 2 and the side force as well as the moment are created. Therefore, the CCPP can generate thrust, as well as manoeuvring forces and moments in different directions. The physical parameter and dynamic model of CCPP will be presented thoroughly in the next chapters.

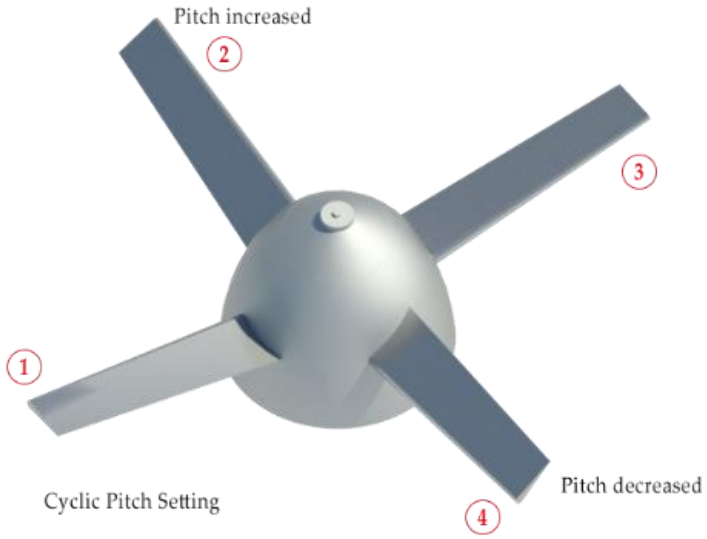

Figure 2.9. Cyclic Pitch Setting of CCPP.

Extensive research has been conducted in the aeronautics on the helicopter main rotor. However, there has been limited publications in the literature considering the unique features of CCPP and its applications to marine underwater vehicles. The complex mechanical design and control system associated with this propulsion system has prevented the extensive research effort. Previous studies have focused on the mechanical design and hardware integration. The prototype

of CCPP utilised in this study was initially built at Memorial University of Newfoundland, Canada (Humphrey, 2005). A prototype CCPP with control system was designed, constructed and tested. A series of initial tests were carried out to study its characteristics in the open water condition. The most recent research was conducted at the Australian Maritime College, University of Tasmania to investigate the performance of an underwater vehicle model equipped with CCPP in straight line model captive test (Niyomka, 2014). In addition, the prediction program for performance of CCPP was also constructed using BEMT and the Leishman-Beddoes dynamic stall model. Although the innovative features of CCPP for underwater vehicle were discovered from previous studies its performance characteristics were not fully demonstrated yet. Additionally, due to the lack of experimental data, the modelling and simulation studies were not conducted in detail. Therefore, the potential application of CCPP to an AUV has not been verified. In response to the shortcomings of previous works, the studies with underwater vehicle model equipped with CCPP have been carried out thoroughly in this thesis. The analytical method, experimental approach and numerical simulation are presented and applied in the next chapters. The methodologies associated with these approaches are also reviewed and explained.

2.5 Summary

The background and literature review of the research project were described in chapter 2. It introduced the reasons for interest in alternative propulsion system to the conventional propeller applied to an AUV. It also presented a review of the state of the art of various underwater vehicle propulsion systems, and more specifically, the propulsion system for the torpedo shaped underwater vehicle. The advantages and disadvantages of these propulsion systems were discussed thoroughly in term of mechanisms and performance characteristics. Chapter 2 concluded with a literature review of previous research conducted for the CCPP to pave way for the current research.

CHAPTER 3

AUV Equations of Motion

This chapter discusses the mathematical model of an underwater vehicle. The modelling of an AUV involves the development of both kinematic and dynamic model. The analytical and theoretical method to estimate the hydrodynamic coefficients are briefly presented. This chapter provides the theoretical foundations for the further investigation conducted in the following chapters.

3.1 Introduction

The works described in this section is concerned with mathematical modelling of the torpedo shaped underwater vehicle. Generally, there are three modelling approaches to obtain a model of an AUV, namely first principles modelling, grey box modelling and black box modelling. The first principle modelling is also known as white box modelling and it is applied to derive the comprehensive mathematical model of an underwater vehicle using the laws of mechanics and hydrodynamics. The relevant first principle modelling approaches are Lagrangian and Newton-Euler modelling. This method provides a comprehensive physical understanding of the vehicle components and their interactions in the development stage.

In this thesis, the Newton-Euler modelling approach is considered. This modelling of an AUV involves the development of both kinematic and dynamic model. The general motion of an AUV is fully described by six degree-of-freedom equations. The non-linear hydrodynamic coefficients of an AUV are calculated using the analytical and theoretical estimation.

An accurate vehicle dynamic model would greatly aid in the development of the simulation program and the controller design. The objective of this chapter is to build the sufficiently high fidelity dynamic model. The mathematical model forms the foundation for investigating the AUV performance with different propulsions. The more precise the mathematical model representing the characteristic of an AUV is, better the performance of the simulation program.

The following assumptions are made in the modelling of the underwater vehicle:

- The AUV is submerged in a homogeneous fluid;
- The AUV is moving in a stationary body of water having constant properties;
- Underwater currents and disturbances are neglected;
- The underwater vehicle is considered as a rigid body of constant mass.

3.2 Coordinate Systems and Transformation

3.2.1 Six Degree of Freedom and Standard Notation

The underwater vehicle operates in a three dimensional space and it is convenient to describe the state variables of the vehicle and the forces acting on it by the six independent coordinates or six degree of freedom (6 DOF). The standard of SNAME (Society of Naval Architects and Marine Engineers) notation is used to describe the 6 DOF quantities and is summarised in the Table 3.1 (SNAME, 1950). In this notation, motion in the horizontal plane is referred to as surge (steady forward motion), sway (sideway motion), and yaw (rotation about the vertical axis). Three remaining DOFs are in the vertical plane including roll (rotation about longitudinal axis), pitch (rotation about transverse axis), and heave (vertical motion).

Table 3.1. Standard Notation for Underwater Vehicle Motion.

DOF	Motions	Forces and Moments	Translational and Rotational Velocity	Positions and Euler Angles
1	Surge	X	u	x
2	Sway	Y	v	y
3	Heave	Z	w	z
4	Roll	K	p	ϕ
5	Pitch	M	q	θ
6	Yaw	N	r	ψ

By convention for underwater vehicles, the positive x direction is taken as forward, the positive y direction is taken as to the right, the positive z direction is taken as down, and the right-hand rule applies for angles (Hajosy, 1994).

3.2.2 Coordinate Systems

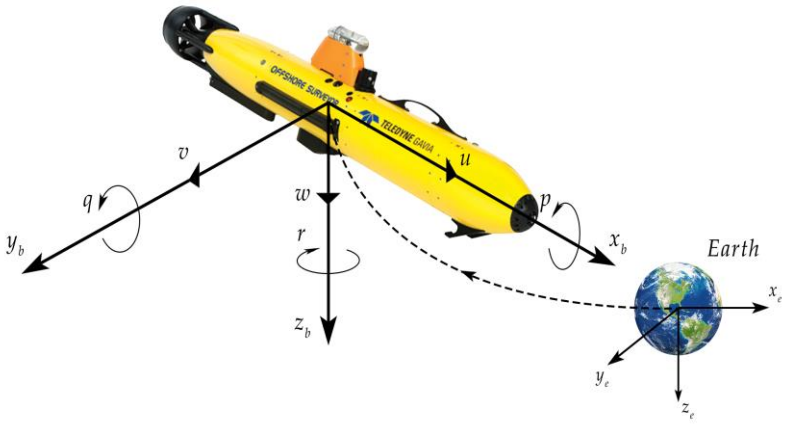

Figure 3.1. Coordinate system.

This section presents the coordinate systems used for measurement of vehicle's position, velocity and acceleration. There are two reference frames describing the state variables of an AUV. There Earth-fixed reference frame is selected as the inertial reference frame since the underwater vehicles travel at low enough speeds so that the acceleration of points on the surface of the Earth can be neglected (Hajosy, 1994). The Earth-fixed coordinate is used to represent the position and orientation of the vehicle relative to a fixed point of the Earth. The body-fixed coordinate with the origin O, is usually selected to coincident with the vehicle centre of gravity CG. The Body-Fixed Coordinate is used to describe the translational and rotational velocities.

Each axis of the coordinate system corresponds to a variable and all variables in both coordinate systems forms the state variables of the system. The position and orientation of the vehicle relative to an Earth-Fixed Coordinate is defined as the position vector η_1 and orientation vector η_2 :

$$\eta_1 = \begin{bmatrix} x & y & z \end{bmatrix}^T \tag{3.1}$$

$$\eta_2 = \begin{bmatrix} \phi & \theta & \psi \end{bmatrix}^T \tag{3.2}$$

where x is the distance in the inertial north direction, y is the distance east, and z is the distance down. ϕ, θ, and ψ are the Euler roll, pitch and yaw angles.

The position and orientation vectors are grouped as vector $\boldsymbol{\eta}$:

$$\boldsymbol{\eta} = \begin{bmatrix} \boldsymbol{\eta}_1^T & \boldsymbol{\eta}_2^T \end{bmatrix} = \begin{bmatrix} x & y & z & \phi & \theta & \psi \end{bmatrix}^T \tag{3.3}$$

The translational velocity vector $\boldsymbol{v}_1 = \begin{bmatrix} u & v & w \end{bmatrix}^T$ is defined in the body-fixed coordinate, where surge velocity u is positive along the vehicle $X-$axis, sway velocity v is positive along the $Y-$axis, and heave velocity w is positive along the vehicle $Z-$axis. The rotational velocity vector $\boldsymbol{v}_2 = \begin{bmatrix} p & q & r \end{bmatrix}^T$ is also defined in the body-fixed coordinate, where roll rate p is right-hand positive about the vehicle $X-$axis, pitch rate q is right-hand positive about the $Y-$axis, and yaw rate r is right-hand positive about $Z-$axis.

The translational and rotational velocities are grouped as vector $\boldsymbol{v}$:

$$\boldsymbol{v} = \begin{bmatrix} \boldsymbol{v}_1 & \boldsymbol{v}_2 \end{bmatrix}^T = \begin{bmatrix} u & v & w & p & q & r \end{bmatrix}^T \tag{3.4}$$

3.2.3 Euler Angles and Vector Transformation

The two coordinate systems have a relationship that is obtained through Euler angles as shown in Figure 3.2. The vehicle coordinate system is rotated relative to the inertial coordinate system by first aligning the coordinate systems such that the X_b-axis points north, the Y_b-axis points east, and the Z_b-axis point down. The vehicle coordinate system is then rotated by the yaw angle ψ about the vehicle Z_b-axis, denoted by Z_3, then by the pitch angle θ about the resulting Y_b- axis, denoted Y_2, then finally by the roll angle ϕ about the resulting X_b- axis, denoted X_1. The sequence of rotations is illustrated in Figure 3.2.

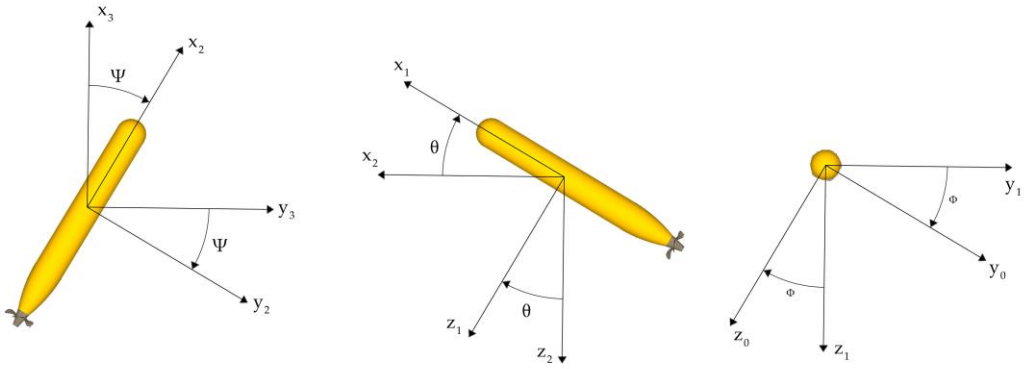

Figure 3.2. Euler's Angle Transformation.

The three rotation matrices about each axis, z, y and x can be defined as:

$$C_{z,\psi}=\begin{bmatrix}\cos\psi & \sin\psi & 0\\ -\sin\psi & \cos\psi & 0\\ 0 & 0 & 1\end{bmatrix},\ C_{y,\theta}=\begin{bmatrix}\cos\theta & 0 & -\sin\theta\\ 0 & 1 & 0\\ \sin\theta & 0 & \cos\theta\end{bmatrix},\ C_{x,\phi}=\begin{bmatrix}1 & 0 & 0\\ 0 & \cos\phi & \sin\phi\\ 0 & -\sin\phi & \cos\phi\end{bmatrix} \tag{3.5}$$

3.3 Kinematics

The kinematic equations represents the transformation between two coordinate systems. The translational velocity vector υ can be mapped to the Earth-fixed coordinate by a rotation matrix J (Fossen, 2011):

$$\dot{\eta}=J(\eta_2)\upsilon \tag{3.6}$$

where:

$$J(\eta_2)=\begin{bmatrix}J_1(\eta_2) & \mathbf{0}\\ \mathbf{0} & J_2(\eta_2)\end{bmatrix} \tag{3.7}$$

The matrices $J_1(\eta_2)$ and $J_2(\eta_2)$ are defined based on the Euler angle transformation as:

$$J_1(\eta_2) = C_{z,\psi}^T C_{y,\theta}^T C_{x,\phi}^T = \begin{bmatrix} c\psi c\theta & -s\psi c\phi + c\psi s\theta s\phi & s\psi s\phi + c\psi c\phi s\theta \\ s\psi c\theta & c\psi c\phi + s\phi s\theta s\psi & -c\psi s\phi + s\theta s\psi c\phi \\ -s\theta & c\theta s\phi & c\theta c\phi \end{bmatrix} \tag{3.8}$$

$$J_2(\eta_2) = \begin{bmatrix} 1 & s\phi t\theta & c\phi t\theta \\ 0 & c\phi & -s\phi \\ 0 & s\phi / c\theta & c\phi / c\theta \end{bmatrix} \tag{3.9}$$

Note that $\sin\psi$ is represented as $s\psi$, $\cos\psi$ as $c\psi$, and $\tan\psi$ as $t\psi$.

3.4 Dynamics

3.4.1 Equations of Motion for Underwater Vehicle

The Equations of Motion (EOM) for an underwater vehicle with 6 DOF, with respect to the Body-fixed frame are derived in this section based on assumptions from section 3.1. These equations are useful for the simulation and the design of control system. The derivation of the EOM is resulted from the Newton's second law and expressed in the component form as (Fossen, 2011):

$$\begin{aligned}
&m\left[\dot{u} - vr + wq - x_G\left(q^2 + r^2\right) + y_G\left(pq - \dot{r}\right) + z_G\left(pr + \dot{q}\right)\right] = X \\
&m\left[\dot{v} - wp + ur - y_G\left(r^2 + p^2\right) + z_G\left(qr - \dot{p}\right) + x_G\left(qp + \dot{r}\right)\right] = Y \\
&m\left[\dot{w} - uq + vp - z_G\left(p^2 + q^2\right) + x_G\left(rp - \dot{q}\right) + y_G\left(rq + \dot{p}\right)\right] = Z \\
&I_x\dot{p} + \left(I_z - I_y\right)qr - \left(\dot{r} + pq\right)I_{xz} + \left(r^2 - q^2\right)I_{yz} + \left(pr - \dot{q}\right)I_{xy} \\
&\qquad + m\left[y_G\left(\dot{w} - uq + vp\right) - z_G\left(\dot{v} - wp + ur\right)\right] = K \\
&I_y\dot{q} + \left(I_x - I_z\right)rp - \left(\dot{p} + qr\right)I_{xy} + \left(p^2 - r^2\right)I_{zx} + \left(qp - \dot{r}\right)I_{yz} \\
&\qquad + m\left[z_G\left(\dot{u} - vr + wq\right) - x_G\left(\dot{w} - uq + vp\right)\right] = M \\
&I_z\dot{r} + \left(I_y - I_x\right)pq - \left(\dot{q} + rp\right)I_{yz} + \left(q^2 - p^2\right)I_{xy} + \left(rq - \dot{p}\right)I_{zx} \\
&\qquad + m\left[x_G\left(\dot{v} - wp + ur\right) - y_G\left(\dot{u} - vr + wq\right)\right] = N
\end{aligned} \tag{3.10}$$

The forces X, Y, Z acting on rigid body are defined in the Body-fixed frame, where X is the force acting along the $X-$axis, Y acts along the $Y-$axis, and Z acts along the $Z-$axis. The moments K, M, N acting on the body are defined similarly, where K is the moment acting about the $X-$axis in a right-hand fashion, M acts about the $Y-$axis, and N acts about the $Z-$axis.

In the matrix form, the equation of motion of an AUV can be rearranged and written as follows:

$$\boldsymbol{M}_{RB}\dot{\boldsymbol{\upsilon}} + \boldsymbol{C}_{RB}(\boldsymbol{\upsilon})\boldsymbol{\upsilon} = \boldsymbol{\tau}_{RB} \tag{3.11}$$

where $\boldsymbol{M}_{RB}$ is the rigid-body inertia matrix, and $\boldsymbol{C}_{RB}(\boldsymbol{\upsilon})\boldsymbol{\upsilon}$ represents the Coriolis and centripetal forces due to the vehicle's motion in a rotating reference frame, $\boldsymbol{\tau}_{RB}$ is the vector of external rigid body force.

Let the vehicle's inertia tensor $\boldsymbol{I}_0$ and the centre of gravity $\boldsymbol{r}_G$ be defined as

$$\boldsymbol{I}_0 = \begin{bmatrix} I_{xx} & -I_{xy} & -I_{xz} \\ -I_{yx} & I_{yy} & -I_{yz} \\ -I_{zx} & -I_{zy} & I_{zz} \end{bmatrix} \tag{3.12}$$

$$\boldsymbol{r}_G = \begin{bmatrix} x_G & y_G & z_G \end{bmatrix}^T \tag{3.13}$$

Then the rigid-body inertia matrix $\boldsymbol{M}_{RB}$ may be defined by $\boldsymbol{r}_G, \boldsymbol{I}_0,$ and vehicle m as

$$\boldsymbol{M}_{RB} = \begin{bmatrix} m\boldsymbol{I}_{3\times 3} & -m\boldsymbol{S}(\boldsymbol{r}_G) \\ m\boldsymbol{S}(\boldsymbol{r}_G) & \boldsymbol{I}_0 \end{bmatrix} = \begin{bmatrix} m & 0 & 0 & 0 & mz_G & -my_G \\ 0 & m & 0 & -mz_G & 0 & mx_G \\ 0 & 0 & m & my_G & -mx_G & 0 \\ 0 & -mz_G & my_G & I_x & -I_{xy} & -I_{xz} \\ mz_G & 0 & -mx_G & -I_{yx} & I_y & -I_{yz} \\ -my_G & mx_G & 0 & -I_{zx} & -I_{zy} & I_z \end{bmatrix} \tag{3.14}$$

The rigid body inertia matrix $\boldsymbol{M}_{RB}$ is constant, positive definite and symmetric.

The Coriolis and centripetal forces $\boldsymbol{C}_{RB}(\boldsymbol{\upsilon})\boldsymbol{\upsilon}$ are determined by the inertia matrix $\boldsymbol{M}_{RB}$ as a function of velocity $\boldsymbol{\upsilon}$. Let $\boldsymbol{M}$ be an arbitrary inertia matrix described as:

$$\boldsymbol{M} = \begin{bmatrix} \boldsymbol{M}_{11} & \boldsymbol{M}_{12} \\ \boldsymbol{M}_{21} & \boldsymbol{M}_{22} \end{bmatrix} \tag{3.15}$$

Then the Coriolis matrix $\boldsymbol{C}(\boldsymbol{v})$ is defined as:

$$\boldsymbol{C}_{RB}(\boldsymbol{v}) = \begin{bmatrix} \boldsymbol{0}_{3\times 3} & -\boldsymbol{S}(\boldsymbol{M}_{11}\boldsymbol{v} + \boldsymbol{M}_{12}\boldsymbol{w}) \\ -\boldsymbol{S}(\boldsymbol{M}_{11}\boldsymbol{v} + \boldsymbol{M}_{12}\boldsymbol{w}) & -\boldsymbol{S}(\boldsymbol{M}_{21}\boldsymbol{v} + \boldsymbol{M}_{22}\boldsymbol{w}) \end{bmatrix} \tag{3.16}$$

The Coriolis and Centripetal matrix $\boldsymbol{C}_{RB}$, is presented with an skew-symmetric form as:

$$\boldsymbol{C}_{RB}(\boldsymbol{\nu}) = \begin{bmatrix} 0 & 0 & 0 \\ 0 & 0 & 0 \\ 0 & 0 & 0 \\ -m(y_G q + z_G r) & m(y_G p + w) & m(z_G p - v) \\ m(x_G q - w) & -m(z_G r + x_G p) & m(z_G q + u) \\ m(x_G r + v) & m(y_G r - u) & -m(x_G p + y_G q) \end{bmatrix} \begin{bmatrix} m(y_G q + z_G r) & -m(x_G q - w) & -m(x_G r + v) \\ -m(y_G p + w) & m(z_G r + x_G p) & -m(y_G r - u) \\ -m(z_G p - v) & -m(z_G q + u) & m(x_G p + y_G q) \\ 0 & -I_{yz}q - I_{xz}p + I_z r & I_{yz}r + I_{xy}p - I_y q \\ I_{yz}q + I_{xz}p - I_z r & 0 & -I_{xz}r - I_{xy}q + I_x p \\ -I_{yz}r - I_{xy}p + I_y q & I_{xz}r + I_{xy}q - I_x p & 0 \end{bmatrix} \tag{3.17}$$

The next section discusses the vector of external rigid body force $\boldsymbol{\tau}_{RB}$.

3.4.2 External Rigid Body Force

The vector of external rigid body force $\boldsymbol{\tau}_{RB}$ consists of the hydrostatic force $\boldsymbol{\tau}_S$, hydrodynamic force $\boldsymbol{\tau}_H$, and propulsion force $\boldsymbol{\tau}_{prop}$. These external forces are described in the next sections.

$$\boldsymbol{\tau}_{RB} = \boldsymbol{\tau}_S + \boldsymbol{\tau}_H + \boldsymbol{\tau}_{prop} \tag{3.18}$$

3.4.2.1 Hydrostatic Force

The hydrostatic force includes the gravitational and buoyant forces, which act on the CG of the vehicle. The hydrostatic force is defined in the Body Fixed Coordinate as (Feldman, 1979):

$$\boldsymbol{\tau}_S = \begin{bmatrix} (W-B)\sin\theta \\ -(W-B)\cos\theta\sin\phi \\ -(W-B)\cos\theta\cos\phi \\ -(y_G W - y_B B)\cos\theta\cos\phi + (z_G W - z_B B)\cos\theta\sin\phi \\ (z_G W - z_B B)\sin\theta + (x_G W - z_B B)\cos\theta\cos\phi \\ -(x_G W - x_B B)\cos\theta\sin\phi - (y_G W - y_B B)\sin\theta \end{bmatrix} \tag{3.19}$$

where $W = mg$ is the submerged weight of the AUV, $B = \rho\nabla g$ is the buoyancy, ρ is the fluid density, ∇ is the volume of the AUV hull, (x_B, y_B, z_B) and (x_G, y_G, z_G) are the centre of gravity and centre of buoyancy respectively.

3.4.2.2 Hydrodynamic Forces

The hydrodynamic forces $\boldsymbol{\tau}_H$ are due to pressure exerted on the body by the surrounding fluid as the vehicle moves and accelerates through the fluid. The hydrodynamic force is decomposed into terms including added mass, added Coriolis-centripetal and hydrodynamic damping as follows:

$$\boldsymbol{\tau}_H = -\left[\boldsymbol{M}_A\dot{\boldsymbol{\upsilon}} + \boldsymbol{C}_A(\boldsymbol{\upsilon})\boldsymbol{\upsilon} + \boldsymbol{D}(\boldsymbol{\upsilon})\boldsymbol{\upsilon}\right] \tag{3.20}$$

The added mass and hydrodynamic damping forces are a function of the density of water, the geometric shape of the vehicle - which is assumed to be a prolate ellipsoid and the vehicle's velocity (Fossen, 2011).

Added mass

The accelerated fluid flow around the moving vehicle generates the component, which accounts for the inertia of the surrounding fluid, termed added mass. The fluid surrounding the vehicle body is accelerated with the body itself, a force is necessary to achieve this acceleration; the fluid exerts a reaction force, which is equal in magnitude and opposite in direction. This reaction force is the added mass contribution (Antonelli, 2013). Added mass effects are modelled as a function of acceleration. The added matrix of inertia is defined as:

$$\boldsymbol{M}_A = \begin{bmatrix} X_{\dot{u}} & X_{\dot{v}} & X_{\dot{w}} & X_{\dot{p}} & X_{\dot{q}} & X_{\dot{r}} \\ Y_{\dot{u}} & Y_{\dot{v}} & Y_{\dot{w}} & Y_{\dot{p}} & Y_{\dot{q}} & Y_{\dot{r}} \\ Z_{\dot{u}} & Z_{\dot{v}} & Z_{\dot{w}} & Z_{\dot{p}} & Z_{\dot{q}} & Z_{\dot{r}} \\ K_{\dot{u}} & K_{\dot{v}} & K_{\dot{w}} & K_{\dot{p}} & K_{\dot{q}} & K_{\dot{r}} \\ M_{\dot{u}} & M_{\dot{v}} & M_{\dot{w}} & M_{\dot{p}} & M_{\dot{q}} & M_{\dot{r}} \\ N_{\dot{u}} & N_{\dot{v}} & N_{\dot{w}} & N_{\dot{p}} & N_{\dot{q}} & N_{\dot{r}} \end{bmatrix} \tag{3.21}$$

The matrix is determined by vehicle external geometry. Each term represents the force generated in a given direction by an acceleration in a given direction. For example, the force Z_A along the $Z-$axis due to an acceleration $\dot{u}$ along the $X-$axis is expressed $Z_A = Z_{\dot{u}}\dot{u}$.

In this study, it is assumed that the vehicle has three planes of symmetry and fully submerged in the water. For a three plane of symmetry AUV, the contribution of the non-diagonal components of the added mass matrix could be neglected. Consequently, only the diagonal components are taken into account and the added mass matrix is presented as:

$$\boldsymbol{M}_A = -diag\left\{X_{\dot{u}}, Y_{\dot{v}}, Z_{\dot{w}}, K_{\dot{p}}, M_{\dot{q}}, N_{\dot{r}}\right\} \tag{3.22}$$

The added mass coefficients are analytically approximated by using the slender body theory or strip theory based on the geometry of the rigid body and its symmetry. A detailed discussion on the added mass for the marine vehicles is can be found in (Korotkin, 2008).

Coriolis-centripetal forces from added mass

The Coriolis and centripetal matrix due to the added mass can be written in simplified form as:

$$\boldsymbol{C}_A(\boldsymbol{v}) = \begin{bmatrix} 0 & 0 & 0 & 0 & -Z_{\dot{w}}w & Y_{\dot{v}}v \\ 0 & 0 & 0 & Z_{\dot{w}}w & 0 & -X_{\dot{u}}u \\ 0 & 0 & 0 & -Y_{\dot{v}}v & X_{\dot{u}}u & 0 \\ 0 & -Z_{\dot{w}}w & Y_{\dot{v}}v & 0 & -N_{\dot{r}}r & M_{\dot{q}}q \\ Z_{\dot{w}}w & 0 & -X_{\dot{u}}u & N_{\dot{r}}r & 0 & -K_{\dot{p}}p \\ -Y_{\dot{v}}v & X_{\dot{u}}u & 0 & -M_{\dot{q}}q & K_{\dot{p}}p & 0 \end{bmatrix} \tag{3.23}$$

Hydrodynamic damping forces and moments

The hydrodynamic forces and moments have a dominant effect in the vehicle motion. The hydrodynamic damping terms may be grouped into linear and quadratic terms as a common simplification as follows:

$$\boldsymbol{D}(\boldsymbol{v}) = \boldsymbol{D}_l + \boldsymbol{D}_q(\boldsymbol{v}) \tag{3.24}$$

where

$$\boldsymbol{D}_l = -\begin{bmatrix} X_u & 0 & 0 & 0 & 0 & 0 \\ 0 & Y_v & 0 & Y_p & 0 & Y_r \\ 0 & 0 & Z_w & 0 & Z_q & 0 \\ 0 & K_v & 0 & K_p & 0 & K_r \\ 0 & 0 & M_w & 0 & M_q & 0 \\ 0 & N_v & 0 & N_p & 0 & N_r \end{bmatrix} \tag{3.25}$$

$$\boldsymbol{D}_q(\boldsymbol{v}) = \begin{bmatrix} X_{|u|u}|u| & 0 & 0 & 0 & 0 & 0 \\ 0 & Y_{|v|v}|v| & 0 & Y_{|p|p}|p| & 0 & Y_{|r|r}|r| \\ 0 & 0 & Z_{|w|w}|w| & 0 & Z_{|q|q}|q| & 0 \\ 0 & K_{|v|v}|v| & 0 & K_{|p|p}|p| & 0 & K_{|r|r}|r| \\ 0 & 0 & M_{|w|w}|w| & 0 & M_{|q|q}|q| & 0 \\ 0 & N_{|v|v}|v| & 0 & 0 & 0 & N_{|r|r}|r| \end{bmatrix} \tag{3.26}$$

The quadratic damping terms dominate as an underwater vehicle operating in an unbounded fluid. For the low velocities, the quadratic terms may be considered negligible (Fossen, 2011). The hydrodynamic damping coefficients are considered constant for the vehicle utilised in this study. In order to simply the model, it is assumed that the angular coupled terms are neglected since their values are relatively small. The detailed estimation of these coefficients is beyond the scope of this work.

3.4.2.3 Control Surfaces Forces

A torpedo shaped underwater vehicle is usually equipped with two different control surface arrangements, namely the cruciform configuration and the X-form configuration. Figure 3.3 shows the two control surface configurations viewed from astern, the cruciform in the left and the X-form in the right. In the cruciform configuration, the vertical rudders and horizontal elevators are controlled independently. On the other hand, for the X-form configuration, all four rudders rotate simultaneously to perform a specific manoeuvre.

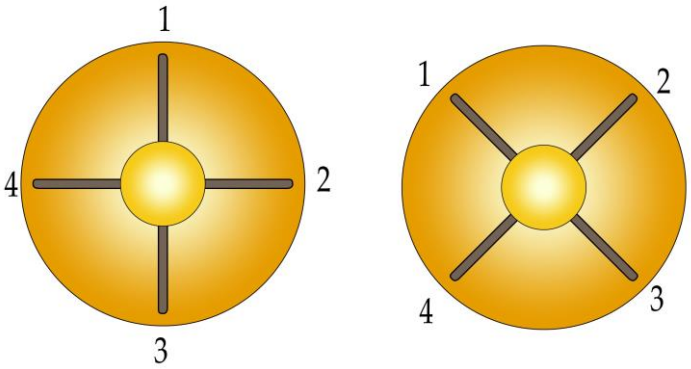

Figure 3.3. Two types of the control surface configuration.

In case of the X –form configuration, the effective (movable) area is greater with respect to the cruciform configuration (all 4 rudders are deflected) and, consequently, a larger manoeuvring (destabilizing) lateral force is exerted to the submarine (Dubbioso et al., 2017). The X-form configuration shares most of the properties of the cruciform configuration, but it has mixed control surface control providing maximum moment in pitch, and yaw manoeuvres.

The Gavia AUV is propelled and manoeuvred with a three-bladed propeller and four independent control surfaces in X-form configuration located aft of the propeller as shown in Figure 3.4. The control surfaces can be commanded separately by independent servomotors and are em-

ployed simultaneously to generate accurate and fast moments. The whole unit is protected inside a Nautican type nozzle. This propulsion configuration is unique to Teledyne Gavia that provides high efficiency in both low-speed and high-speed manoeuvers.

Figure 3.4. Gavia Propulsion system.

Assuming that the cross-configuration has a mounting of 45 degrees from the AUV vertical line, the hydroplane force for one blade for each configuration will be:

$$F_{\delta y}^{*} = \frac{F_{\delta y}}{\sqrt{2}} \tag{3.27}$$

where $F_{\delta y}$ is the force of one blade in the cruciform configuration.

The forces and moments created by the actuators are directly proportional to the angle of deflection and to the square of the AUV forward speed. Forces and moments due to control surface deflection can be approximated by a second order polynomial function if the deflection angle is small enough that the flow over the control surface does not stall.

3.4.3 Determination of the Hydrodynamic Coefficients

A Gavia class modular, torpedo-shaped AUV was used as the platform this study. The vehicle in its tested configuration consisted of a Nose Cone Module, Battery Module, Acoustic Doppler Current Profiler module, Inertial Navigation System module, Control Module and a Propulsion module. There are some transducers equipped with AUV such as the obstacle avoidance sonar,

acoustic modem transducer, and side scan sonar. The overall length of the vehicle was 2.7 m and a maximum hull diameter of 0.2 m and the dry weight in air was approximately 70 kg.

Techniques for estimating the hydrodynamic coefficients of fully submerged vehicles can be traced back to the tools originally developed to predict the aerodynamic coefficients of airships and subsequently adopted for submarines (De Barros et al., 2008). There are generally four main approaches to estimate the hydrodynamic coefficients of an underwater vehicle, including the CFD method, analytical method, experimental approach using model test in towing tank, and the system identification (SI) approach using real system test. In this thesis, the analytical method and the SI approach are utilised. The analytical method is applied to estimate the coefficients in the non-linear model used for the simulation study. The SI approach is employed for the control design that is discussed thoroughly in chapter 7.

The nonlinear hydrodynamic coefficients in this chapter are estimated using the Prestero approach and Fossen model as illustrated in (Prestero, 2001b) and (Fossen, 2011).

The added mass in the x-axis is derived by approximating the hull of the vehicle by an ellipsoid with a minor axis is haft of the vehicle diameter and a major axis is haft of the vehicle length (Blevins, 1979):

$$X_{\dot{u}} = -\frac{4\chi\rho\pi}{3}\frac{l}{2}r^2 \tag{3.28}$$

where χ is empirically determined by the ratio of the vehicle to the diameter.

For the calculation of crossflow and roll added mass, the strip theory is applied. In the strip theory, the crossflow and roll added mass is approximated as a sum of slices along the body. These added mass coefficients are calculated using integrals along the x-axis as shown in the following equations:

$$Y_{\dot{v}} = Z_{\dot{w}} = -\int_x m_a(x)dx \tag{3.29}$$

$$M_{\dot{w}} = -N_{\dot{v}} = -Y_{\dot{r}} = Z_{\dot{q}} = -\int_x x m_a(x)dx \tag{3.30}$$

$$M_{\dot{q}} = -N_{\dot{r}} = -\int_x x^2 m_a(x)dx \tag{3.31}$$

$$K_{\dot{p}} = -\int_{x_f} \frac{2}{\pi}\rho a^4 dx \tag{3.32}$$

where m_a represents the added mass per length unit and is defined as:

$$m_a(x) = \begin{cases} \pi\rho R(x)^2 \text{ for cylinder} \\ \pi\rho\left(a_f^2 - R(x)^2 + \frac{R(x)^4}{a_f^2}\right) \text{ for the cylinder with fin} \end{cases} \tag{3.33}$$

a is the length of fin taken from the central axis

x_f is the sector along the x-axis where the fins are located.

The nonlinear axial drag coefficients is calculated as

$$X_{u|u|} = -\frac{1}{2}\rho C_D A_f \tag{3.34}$$

where C_D is an empiric coefficient.

A_f is the vehicle frontal area.

The nonlinear crossflow drag is considered to the summation of the vehicle hull and fin cross-flow drag. It is calculated due to the symmetry of vehicle using integrals from the strip theory as:

$$Y_{v|v|} = Z_{w|w|} = -\gamma \int_x 2R(x)dx - 2\upsilon \tag{3.35}$$

$$M_{w|w|} = -N_{v|v|} = -\gamma \int_x 2xR(x)dx - 2x_{fin}\upsilon \tag{3.36}$$

$$Y_{r|r|} = -Z_{q|q|} = -\gamma \int_x 2x|x|R(x)dx - 2x_{fin}|x_{fin}|\upsilon \tag{3.37}$$

$$M_{q|q|} = N_{r|r|} = -\gamma \int_x 2x^3|x|R(x)dx - 2x^3{}_{fin}\upsilon \tag{3.38}$$

where $\gamma = \frac{1}{2}\rho c_{dc}$

$\upsilon = \frac{1}{2}\rho S_{fin} c_{df}$

c_{dc} is the crossflow drag coefficient of a cylinder.

c_{df} is the damping crossflow coefficient.

The crossflow drag coefficient c_{dc} is estimated taking the empirical values.

The damping crossflow coefficient c_{df} can be expressed using the following equations:

$$c_{df} = 0.1 + 0.7t \tag{3.39}$$

where t is the ration of the widths of the top and bottom of the fin along the vehicle x-axis.

The developed coefficients were non-dimensionalised with the length of the vehicle. A number of studies on the hydrodynamic coefficient estimation of Gavia AUV have been conducted in the literature. The hydrodynamic coefficients are verified by comparing with similar works reported in the literature (Porgilsson, 2006) (Helgason, 2012) and with the data provided by the manufacturers.

3.5 Summary

A complete mathematical model for an autonomous underwater vehicle was discussed in chapter 3. This chapter covered the system of equations used for the experiments and simulations described in subsequent chapters. The modelling of an AUV involved the development of both kinematic and dynamic model. The analytical and theoretical method to estimate the hydrodynamic coefficients were briefly presented. The hydrodynamic coefficients were then incorporated into the equations of motion to obtain the complete mathematical model of an AUV.

CHAPTER 4

Experimental Study of the Conventional Fixed Pitch Propeller

This chapter presents the open water propeller characteristics and the four-quadrant propeller models as applied to a torpedo shaped underwater vehicle. A series of experiments with a Gavia AUV propeller were conducted in the towing tank using a rotor testing apparatus. The purpose of these tests was to measure the propeller thrust and torque under varying flow conditions to then be used as the basis of the developed propeller models. These mathematical models were constructed using two regression models, a polynomial and a Fourier series. Model coefficients were derived using the method of least squares and a comparison analysis was also conducted to test the robustness of the methodology. Results show that the Fourier series models are able to produce a reasonable and accurate approximation of thrust and torque coefficients with a small number of parameters in the examined condition of this study. The obtained four-quadrant open water characteristics of the AUV propeller model were utilised to improve the system mathematical model for more accurate simulation and controller design, to compare the AUV performance equipped with CCPP propulsion system.

Part of this chapter has been published in the "*Proceedings of the Institution of Mechanical Engineers, Part M: Journal of Engineering for the Maritime Environment*". The citation for the journal paper is:

Tran M, Binns J, Chai S, et al. (2017). A practical approach to the dynamic modelling of an underwater vehicle propeller in all four quadrants of operation. *Proceedings of the Institution of Mechanical Engineers, Part M: Journal of Engineering for the Maritime Environment*.

4.1 Introduction

There have been significant attempts to determine the performance of marine propellers in the literature by applying analytical approximations, experimental fluid dynamics (EFD), and computational fluid dynamics (CFD). A simplified model operating in the first quadrant is commonly utilised and, in several cases, the detailed modelling in all the four quadrants of operation is necessary. For ships and vessels in conventional operation, obtaining accurate thrust and torque values for positive shaft speed and advance speed are commonly investigated and modelled (Carlton, 2012). For underwater vehicles such as AUVs, it is important to model propeller thrust and torque in all four quadrants since the four-quadrant propeller model is able to cover a full range of operation which include a complete representation of propeller thrust and torque for both directions of propeller and fluid velocity (Brown, 1993). By applying the four-quadrant propeller model in the vehicle simulation and control model, the performance prediction in the conditions such as braking, stopping and running astern would be obtainable. Another important advantage of the four-quadrant model is that it provides a continuous function to estimate the thrust and torque applied in the simulation and control design. The four quadrants of operation are defined and summarised in Table 4.1 with the (+) and (−) signs represented for the positive and negative direction accordingly.

Table 4.1. Definition of four quadrants

Quadrant	Vehicle Speed V_A	Propeller Speed n	Advance angle β
1^{st}	+	+	$0^\circ - 90^\circ$
2^{nd}	+	−	$90^\circ - 180^\circ$
3^{rd}	−	−	$180^\circ - 270^\circ$
4^{th}	−	+	$270^\circ - 360^\circ$

Some of early studies on four-quadrant models have been discussed for the well-known Wageningen propeller B-series (Van Lammeren et al., 1969; Kuiper, 1992; Oosurveld and Van Oossanen, 1975; Oosterveld, 1970) and recently for the C and D-series (Dang et al., 2012) developed by the Maritime Research Institute Netherlands. These fixed pitch propeller (FPP) and controllable pitch propeller (CPP) series comprise the propeller characteristics primarily designed for the merchant ships (Dang et al., 2012). The four-quadrant mathematical models of the propeller derived from the Wageningen B-series were implemented in the ship manoeuvring simulation systems in (Sutulo et al., 2002; Khaled and Chalhoub, 2011; Tannuri et al., 2014; Woodward et al., 2005; Delefortrie and Vantorre, 2009). The method to experimentally determine the four-quadrant model for marine thruster employ thin aerofoil theory and experimental data (Bachmayer et al., 2000). However, the proposed model was intentionally applied for the low-speed and hovering manoeuvrability of an underwater vehicle since it was derived with the assumption of zero advance velocity, the "Bollard-pull" condition. This was taken further to a nonlinear model for the axial flow velocity through the propeller blade and included a propeller model to reproduce the thrust over the four-quadrant range (Pivano et al., 2006). The feed forward neural networks (FFNN) was utilised to train a neural network using the data obtained from previous four-quadrant tests of the Wageningen propeller B-series (Roddy et al., 2007). This method provides a means for estimating the four-quadrant model of the propellers in the series for which the measured data is not available.

Although there is a wealth of information on the propeller modelling, the published data in the literature did not provide sufficient information to reproduce the propeller performance characteristics in four quadrants, especially for the investigation of underwater vehicle manoeuvrability. The available data is exclusively applied to ship and vessel propeller in the first quadrant. In addition, the approach to derive the approximation functions representing the experimental results for the four quadrant measurements have not been thoroughly examined.

This chapter presents an experimental study on the propeller of the Gavia AUV, a vehicle manufactured by Hafmynd ehf and currently in service at the Australian Maritime College. Results are presented from two different regression models, polynomial and Fourier series, to describe experimental data for a four-quadrant propeller model. The model coefficients of these two models are derived by using the curve fitting technique - Least Squares method.

4.2 Propeller Dynamic Modelling

Modelling the thrust and torque produced by a propeller is a complicated task, since it is difficult to develop a finite-dimensional analytical model from the laws of physics (Pivano et al., 2009). A combination of simplified analytical and empirical models is therefore the commonly utilised since it is reliable and computational efficient. This approach utilises the analysed experimental data combined with the empirical equations to estimate the fundamental propeller characteristics. From the simulation and control point of view, the models are required to be identified accurately to capture the primary hydrodynamic performance. If the models were too complicated, the controller designed would be of high order with weak robustness and low reliability. As a result, the system would experience unstable conditions. The relevant practical method is the estimation of thrust and torque using the empirical equations that relate the non-dimensional coefficients. In this chapter, the fully submerged underwater vehicle propeller is considered so that the unsteady flow effects such as air suction, cavitation, Wagner's effect, and Kuessner effect can be neglected (Fossen and Blanke, 2000). The following models are therefore presented based on quasi-steady thrust and torque modelling.

4.2.1 The Propeller Open Water Characteristics Curves

The propeller open water characteristics curves refer to the first quadrant performance of the four-quadrant operation in uniform flow conditions. The results of open water tests of propeller

are presented in the form of non-dimensional coefficients of speed, thrust and torque. The advance ratio J, the thrust coefficient K_T and the torque coefficient K_Q are defined as:

$$J = \frac{V_A}{nD} \tag{4.1}$$

$$K_T = \frac{T}{\rho n^2 D^4} \tag{4.2}$$

$$K_Q = \frac{Q}{\rho n^2 D^5} \tag{4.3}$$

where the propeller thrust T and torque Q are characterized by the dimensionless open water coefficients $K_T(J)$ and $K_Q(J)$, respectively, where J is the advance ratio and n (RPS) is the propeller rotational speed, D (m) is the propeller diameter, V_A (m/s) is the vehicle advance speed, and ρ (kg/m^3) is the water density.

The values of the non-dimensional thrust coefficient K_T and torque coefficient K_Q calculated from experimental data are approximated with sufficient accuracy using nonlinear polynomial regression analysis. They are defined as the function of advance ratio J in the form:

$$K_T(J) = \sum_{x=0}^{k} m_x J^x \tag{4.4}$$

$$K_Q(J) = \sum_{x=0}^{k} n_x J^x \tag{4.5}$$

where the polynomial coefficients m_x and n_x are determined by using the least-squares curve fitting technique.

The K_T and K_Q versus J characteristic curves contain all of the information necessary to define the propeller performance at a particular design operating condition (Carlton, 2012). For the testing of a propeller series, the Wageningen B-series for example, the results of K_T and K_Q

values could be presented systematically as the polynomial functions of J and other propeller geometric parameters such as the number of blades (Z), the pitch to diameter ratio (P/D), blade area ratio (A_E/A_O) and Reynolds number R_n (Carlton, 2012; Van Lammeren et al., 1969; Oosurveld and Van Oossanen, 1975; Kuiper, 1992):

$$K_T = f(J, Z, P/D, A_E/A_O, R_n) \tag{4.6}$$

$$K_Q = g(J, Z, P/D, A_E/A_O, R_n) \tag{4.7}$$

The open water efficiency is defined as the ratio of the thrust horsepower to delivered horsepower (Carlton, 2012):

$$\eta_O = \frac{\text{THP}}{\text{DHP}} = \frac{TV_a}{2\pi nQ} = \frac{K_T}{K_Q}\frac{J}{2\pi} \tag{4.8}$$

The models based on these coefficients are only applicable in the regime of non-zero propeller velocities, where the rotational direction must be the one that drives the vehicle forward. This is the conventional way of operating a propeller, but for studying manoeuvring situations or astern performance of vehicle other data is required (Carlton, 2012). A zero-crossing of the propeller speed in such conditions would make the advance ratio go to infinity.

4.2.2 The Propeller Four-quadrant Mathematical Model

Despite being available for decades, four-quadrant propeller models are not widely used in the marine simulation and control study. In the case of the fixed pitch propeller it is possible to define four-quadrant propeller characteristics model which is based on the advance angle β of the propeller blade at radius $0.7R$:

$$\beta = \arctan\left(\frac{V_A}{0.7\pi nD}\right) = \arctan\left(\frac{J}{0.7\pi}\right) = \arctan\left(\frac{V_A}{0.7\omega R}\right) \tag{4.9}$$

where $R = \frac{D}{2}$ is the propeller radius, and $\omega = 2\pi n$ is the propeller angular velocity.

For multi-quadrant studies, the advance angle notation β offers a considerably more flexible representation than the conventional advance coefficient J, for example when propeller speed approaches zero, the advance coefficient J_0, thrust and torque coefficients K_T and K_Q all approach infinity and have a discontinuity. This formulation has many advantages over the open-water characteristics, since it is based on a physical foundation: it is valid for any shaft speed and inflow, and covers all four quadrants of operation.

4.2.3 Four-quadrant Model Representations

Provided sufficient experimental data is available it becomes possible to define the thrust and torque characteristics of the propeller in each quadrant (Carlton, 2012). To determine the performance characteristics at other quadrants other than the first quadrant the open water diagrams has to be expanded. The four-quadrant propeller characteristic is usually presented using the non-dimensional thrust and torque coefficients C_T and C_Q as functions of β. C_T and C_Q are computed as follows (Carlton, 2012; Kuiper, 1992):

$$C_T = \frac{T}{\frac{1}{2}\rho\left[V_A^2 + \left(0.7\omega R\right)^2\right]\frac{\pi}{4}D^2} = \frac{8K_T}{\pi\left(J^2 + \left(0.7\pi\right)^2\right)} \tag{4.10}$$

$$C_Q = \frac{Q}{\frac{1}{2}\rho\left[V_A^2 + \left(0.7\omega R\right)^2\right]\frac{\pi}{4}D^3} = \frac{8K_Q}{\pi\left(J^2 + \left(0.7\pi\right)^2\right)} \tag{4.11}$$

The propeller characteristic curves are periodic over the range $0 \le \beta \le 360^0$ and can be determined by experiment and smoothly interpolated in four quadrants by using the nonlinear polynomial and the Fourier series approximation.

$$C_T(\beta) = \sum_{x=0}^{k} m_x \beta^x \tag{4.12}$$

$$C_Q(\beta) = \sum_{x=0}^{k} n_x \beta^x \tag{4.13}$$

$$C_T(\beta) = m_0 + \sum_{k=0}^{i} \left[m_k \cos\left(k\omega\beta\right) + n_k \sin\left(k\omega\beta\right) \right] \tag{4.14}$$

$$C_Q(\beta) = m_0 + \sum_{k=0}^{i} \left[m_k \cos\left(k\omega\beta\right) + n_k \sin\left(k\omega\beta\right) \right] \tag{4.15}$$

where ω is the frequency of the signal,

i is the number of terms,

m_x, m_k, n_x, n_k are the function coefficients determined by applying the method of LS.

Similar to the coefficient representation in the first quadrant, the non-dimensional coefficients of a propeller series cover four quadrants operation could be expressed systematically as the functions of a range of number of blades (Z), the pitch to diameter ratio (P/D), blade area ratio (A_E/A_O) and Reynolds number R_n.

$$C_T = f(\beta, Z, P/D, A_E/A_O, R_n) \tag{4.16}$$

$$C_Q = g(\beta, Z, P/D, A_E/A_O, R_n) \tag{4.17}$$

For an effective computation in the simulator, a simplified four-quadrant model is obtained by utilising fewer terms associated with sines and cosines functions in the expansion of C_T and C_Q. In (Smogeli, 2006), the authors derived the model by applying only the first terms:

$$C_T(\beta) = m_{T0} + m_{T1}\cos\beta + n_{T1}\sin\beta \tag{4.18}$$

$$C_Q(\beta) = m_{Q0} + m_{Q1}\cos\beta + n_{Q1}\sin\beta \tag{4.19}$$

4.2.4 The Least Squares Fitting Method

The curve fitting techniques or regression methods use the provided series of experimental data to estimate the coefficients of an empirical parametric model. The coefficients are estimated by applying the least squares method, which minimises the sum square of residual ε or the difference between the measured data and the fitted data.

Let y denote the empirical function to be determined and can be written in the form of equation (4.20):

$$y = f(x, \theta) \tag{4.20}$$

where x is the input data and θ is the vector of model coefficients.

The measured data y_i^* of y_i in the experiment is defined as:

$$y_i^* = y_i + \varepsilon_i \tag{4.21}$$

where ε_i is the estimation error.

The identification of coefficient θ is equivalent to the minimization of a scalar cost function

$$J(\theta) = \frac{1}{2}\sum \varepsilon_i^2 = \frac{1}{2}\sum (y_i^* - f(x_i, \theta)) \tag{4.22}$$

Solving equation $\frac{\partial J}{\partial \theta} = 0$ for the unknown parameter θ gives the estimation of θ. The comprehensive solutions to this equation are described in relevant reference (Van Der Heijden et al., 2005; Klein and Morelli, 2006).

In this study, the polynomial functions and the Fourier series expressed in equations (4.12-4.15) are the empirical functions to be examined for representing the experimental data.

4.3 Experimental Study

The objectives of the tests were to derive a set of Gavia AUV propeller thrust and torque data under the four-quadrant conditions. A three-bladed Gavia AUV FPP, as shown in Figure 4.1, was selected for the tests. This propeller is made from aluminium alloy and particularly designed for the torpedo shaped underwater vehicle. An adapter was specifically designed and manufactured to fit the propeller into the driving shaft of the testing apparatus as shown in Figure 4.2. The fundamental specifications of the tested Gavia propeller are also listed in Table 4.2 below.

Figure 4.1. Gavia AUV propeller.

Figure 4.2. Propeller attached into an adaptor.

Table 4.2. Fundamental specifications of tested propeller.

Symbol	Description	Value	Unit
	Scale	1:1	
Z	Number of blades	3	
D	Diameter	0.143	m
P/D	Pitch ratio	1.7	
A_E / A_O	Blade area ratio	0.4	
A_O	Disk area	0.0161	m^2

4.3.1 Open Water Test Setup

The open water tests are usually performed in the towing tank. The experiments in this study were conducted in the towing tank at AMC as shown in Figure 4.3. The primary dimensions of the AMC towing tank are listed in Table 4.3.

Table 4.3. Towing tank dimensions.

Length	Width	Depth	Maximum speed
100 m	3.55 m	0 to 1.5 m	0 to 4.6 m/s

Figure 4.3. The towing tank at AMC-UTAS.

The key equipment for the open water tests was the propeller open water dynamometer, shown in Figure 4.4. Further details of the propeller open water dynamometer can be found in (Liu et al., 2015; Liu et al., 2014), which was designed and built during the that project.

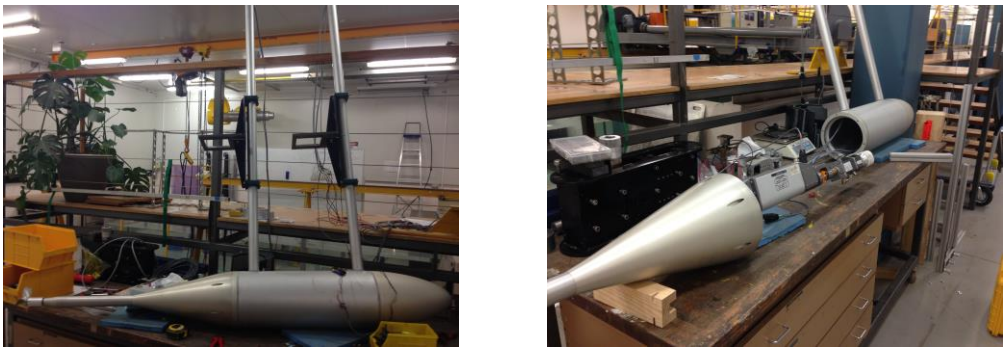

Figure 4.4. Propeller Open Water Dynamometer.

The thrust and torque of propeller were measured by a Cussons Propulsion Dynamometer R31. This R31 dynamometer was mounted in line with the shaft of the propeller, and the dynamometer static calibration was carried out before the test. The driving motor was the Dunkermotoren BG 75 attached behind the dynamometer. An encoder was used to measure propeller rotational speed (RPM) and the motor speed was controlled from the computer on the carriage by the encoder feedback signal. Both the dynamometer and the driven motor were located inside the Propeller Open Water Dynamometer as shown in Figure 4.5.

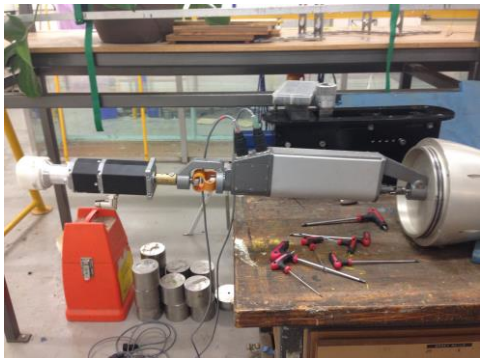

Figure 4.5. Internal assembly of Propeller Open Water Dynamometer.

4.3.2 Data Acquisition and Post Processing

The measured data were acquired with the National Instruments BNC-2090 acquisition system and a LabVIEW software program was developed to ensure accurate data acquisition. The in-house developed program was able to control the propeller rotational speed at desired constant values and acquire the measured data via different channels. A sampling rate of 1000 Hz was selected with sampling time was 20s for the acquired signals. The low pass Kalman filter was also applied in order to reduce the high frequency noise of collected raw data. A schematic diagram and a photo of the experimental setup and data acquisition system are given in Figure 4.6.

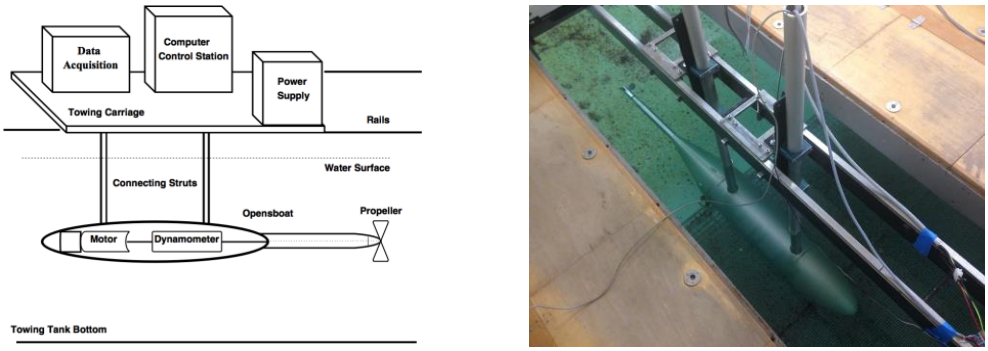

Figure 4.6. The experimental setup of Propeller Open Water Test.

The four-quadrant tests were conducted by varying the carriage speed and direction, the propeller rotational speed and the direction of rotating propeller. The experiments were run at a

wide range of advance ratio, especially at off design conditions on both ends of the range in order to evaluate the performance characteristics of the AUV equipped with this propeller during manoeuvring. In a conventional open water propeller test, for each quadrant condition, the propeller rotational speed is kept constant while the advance speed of the propeller varies, as recommended by procedures and guidelines of the International Towing Tank Conference (ITTC) (ITTC, 2008a). The carriage speed was set at different constant speed in the range from 0.5 m/s to 3 m/s during these tests. The tests with negative advance speed were conducted with reversely mounted propeller without changing motion direction of the carriage to avoid effect of the submerged testing apparatus on the propeller. From equation (4.9), the relationship between β and J over the four quadrants is intensively described in Table 4.4 below:

Table 4.4. The relationship between β and J in the four quadrants.

	First quadrant				**Second quadrant**			
β	0°	26°	69°	90°	95°	112°	146°	180°
J	0	1.1	5.7	∞	-28	-5.5	-1.5	0
	Third quadrant				**Forth quadrant**			
β	190°	206°	241°	270°	275°	300°	327°	360°
J	0.4	1.1	3.9	∞	-25	-3.7	-1.5	0

It can be seen from Table 4.4 that to cover the full range of β in each quadrant, the advance ratio J had to be adjusted progressively from 0 to very high values in the tests. This procedure was difficult to manage in practice due to the physical limitations of the facility. In addition, the high values of J refer to the off-design conditions in which the underwater vehicles would not manoeuvre in practical application as they are not realistic. Therefore in the presented tests, within

the capability of models and instrumentations, the advance ratio J was controlled up to 1.5 in the first and third quadrant and to -1.5 in the second and forth quadrant. It should be noted that when $\beta = 0^{\circ}$ and $\beta = 360^{\circ}$, or $J = 0$ the model was at the bollard pull conditions. Moreover, for the condition when $\beta = 90^{\circ}$ and $\beta = 270^{0}$ the propeller was stationary and the loads were obtained by dragging the propeller through the water without rotating in both forward and backward directions. The measured data at these cases are important in the estimation of the curve fitting functions.

4.3 Results and Discussions

4.3.1 Open Water Performance Results

The first quadrant performance or the open water characteristic curve of the Gavia AUV propeller is presented in this section. The propeller model in the first quadrant is initially discussed since it is the most important phase in which the underwater vehicles are primarily designed to operate.

The collected raw data was processed and characterised in the regression analysis. For most propellers, the open water characteristic curves can be approximated with sufficient accuracy by a second-degree polynomial:

$$K_T(J) = -0.1436J^2 - 0.1633J + 0.2860 \tag{4.23}$$

$$10K_Q(J) = -0.3095J^2 - 0.0572J + 0.4004 \tag{4.24}$$

The presented curves are drawn based on the second order polynomials and is given in Figure 4.7. In this diagram, the non-dimensional open water thrust coefficient K_T, torque coefficient K_Q and the efficiency η_0 are plotted against the advance ratio J.

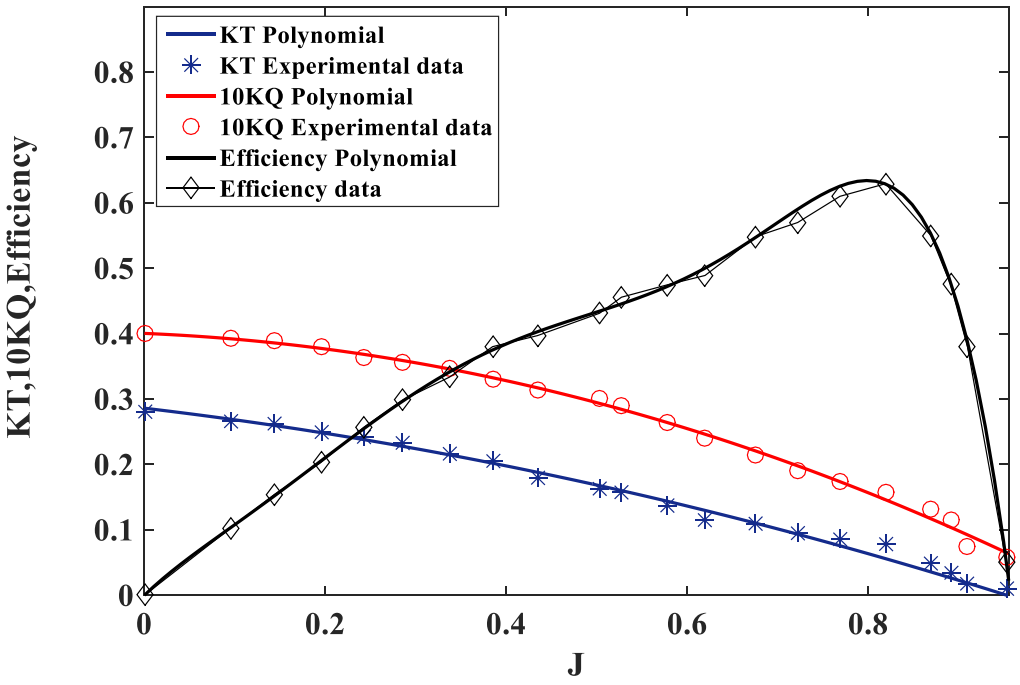

Figure 4.7. Gavia AUV propeller open water diagram.

The largest values of K_T and $10K_Q$ are 0.28 and 0.4, respectively at $J=0$, the condition in which the propeller is rotating without translating. The maximum efficiency is 62% at $J=0.8$. Some minor oscillations occur at the high J value due to the system mechanical vibration. The experimental measurements were filtered and analysed based on the mechanical vibration frequency measured by a separated accelerometer attached on the system.

4.3.1 Four-quadrant Models Results

4.3.1.1 Polynomial Regression Models

The thrust coefficient C_T and torque coefficient C_Q for the Gavia AUV propeller in the range of advance angle β from 0° to 360° are described by the nonlinear polynomial regression models with the degree from 2 to 9 as shown in Figure 4.8 and Figure 4.9.

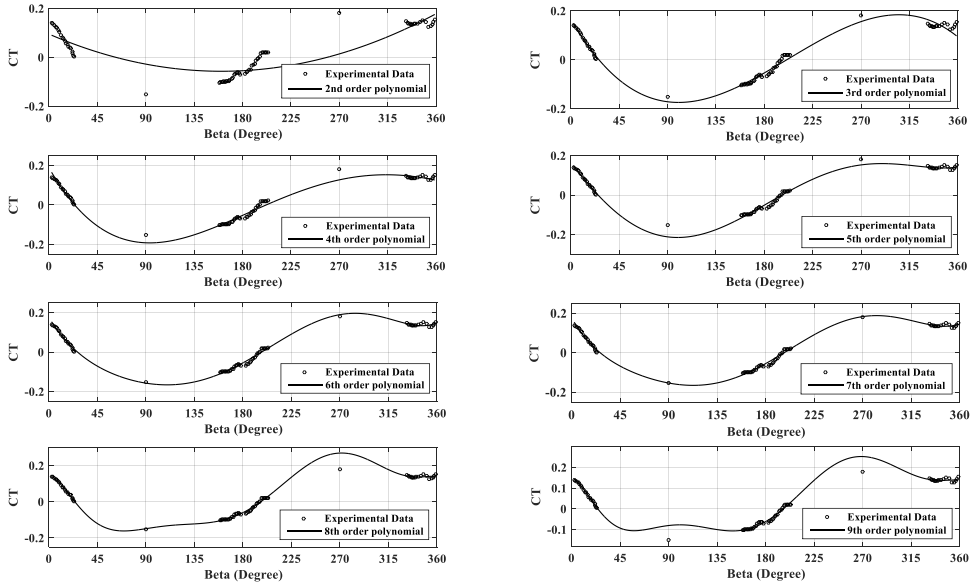

Figure 4.8. Comparison of different polynomial regression models with measured experimental data for torque coefficient C_T.

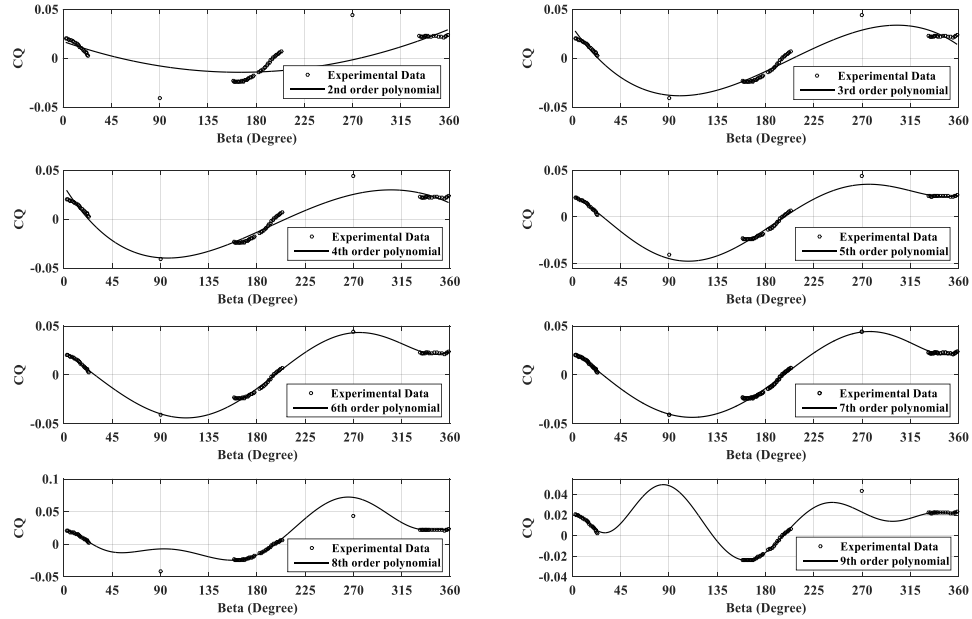

Figure 4.9. Comparison of different polynomial regression models with measured experimental data for thrust coefficient C_Q.

As was mentioned in the previous section, the measured data in the entire range of β could not be practically obtained. Therefore, the experimental data were allocated in specific regions on the graphs where the testing conditions were feasible. It is seen from Figure 4.8 that the polynomial models for C_T represent the data really well at high degrees, such as the sixth and seventh order polynomial. However, for the polynomials with the order higher than seven, the over-fittings occur at $\beta = 90^\circ$ and $\beta = 270^\circ$. In the same manner, the polynomial up to seventh order appears to be adequate for describing the C_Q data as demonstrated in Figure 4.9. The low order polynomials are not able to fit the data in the range of β from 150° to 220^0. The over-fittings are resulted from the high order polynomials and the curve characteristics are varied that is not able to present the nature of the propeller performance.

After fitting the data by using polynomial regression models with different orders, the applicability of fit is assessed to evaluate the validity. There are three statistic criteria to be considered: the Sum of Squares due to Error SSE, the Root Mean Squared Error $RMSE$, and coefficient of determination R^2. The SSE calculates the total deviation of the output values from the fitted curve to the output values and the $RMSE$ is an estimation of the standard deviation of the random value in the data. These values closer to 0 show that the obtained model is more useful and effective for prediction. Coefficient of determination R^2 indicates the proportionate of variation in the output variables explained by the input variables in the regression model. The values of R^2 close to 1 demonstrate that the regression models are appropriate for extrapolation. The statistic criteria SSE, $RMSE$, and R^2 for the C_T and C_Q coefficients are calculated and listed in the Table 4.5.

Table 4.5. Statistical properties for polynomial regression.

	Thrust coefficient C_T			**Torque coefficient** C_Q		
Number of Orders	SSE	$RMSE$	R^2	SSE	$RMSE$	R^2
2	0.1213	0.0402	0.8178	0.0026	0.0058	0.9147
3	0.0168	0.0151	0.9748	0.0003	0.0022	0.9883
4	0.0132	0.0134	0.9802	0.0004	0.0025	0.9851
5	0.0069	0.0098	0.9896	0.0004	0.0025	0.9866
6	0.0059	0.0091	0.9911	0.0004	0.0025	0.9862
7	0.0057	0.0090	0.9914	0.0002	0.0018	0.9923
8	0.0040	0.0076	0.9940	0.0001	0.0015	0.9952
9	0.0038	0.0075	0.9943	0.0001	0.0015	0.9956

It can be seen in Table 4.5 that the ninth order polynomial has the least SSE and $RMSE$ values for both C_T and C_Q coefficients. In addition, its coefficient of determination R^2 is highest and close to 1 compared to others. However, as previously discussed the polynomials with the order higher than seven overfit the data for both C_T and C_Q coefficients. Increasing the number of order in the polynomial would give better the applicability of fit but cause the over-fitting. For the polynomials with the order from two to seven, the seventh order polynomial has the least SSE and $RMSE$ values, and highest R^2 value. Therefore, the seventh order polynomial is considered the finest polynomial model in the examined condition.

4.3.1.2 Fourier Series Regression Models

The Fourier series regression models with the number of terms from one to six are applied to represent the thrust coefficient C_T and torque coefficient C_Q for the propeller in the range of advance angle β from 0° to 360°. The comparison of different Fourier series regression models with measured experimental data for C_T and C_Q are shown in Figure 4.10 and Figure 4.11. It can be seen in Figure 4.10 that the four-term and five-term Fourier series provide the better fit to the experimental data than the lower term models for C_T. For the Fourier series with the number of term higher than five, the over-fittings occur as seen in the range of β from 45° to 135° and from 270° to 315°. It is also observed from Figure 4.11 that three-term Fourier series provide the better fit to the experimental data compared to other models for the values of C_Q. As the number of term increases the curves reach unreasonably high values, which is considered as over-fitting. Additionally, the nature of these curve forms are incorrectly changed.

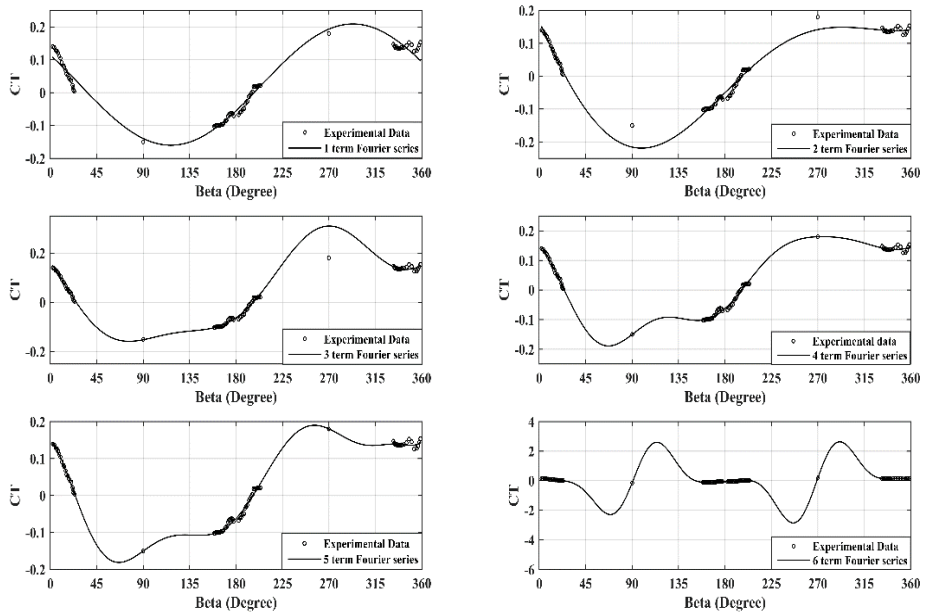

Figure 4.10. Comparison of different Fourier series regression models with measured experimental data for thrust coefficient C_T.

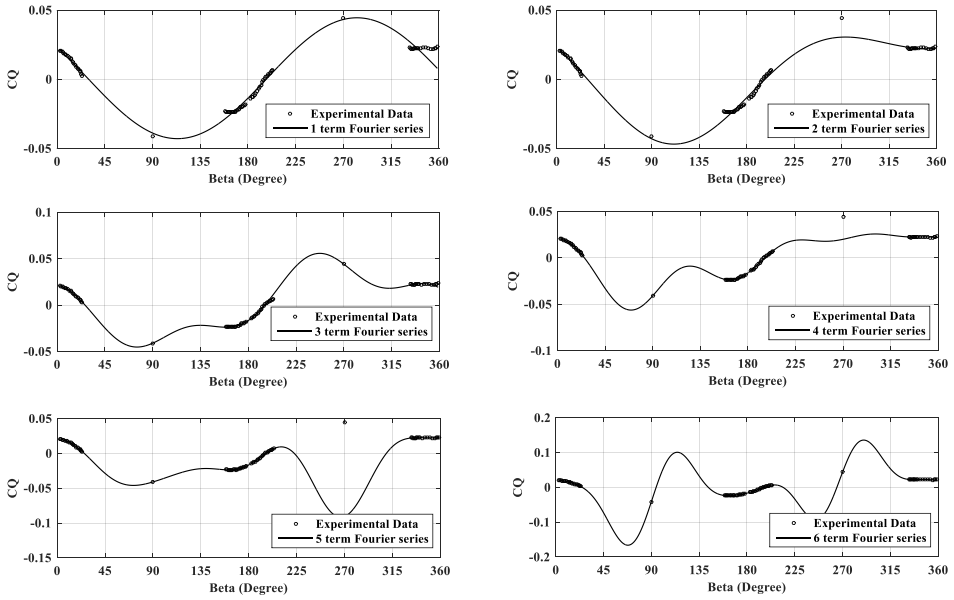

Figure 4.11. Comparison of different Fourier series regression models with measured experimental data for torque coefficient C_Q.

Table 4.6. Statistical properties for Fourier series regression.

	Thrust coefficient C_T			**Torque coefficient** C_Q		
Number or Terms	*SSE*	*RMSE*	R^2	*SSE*	*RMSE*	R^2
1	0.0270	0.0191	0.9595	0.0005	0.0027	0.9797
2	0.0071	0.0099	0.9893	0.0003	0.0020	0.9887
3	0.0045	0.0080	0.9932	0.00003	0.00066	0.9989
4	0.0036	0.0072	0.9947	0.00001	0.00049	0.9994
5	0.0037	0.0074	0.9945	0.00001	0.00049	0.9994
6	0.0024	0.0061	0.9964	0.00001	0.00045	0.9995

Three similar statistic criteria used above are also be considered for evaluating Fourier series regression models: SSE, $RMSE$, and R^2. They are calculated and listed in Table 4.6.

It can be seen in Table 4.6 that the SSE and $RMSE$ values decrease and R^2 value increases in general as the number of terms increase for both C_T and C_Q coefficients. This fact illustrates that increasing the number of terms could make the resulting curves fit with the experimental data better. However, it is noted previously that the Fourier series models with the number of term higher than five overfit the thrust coefficient C_Q and the models with the number of term higher than three overfit the torque coefficient C_Q. In addition, considering the four-term and five-term Fourier series model for C_T coefficient they are almost identical as can be seen in Table 4.6. Nevertheless, there is a difference in their statistical properties, which show that the four-term Fourier series model provides a better fitting curve. It has lower values of SSE and $RMSE$, and higher R^2 value compared to the five-term Fourier series model . Therefore, the four-term Fourier series and the three-term Fourier series models are considered the most suitable Fourier models for the thrust coefficient C_T and the torque coefficient C_Q, respectively, in the examined condition of this study.

4.3.1.3 Results Comparisons

Based on the information and calculations in previous sections, the comparison between the polynomial and Fourier series model in describing the four-quadrant propeller model is presented. For the thrust coefficient C_T, the seventh order polynomial model and the four-term Fourier series model are compared based on the applicability of fit shown in Table 4.5 and Table 4.6. Although both models are able to produce acceptable approximation of C_T as seen on the graphs, it can be noted that the statistical results for the thrust coefficient C_T in the four-term Fourier series model are better than the seventh order polynomial model. The Fourier model

has lower values of SSE and $RMSE$, and higher value considering the R^2 compared to the polynomial model. For the torque coefficient C_Q, the comparison between the seventh order polynomial model and the three-term Fourier series model is performed based on the statistical values. It can also be noted that the Fourier model has significantly lower values of SSE and $RMSE$ compared to those of the polynomial model. In addition, the Fourier model has higher value considering the R^2 as well. It is derived from the examination that the Fourier series model gives the results to a better agreement for all three statistic criteria: lower SSE, $RMSE$ value and higher R^2 value. It is therefore concluded that the four-term Fourier series and three-term Fourier series regression models are considered the most appropriate models in representing the C_T and C_Q coefficients respectively in the specified condition of this study. The model coefficients from equation (4.14) and (4.15) are calculated and listed in Table 4.7.

Table 4.7. The Fourier series regression function coefficients.

Coefficients	m_0	m_1	n_1	m_2	n_2
C_T	0.0432	-0.0967	0.1455	0.0325	0.0344
C_Q	-0.0055	-0.0152	0.0493	0.0066	0.0020
	m_3	n_3	m_4	n_4	ω
C_T	-0.0394	-0.0385	-0.0151	0.0193	1.7390
C_Q	-0.0063	-0.0120			2.0540

4.4 Summary

The experiment of an underwater vehicle propeller was tested at the towing tank in all four quadrants of operation. The conventional open water performance in the first quadrant and the performance characteristic in four-quadrant operation were presented in this chapter. An analysis of using polynomial and Fourier series regression model in representing the experimental data sets was examined. The applicability of fit was assessed to compare and evaluate the validity of the proposed models. It was concluded that the four-term and three-term Fourier series regression models were considered the most appropriate models in representing the thrust and torque coefficient curves respectively in the specified condition of this study. These two models formed the four-quadrant underwater propeller model. They were able to produce a reasonable approximation of thrust and torque coefficients with a small number of parameters.

CHAPTER 5

Experimental Study of the Collective and Cyclic Pitch Propeller CCPP

A series of experimental studies of the innovative propulsor named Collective and Cyclic Pitch Propeller (CCPP) applied to an underwater vehicle are presented in chapter 5. The bollard pull and captive model tests were conducted to investigate the characteristics of CCPP and to examine the effect of different parameter settings to its performance. The obtained results in the form of force coefficients provide a useful empirical model for the simulation and control of an underwater vehicle equipped with this propulsor.

Part of this chapter has been accepted for publication in the "*Journal of Marine Science and Application*". The citation for the journal is:

Minh Tran, Hung Nguyen, Jonathan Binns, Shuhong Chai and Alex Forrest, Experimental Study of the Collective and Cyclic Pitch Propeller, *The Journal of Marine Science and Application.*

5.1 Introduction

Although the innovative features of CCPP for an underwater vehicle were discovered from previous research studies its performance characteristics have not been fully demonstrated yet. In response to the shortcomings of previous works, the experimental studies with underwater vehicle model equipped with the CCPP propulsion system have been conducted at the AMC towing tank.

In this chapter, the thrust and manoeuvring forces of the CCPP are experimentally investigated by conducting a series of model tests, including bollard pull test, captive model test, and resistance test. In the bollard pull tests, the CCPP was tested in the stationary condition with different rotational speeds and pitch angle settings. These tests are important to evaluate the CCPP capability in the operational conditions of no advance speed and at low speed. In the captive model tests, the CCPP experiments were carried out in the behind hull condition with a series of different advance coefficients and pitch angle settings to primarily examine its propulsive performance whilst cruising. In addition, the resistance tests were also conducted and would be presented in the future study to enable the assessment of the propulsor and model hull interaction.

The main objectives of the present experimental study is to evaluate the characteristics of CCPP thrust and manoeuvring forces for a range of rotational speed, advance coefficients and pitch angle settings. The knowledge of these forces is necessary to gain the better understanding of the innovative design of CCPP and for the optimisation of CCPP system. Moreover, with an extensive measurement data obtained from the experiments, empirical propulsion model would be constructed and embedded into the AUV mathematical model to precisely simulate its manoeuvrability.

5.2 Experimental Design

5.2.1 Experimental setup

The experiments in this study were conducted at the AMC towing tank at the University of Tasmania. The primary specification of the towing tank was described in the previous chapter.

The main components of the testing apparatus including the underwater vehicle model, power system, transducers, data acquisition system and control system were attached on the towing carriage. The towing carriage was moved forward and backward with specific speed by the built-in speed controller.

The underwater vehicle model was mounted from a pair of aluminium vertical struts attached to the external force balance fixed at the centre of the towing carriage. The height of the struts were adjusted such that the whole vehicle was immersed 0.9 m below the water surface. Since the ratio of the tank width to the model transverse dimension is less than 5:1 the tank walls could be considered not to have significant effect on the propeller force measurements in this experiment (Chakrabarti, 1994).

The entire experimental apparatus is shown in Figure 5.1.

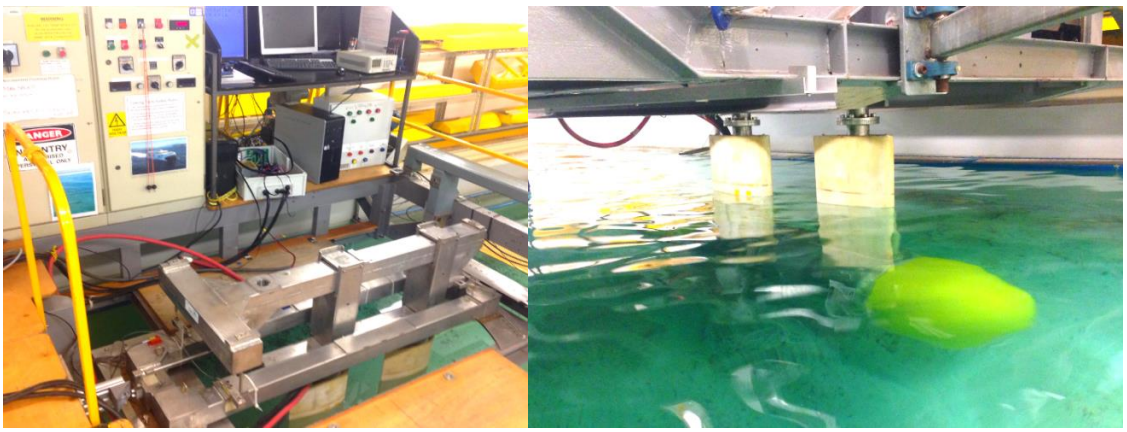

Figure 5.1. The experimental apparatus.

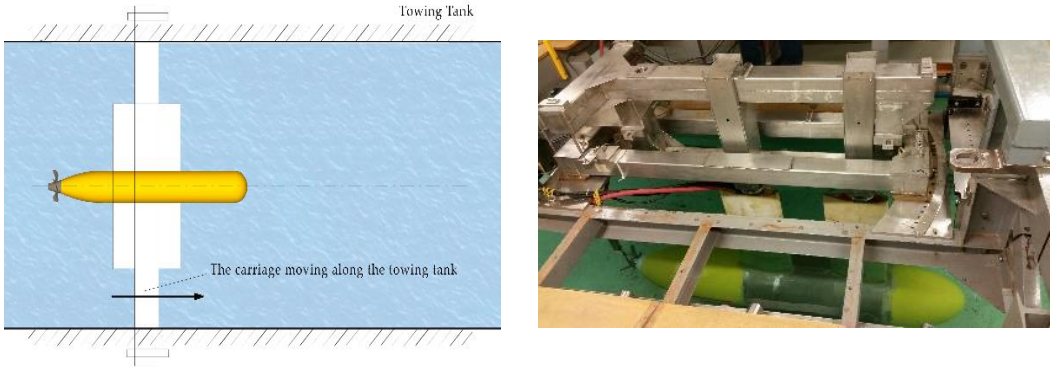

Figure 5.2. The Experimental setup in the Towing Tank.

5.2.2 Force and moment measurements

The experiments were conducted using two types of force balance, an internal force balance and an external force transducer. The internal balance was a six DOF load cell manufactured by JR3 Multi-Axis Load Cell Technologies. The balance was placed inside a waterproof block and inserted behind the propulsion unit. This arrangement enabled the direct measurements of force and moment generated by the CCPP during the tests. The wires from the load cell were covered by a watertight seal and connected to the data acquisition system on the towing carriage. The internal force transducer had the capability of measuring up to 400 N of axial force and 200 N of side forces.

The external balance was a force transducer designed and manufactured at AMC. It was mounted at the centre of the towing carriage. This force balance of six single axis load cells was placed at specific positions enabling the measurement of force and moment experienced by the entire underwater vehicle model in the six DOF. Each load cell had the measurement capacity of 225 kg. Figure 5.3 shows the internal and external force transducers used in the experiment.

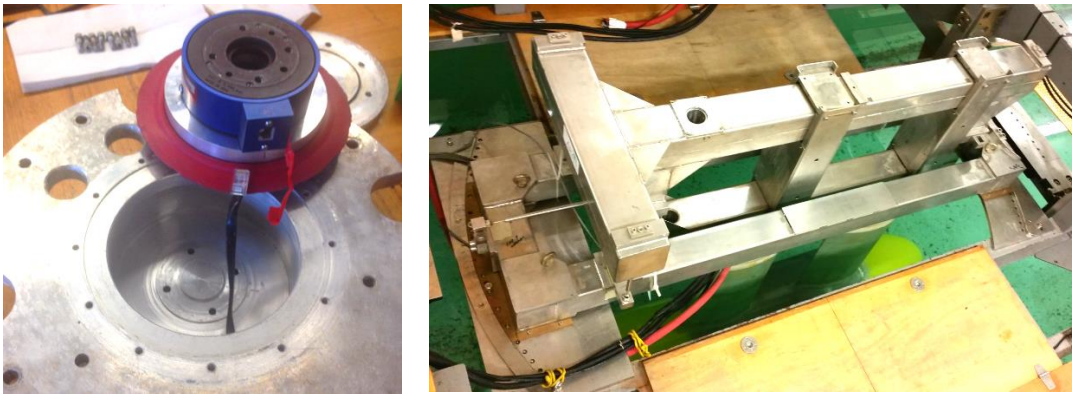

Figure 5.3. The internal and external force balances.

The balance axis system is given in Table 5.1.

Table 5.1. The force balance axis system.

Balance Axis System	Description	Positive Direction
X	Axial Force or Thrust	Forward
Y	Horizontal Force	To starboard
Z	Vertical Force	Up
K	Rolling moment	Roll to starboard
M	Pitching moment	Turn up
N	Yawing moment	Turn to starboard

The calibration process was conducted prior to the experiment. A test stand was specifically designed for the internal force transducer calibration as shown in Figure 5.4. Two force transducers were carefully calibrated separately. The known loads from 1 kg to 10 kg were applied to the transducers in each direction and a multiple linear regression analysis was applied to form the calibration matrix. The calibration process was based on standard procedure described in the reference (ITTC, 2008b).

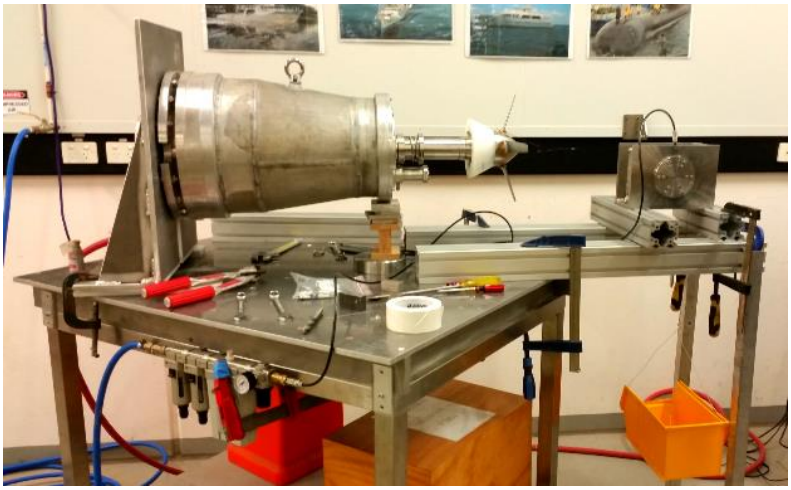

Figure 5.4. The internal force transducer calibration stand.

5.2.3 Data acquisition system and signal conditioning

The response signals from the external force transducer were recorded simultaneously and pre-processed by the National Instrumentation data acquisition and filtering system PCI-6254M series equipped on the towing carriage. The carriage speed was also captured via an analogue channel of this system. The data from the internal force transducer were acquired directly by the National Instrumentation DAQ PCI-6036 fitted into the PCI slot of a desktop computer. The data acquisition program was developed by using the LABVIEW software to capture signal from both transducers. The sample rate were set to 100 Hz and 200 Hz for the internal and external force transducer respectively. The sampling times were set for 20 seconds. The high frequency noise from the system vibration were removed by applying the low-pass filter. These data were then stored on the on-board desktop hard drive and then analysed by using Excel and MATLAB/Simulink™.

5.2.4 Experimental program

The objectives of the experiment were to investigate the CCPP performance characteristics by conducting the bollard pull and captive model tests. The tests included the measurements of

forces and moments generated by the CCPP over the range of propeller rotational speed, CCPP pitch settings and towing carriage speed.

The experiments were conducted in accordance with the ITTC recommended procedures and guidelines, Propulsion/Bollard Pull Test (ITTC, 2011a), Captive Model Test Procedure (ITTC, 2014) and Resistance Test (ITTC, 2011b).

In the bollard pull tests with the towing carriage at a standstill, the experiments were performed at the propeller rotational speed of 100 RPM, 200 RPM, 300 RPM, 400 RPM and 500 RPM with the collective angles δ_{col} from -29° (-100%) to 29° (100%) in the increments of 25% and cyclic angles δ_{cyc} from -20° (-100%) to 20° (100%) in the increments of 25%. In the captive model tests, the collective and cyclic angles were adjusted at fixed values prior to each run while the propeller rotational speed and the towing carriage speed were set at specific values. The tests were conducted at different advance coefficient J ranging from $J=0$ to $J=1.5$. The propeller collective and cyclic angles settings were varied similarly to the bollard pull condition's settings. The resistance test was also conducted to calculate the total resistance resulted from the under-water vehicle model hull and the connecting struts. In the resistance tests, the model was towed in both the forward and reverse directions with the similar advance coefficients in the captive model tests. 2000 runs were performed in total during the two weeks of testing.

5.2.5 Data reduction and representation

The collected raw data from transducer were corrected for zero offset and then multiplied by the calibration matrix to determine the forces and moments. These values were then averaged over a steady period. The non-dimensional coefficients describing the propulsor performance derived from the experimental data are defined as (Carlton, 2012):

$$J = \frac{V_A}{nD} \tag{5.1}$$

$$K_T = K_X = \frac{X}{\rho n^2 D^4} \tag{5.2}$$

$$K_Y = \frac{Y}{\rho n^2 D^4} \tag{5.3}$$

$$K_Z = \frac{Z}{\rho n^2 D^4} \tag{5.4}$$

$$K_Q = K_K = \frac{K}{\rho n^2 D^5} \tag{5.5}$$

$$K_M = \frac{M}{\rho n^2 D^5} \tag{5.6}$$

$$K_N = \frac{N}{\rho n^2 D^5} \tag{5.7}$$

where J is the advance coefficient, n (rps) is the propeller rotational speed, D (m) is the propeller diameter, V_A (m/s) is the vehicle advance speed, and ρ (kg/m^3) is the water density.

In addition, the open water efficiency is defined as:

$$\eta = \frac{K_T}{K_Q}\frac{J}{2\pi} \tag{5.8}$$

5.2.6 Error analysis

An elementary error analysis on the experimental data were conducted in accordance with the ITTC recommended procedures for uncertainty analysis (ITTC, 2002). The total uncertainty in the thrust and torque coefficient U respectively were calculated from the precision error P and the bias error B. The precision error was approximated by conducting repeated tests in specific

conditions. The bias error consists of the errors resulted from the transducer sensitivity in measurements of water temperature, propeller diameter, carriage speed, propeller rotational speed, thrust, and torque. The total uncertainties for thrust and torque coefficients are estimated as 2.4% and 3.6% respectively.

5.2 Results and Discussions

During the tests, a wide variety of the measurements was recorded and the data analysis was conducted to present the preliminary results. The main results presented in this section are the performance curves of thrust, torque coefficients as function of the pitch angles in bollard pull condition, and as function of advance coefficient in captive model test condition. The values of δ_{col} and δ_{cyc} are presented in percentage for the ease of application in simulation and control study.

5.2.1 Bollard pull test

5.2.1.1 Effect of Collective Pitch Angle Settings

Figure 5.5 shows the thrust coefficient K_T and the torque coefficient K_Q as functions of the collective pitch angle δ_{col} for different propeller rotational speeds ranging from 100 RPM to 500 RPM.

As can be seen in the first graph for K_T curve, the thrust magnitude increases gradually to the maximum positive and negative values as δ_{col} expands from 0 to 100% and from 0 to -100% respectively. The K_T absolute values for the positive δ_{col} is slightly higher than that of the negative δ_{col} which means that the CCPP produce more thrust in forward direction than in the reverse direction. There is also a difference in the torque coefficient K_Q as δ_{col} varied from -100% to 100%. The reason for the differences in K_T and K_Q at positive and negative δ_{col} is due to the

flow recirculation resulted from the hull interaction. Moreover, as previously noted, the rake angle makes the CCPP asymmetrical in the rotational plane which causes the lower reverse thrust.

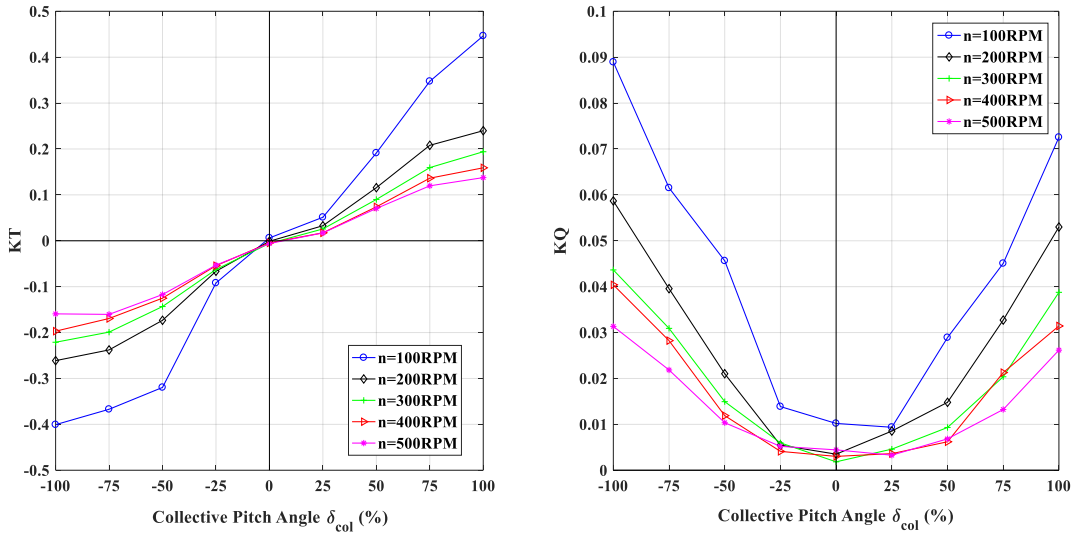

Figure 5.5. Effect of Collective Pitch Angle Settings to K_T and K_Q.

In addition, it can be seen that at a particular δ_{col}, K_T increases as rotational speed n decreases. For the fixed pitch propeller (FPP), changing the rotational speed is the only way to adjust the thrust magnitude. On the other hand, for the CCPP, the thrust magnitude and direction could be changed by controlling the combination of the rotational speed and the collective pitch angles. This mechanism is found to be similar to the CPP, which offers significant advantages such as the capability to gain high efficiency at different cruising speed, high thrust rate of change, flexibility in straight-line motion with both forward and reverse direction, stability in the power generation by not changing the rotor shaft speed continuously.

5.2.1.2 Effect of horizontal cyclic pitch angle settings

In Figure 5.6, the horizontal force coefficient K_Y is plotted against the cyclic pitch angle δ_{cyc}, which are presented in percentage for a range of different rotational speeds.

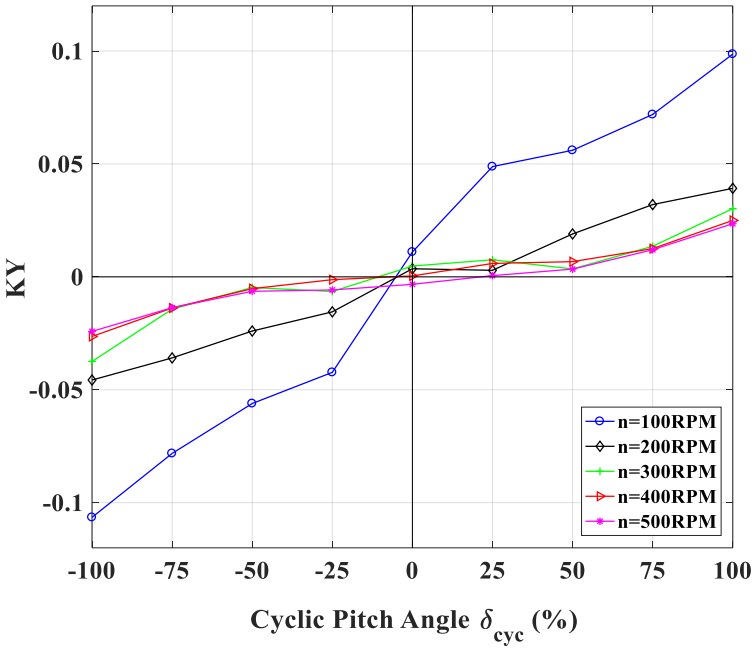

Figure 5.6. Effect of horizontal cyclic pitch angle settings.

The results show that the K_Y absolute value increases as δ_{cyc} ranging from -100% to 100% the limitation at both ends. The positive δ_{cyc} settings would result in a horizontal force to starboard with positive K_Y. On the contrary, the negative δ_{cyc} would result in a horizontal force to the port. This trend is observed at every rotational speed setting.

In addition, K_Y increases with the decrease of rotational speed. However, at the high rotational speeds, above 300 RPM, K_Y appears to be independent of rotational speed to within the experimental errors in this data.

5.2.1.3 Effect of vertical cyclic pitch angle settings

Figure 5.7 illustrates the relationship between the vertical force coefficient K_Z and the cyclic pitch angle δ_{cyc} presented in percentage for a range of propeller rotational speeds.

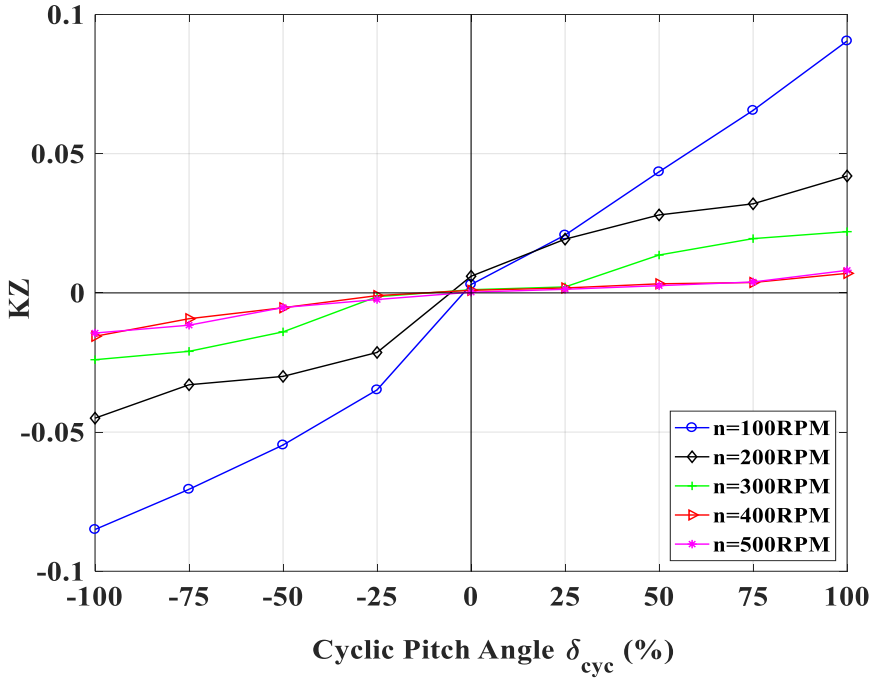

Figure 5.7. Effect of Vertical Cyclic Pitch Angle Settings.

It can be seen that the results show the similar trend in the CCPP side force performance, which has been observed in the previous case. The positive δ_{cyc} settings would result in a vertical force upwards with positive K_Z. On the contrary, the negative δ_{cyc} would result in a vertical force downwards.

In the cases of pure cyclic pitch angle settings, it could be concluded that CCPP are able to generate a significant side forces, which are observed with steady trend. Nevertheless, increasing the rotational speed would result in the dramatic decrease in the side forces, horizontal force and vertical force.

5.2.1.4 Effect of collective and horizontal cyclic pitch angle settings

Considering the effect of both collective and horizontal cyclic pitch angle setting to the CCPP horizontal force and thrust, Figure 5.8 shows the relationship between the horizontal force coefficient K_Y and cyclic pitch angle at various collective pitch angles.

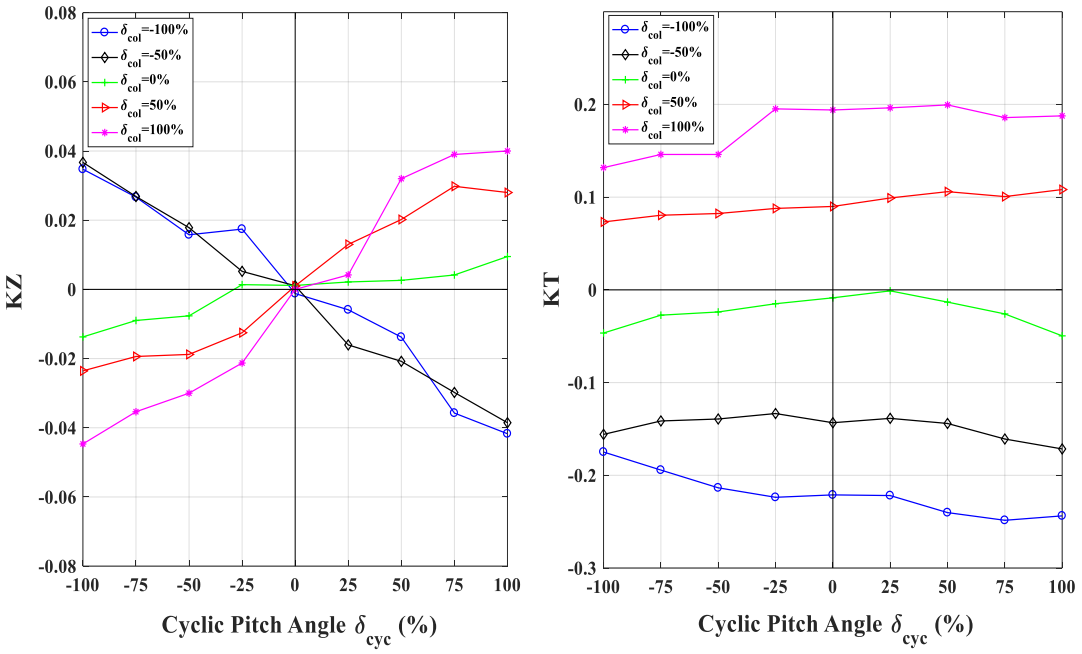

Figure 5.8. Effect of collective and horizontal cyclic pitch angle settings.

From the figure it can be seen that at the positive δ_{col}, in the range of δ_{cyc} from -100% to 100%, the CCPP has the horizontal force performance in the same fashion as in the pure cyclic settings discussed in previous section. However, at the negative δ_{col}, the horizontal force direction changes in the opposite manner. The positive δ_{cyc} settings would result in a horizontal force to the port with negative K_Y. On the contrary, the negative δ_{cyc} would result in a horizontal force to the starboard.

It also noted that the δ_{cyc} does not have dramatic influence on thrust at different δ_{col} settings. This means that the underwater vehicles equipped with CCPP would be able to make a turning manoeuvre without loss in thrust.

5.2.1.5 Effect of collective and vertical cyclic pitch angle settings

Similarly to the previous case, the relationship between the vertical force coefficient K_Z and cyclic pitch angle at various collective pitch angles is presented in Figure 5.9.

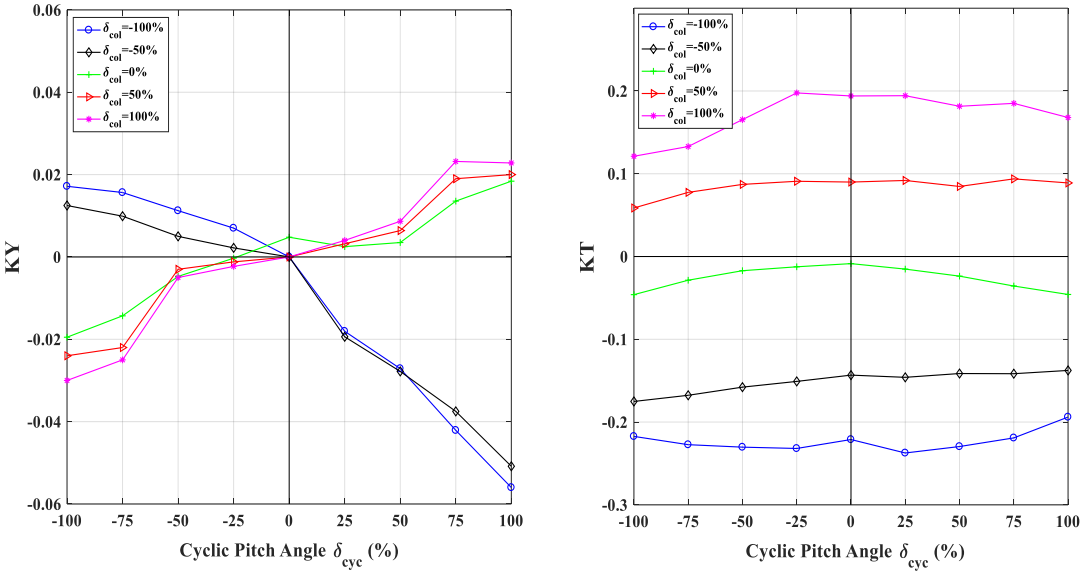

Figure 5.9. Effect of collective and vertical cyclic pitch angle settings.

Similar to the horizontal force coefficient, the vertical force coefficient is affected by the change of δ_{cyc} at different δ_{col}. At the positive δ_{col}, the CCPP has the vertical force performance in the same way to the pure cyclic settings. At the negative δ_{col}, the positive δ_{cyc} settings would result in a vertical force downwards with negative K_Z. On the contrary, the negative δ_{cyc} would result in a horizontal force upwards.

In both cases of horizontal force and vertical force performance from the effect of the cyclic pitch angle, it could be concluded that the CCPP is able to generate effective side forces with and without the presence of thrust. In contrast to the FPP, CPP and vectored thrusters, these propulsors only produce thrust effectively in one direction. This feature enable the manoeuvrability of underwater vehicle at various operational conditions, low speed and cruising speed.

5.2.2 Captive model test

5.2.2.1 Effect of collective pitch angle settings

Figure 5.10 and Figure 5.11 show the thrust coefficient K_T and torque coefficient K_Q as the function of advance coefficient J for a range of the collective pitch angle δ_{col}, which is presented in percentage. In the captive model experiment, the rotational speed was maintained as constant during the tests.

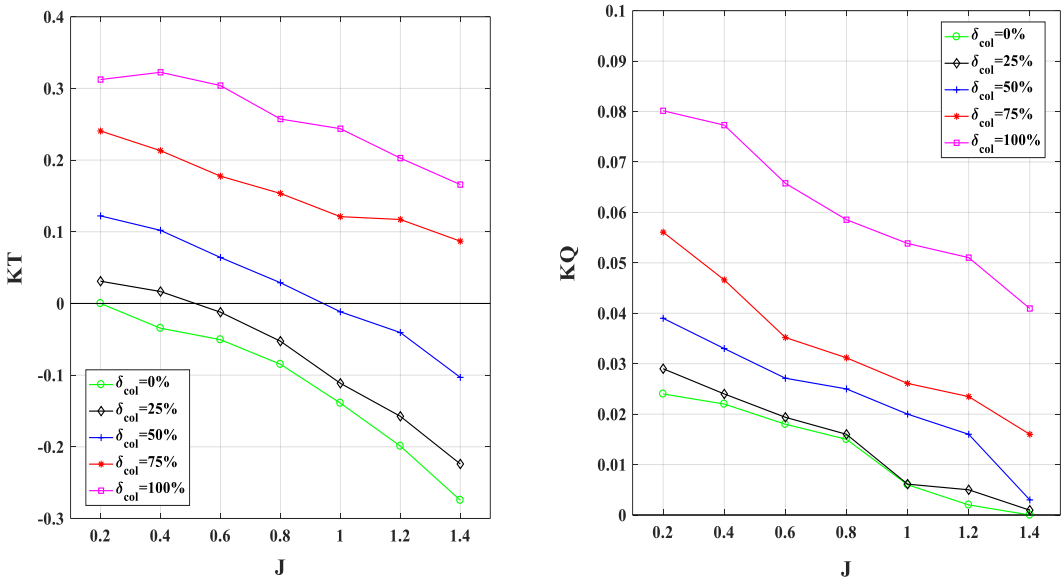

Figure 5.10. Effect of positive collective pitch angle settings.

As can be seen in the graphs for K_T with positive and negative δ_{col}, the thrust coefficients decreases and increases gradually in absolute values as J increases respectively. Advance coefficient J dramatically influences K_T. The presented characteristics curve of CCPP is found to be similar to that of the conventional propeller. It is noted that at a specific J, K_T increases with the rise of δ_{col}. The torque coefficient K_Q curves have the similar tendency as the thrust coefficient curves.

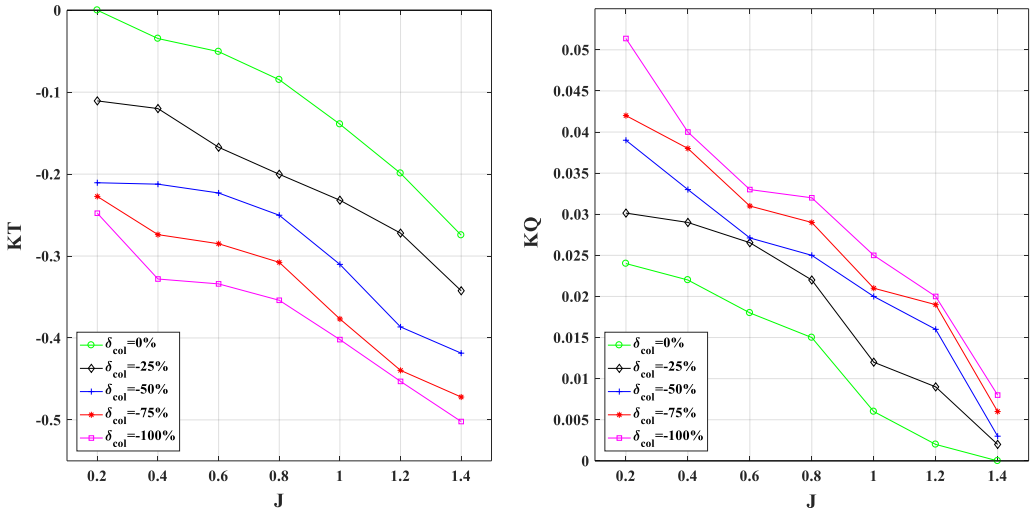

Figure 5.11. Effect of negative collective pitch angle settings.

The difference in the forward and reverse thrust with the positive and negative δ_{col} has been discussed in the previous section. The ability to rapidly generate significant reverse thrust could assist the underwater vehicle in the crash-back manoeuvre as well as in the stopping manoeuvre.

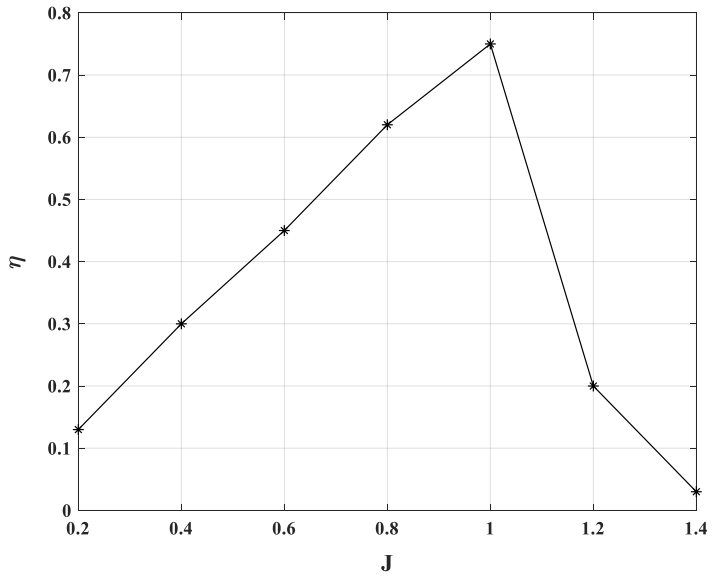

Figure 5.12. Maximum open water efficiency of CCPP in the range of advance coefficient.

The maximum open water efficiency of CCPP for different positive collective pitch settings, shown in Figure 5.12, are presented in the range of advance coefficient. The experimental results show that CCPP has the maximum efficiency at $J = 0.2,\ 0.4,\ 0.6$ with $\delta_{col} = 75\%$ and at $J = 0.8,\ 1.0,\ 1.2$ with $J = 100\%$. In general, the maximum open water efficiency of CCPP is $\eta = 0.73$ at $J = 1$ with the collective pitch setting $\delta_{col} = 100\%$.

5.2.2.2 Effect of horizontal cyclic pitch angle settings

The relationship between the horizontal force coefficient K_Y and the advance coefficient J for different cyclic pitch angle settings is presented in Figure 5.13.

It is interesting to note that K_Y sharply increases its absolute value as J increases. The reason for this characteristics is that it is due to the effect of water inflow velocity which alter the lift generated on each blade of the CCPP. Additionally, in a particular J value, the performance is consistent with the bollard pull condition.

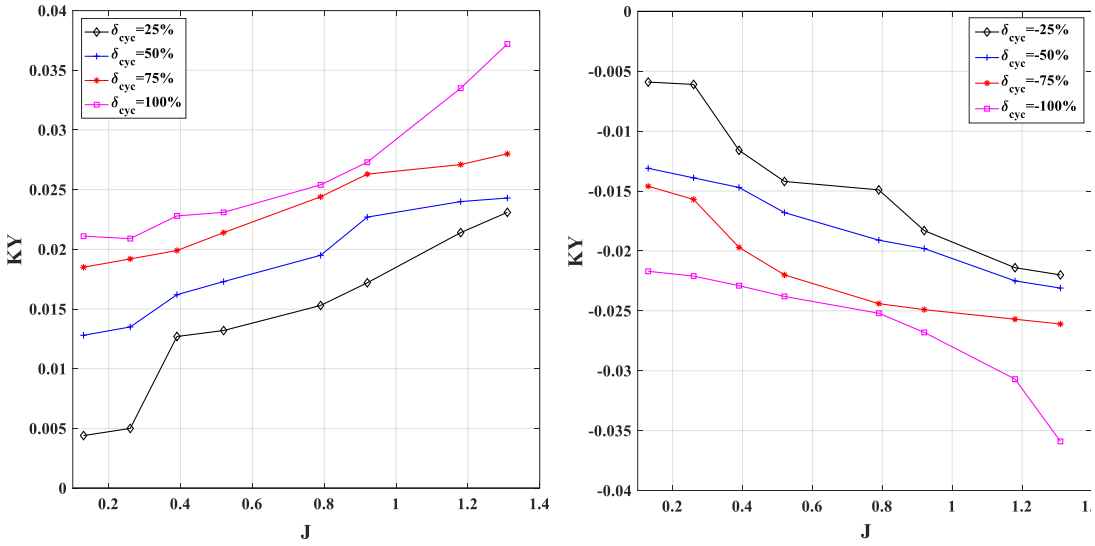

Figure 5.13. Effect of horizontal cyclic pitch angle settings.

5.2.2.3 Effect of vertical cyclic pitch angle settings

Similar to the previous section, the effect of vertical cyclic pitch angle settings on the CCPP performance is illustrated in Figure 5.14 by plotting the vertical force coefficient K_Z against the advance coefficient J for a range of cyclic pitch angles δ_{cyc}.

The behaviour of the vertical force coefficient K_Z with respect to J is similar to the behaviour of the horizontal force coefficient K_Y. It can be found that the side force coefficients, K_Y and K_Z, are not only dependent on δ_{cyc} but also on J. These results suggest that the side forces could be controlled by both variables δ_{cyc} and J for the optimum performance.

Generally, the findings from the captive model test show a fairly consistent CCPP performance in the range of advance coefficients as in the bollard pull condition. In the underwater vehicle simulation at different manoeuvring, all effects have to be taken into account for the accurate performance prediction. The obtained empirical values can be analysed and saved in the form

of look-up table which predict the CCPP manoeuvring forces as a function of pitch angle settings and advance coefficient.

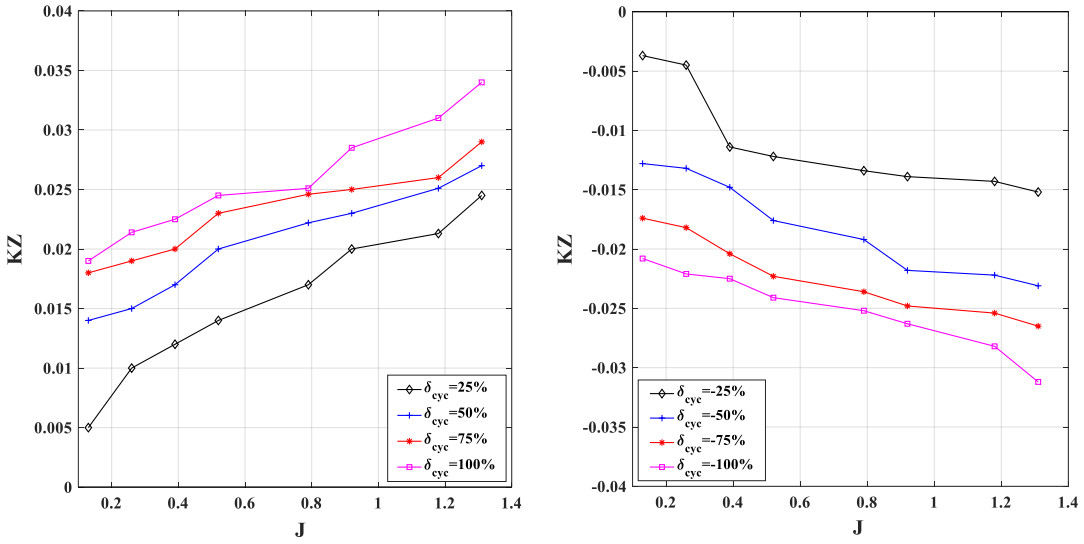

Figure 5.14. Effect of vertical cyclic pitch angle settings.

5.3 Summary

A series of comprehensive bollard pull and captive model tests were designed and conducted on the innovative propulsor named CCPP to evaluate its performance. The effects of the collective and cyclic pitch settings on the CCPP performance have been examined and discussed. According to the obtained results, it is shown that the CCPP is capable of generate an effective manoeuvring forces in both bollard pull and captive model conditions. The results also provide an insight into the relationship between these manoeuvring forces and controlled parameters that enables the simulation and control study of the underwater vehicle equipped with CCPP. As part of the research project, the experimental results from this study is used in a comparison study with experimental data of FPP to evaluate the effectiveness of an underwater vehicle performance

CHAPTER 6

Manoeuvring Simulation

In chapter 6, an AUV simulation program named AUVSIPRO is proposed in the preliminary design stage to predict and compare the AUV manoeuvrability equipped with different propulsion configurations. A series of primary manoeuvres standard for underwater vehicles are presented to investigate the system feasibility. In order to derive the mathematical model in the simulator, the propulsor models are experimentally conducted in the towing tank, the hull hydrodynamic coefficients are calculated using analytical, and system identification approaches. The system outputs are achieved by numerical method. The simulation program provides an effective platform to examine different the propulsion system configurations to an AUV as well as a torpedo shaped submarine.

Part of this chapter has been presented at *"The Forth International Conference on Modelling and Simulation for Autonomous System in Rome, Italy 2017"* and has been submitted to the "*Ocean Engineering, An International Journal of Research and Development*". Citations for conference paper and journal paper are:

Tran M, Binns J, Chai S, et al. (2017). AUVSIPRO–A Simulation Program for Performance Prediction of Autonomous Underwater Vehicle with Different Propulsion System Configurations. *International Conference on Modelling and Simulation for Autonomous Systems.* Springer, 72-82.

Minh Tran, Hung Nguyen, Jonathan Binns, Shuhong Chai and Alex Forrest, A comparison study of two propulsion system configurations for an autonomous underwater vehicle, *Ocean Engineering, An International Journal of Research and Development.*

6.1 Introduction

In this chapter, a simulation program named AUVSIPRO is proposed using the MATLAB/Simulink™. The program is able to rapidly simulate the underwater vehicle equipped with different propulsion systems in various defined standard manoeuvrability. This would greatly facilitate the design of vehicle propulsion system and provide a good understanding of the performance of an AUV. In addition, a wide range of control strategies could be applied in AUVSIPRO to validate the vehicle performance prior to practical implementation.

The chapter is structured as follows: Section 2 briefly describe the basic components and features of AUVSIPRO. A general description of the mathematical model of an underwater vehicle incorporated in AUVSIPRO is presented in Section 3. Fundamental manoeuvrability to examine an underwater vehicle performance are proposed and the simulation results are presented in section 4. Section 5 summarises the chapter.

6.2 AUVSIPRO – The Simulation Program Description

The AUVSIPRO is built using Simulink™ blocks and a set of MATLAB™ defined functions as shown in Figure 6.1. There are five basic components in the program including the propulsion system blocks, vehicle dynamic blocks, transformation blocks, display blocks and output-saving blocks. These components are coloured in orange, cyan, white, yellow and blue respectively for the easy of presentation.

The main component is the vehicle dynamic block, which describes the equations of motion and dynamic model of an underwater vehicle. The Gavia AUV is selected as the vehicle platform for the simulation in this study. In addition to the Gavia AUV, the AUVSIPRO also includes other underwater vehicle model such as REMUS AUV presented in different parameter block.

The propulsion system component consists of the input control signals and the mathematical model relating the inputs to the corresponding generated forces. There are two different propulsion systems examined in the study including the conventional propulsion system with FPP and the CCPP.

In the propulsion system block, the control signals were defined using the *Signal Builder* block as shown in Figure 6.2. A series of *Signal Builder* blocks were built in accordance with the fundamental manoeuvring ability tests, which were illustrated in next section. In the FPP propulsion module, the empirical model developed in chapter 4 was utilised. It should be noted that a minor modification was made to the FPP mathematical model in AUVSIPRO due to the presence of the duct in the FPP configuration. The tested propeller was utilised to operate inside a Nautican accelerating nozzle. Since this nozzle is equipped with supporting mechanical and electrical components in the propulsion unit the experiment to measure the nozzle thrust could not be conducted. It is known that the accelerating flow type of nozzle itself produces a positive thrust and offers a means of increasing the efficiency of open propellers (Oosterveld, 1970). Compared to open propeller with the same design conditions, a nozzle can produce between 25% and 30% more thrust at towing speed (Bose, 2008). These estimated values would be used to modify the nozzle effect to the open propeller in the AUVSIPRO as the experimental data are not currently available. In this study, the value of 25% were applied in the simulation model.

In the CCPP propulsion block, the *Lookup Table* blocks were utilised to construct the propulsion mathematical model, shown in Figure 6.3. In the *Lookup Table*, the relationship between the input control signals and output forces were presented based on the experimental data in chapter 5. The output signals from these propulsion system blocks were then sent to the dynamic block to form the complete equations of motions. Using the pre-defined hydrodynamic coefficients, the

differential equations were solved and integrated in the transformation blocks to provide the vehicle state values such as positions and velocities.

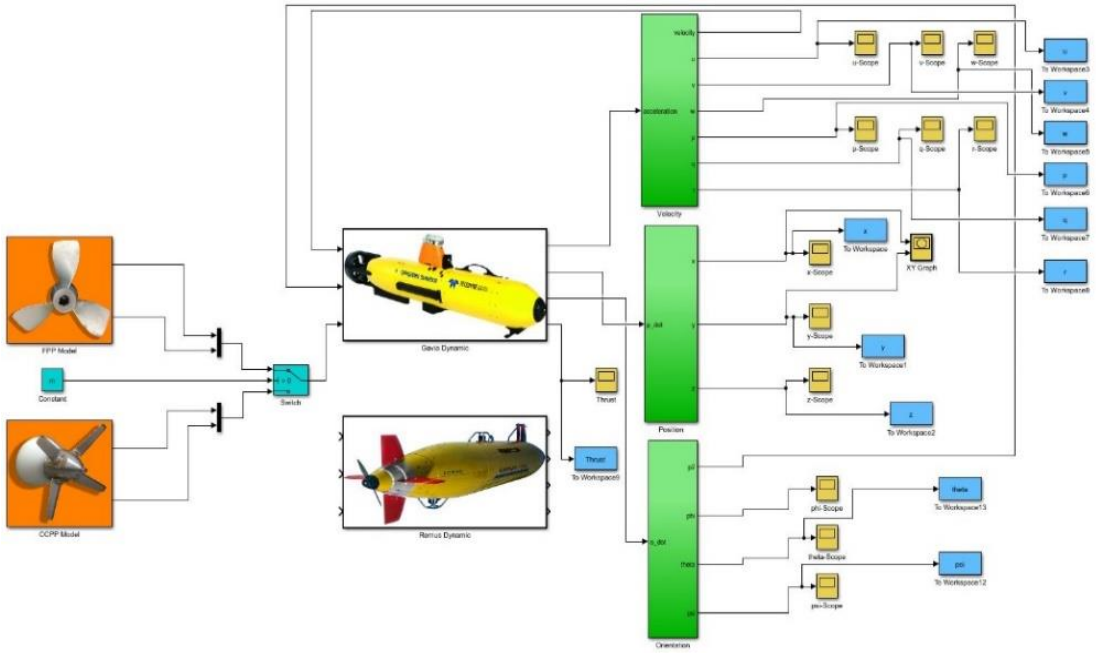

Figure 6.1. The layout of the AUVSIPRO Simulink Model.

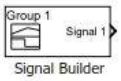

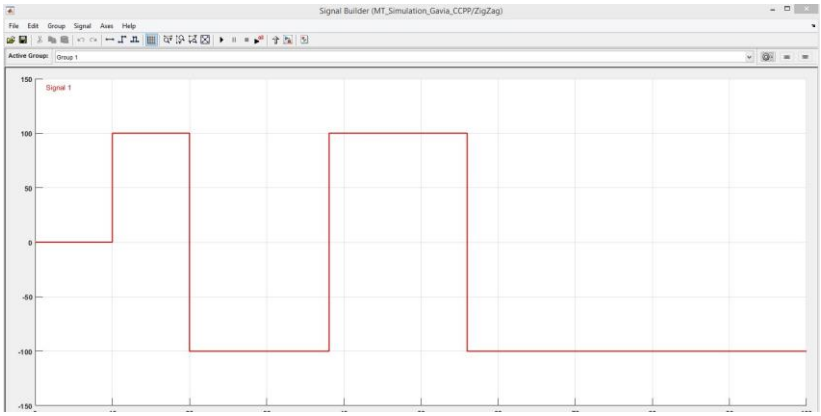

Figure 6.2. The Signal Builder block as the input signal in the propulsion component.

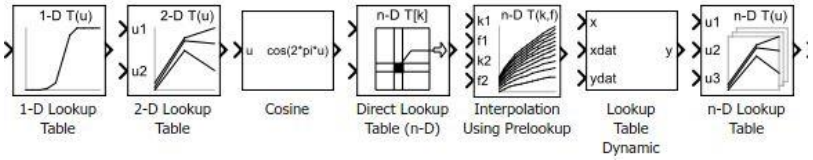

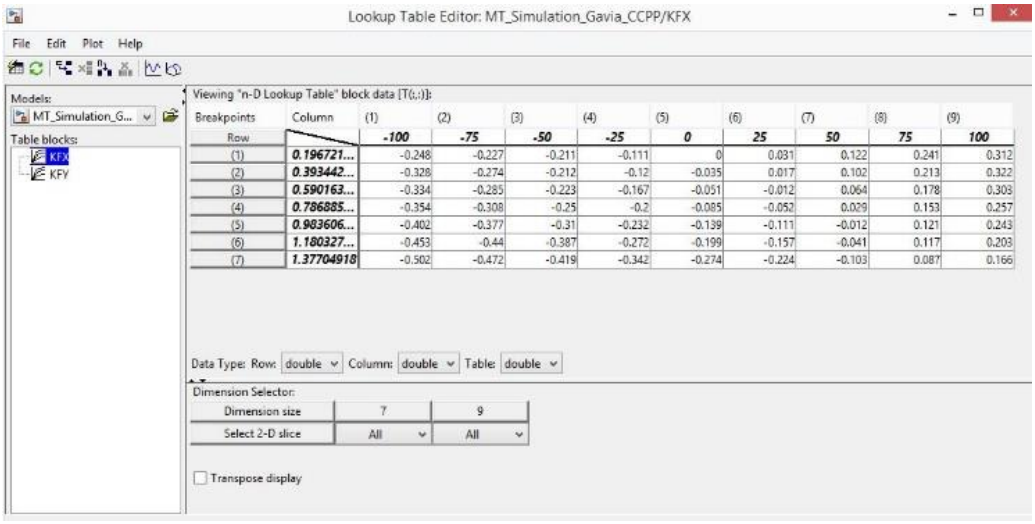

Figure 6.3. The Lookup Table block representing the CCPP system mathematical model.

In the simulation program, the general AUV equations of motion developed from the Chapter 3 are converted into the standard state-space equations in the simulation program. The state-space equations are presented as follows:

$$\begin{bmatrix} \dot{\eta} \\ \dot{\upsilon} \end{bmatrix} = \begin{bmatrix} J(\eta)\upsilon \\ M^{-1}\left\{-C(\upsilon)-D(\upsilon)\upsilon-g(\eta)+\tau\right\} \end{bmatrix} \tag{6.1}$$

The general non-linear matrix-vector form is:

$$\dot{x} = F(x,u) \tag{6.2}$$

where x is the state vector and u is the control input signal.

The Runge-Kutta numerical integration is utilised to numerically solve the underwater vehicle equations of motion. The continuous equation (6.2) is defined in the discrete time domain as:

$$\dot{x}_n = f\left(x_n, u_n\right) \tag{6.3}$$

where x_n is the state vector, and u_n is the input control vector.

In the Runge-Kutta Fourth-order method, the following equations are calculated:

$$\begin{aligned} k_1 &= x_n + f\left(x_n, u_n\right) \\ k_2 &= f\left(x + \frac{\Delta t}{2} k_1, u_{n+1/2}\right) \\ k_3 &= f\left(x + \frac{\Delta t}{2} k_2, u_{n+1/2}\right) \\ k_4 &= f\left(x + \Delta t k_4, u_{n+1}\right) \end{aligned} \tag{6.4}$$

where the interpolated vector is

$$u_{n+1/2} = \frac{1}{2}\left(u_n + u_{n+1}\right) \tag{6.5}$$

State vector at x_{n+1} is calculated based on state vector x_n as:

$$x_{n+1} = x_n + \frac{\Delta t}{6}\left(k_1 + 2k_2 + 2k_3 + k_4\right) \tag{6.6}$$

It is also noted that the current effects on the AUV in the simulation have not been included in the open loop simulation. In the context of the comparison study between the two systems, this effect is assumed not significant.

6.3 Manoeuvring Design

The basic concept behind the manoeuvring of a submarine are very similar to that of a surface ship (Renilson, 2015). In general, there are typical manoeuvres applied to examine the manoeuvrability and performance characteristics of an underwater vehicle, including the acceleration manoeuvre, stopping manoeuvre, turning circle manoeuvre, static turning manoeuvre, pull-out manoeuvre, zig-zag manoeuvre, depth-changing manoeuvre, meander manoeuvre, spiral manoeuvre and reverse spiral manoeuvre.

6.3.1 Acceleration Manoeuvre Test

This test illustrates how the AUV travel during acceleration. An acceleration test is performed by increasing the speed of the AUV from rest or from a particular ahead speed to a higher ahead speed (Issac et al., 2007; Lewis, 1988). The acceleration test is important for vehicles that may have a change position rapidly or accelerate suddenly for a mission (Lewis, 1988).

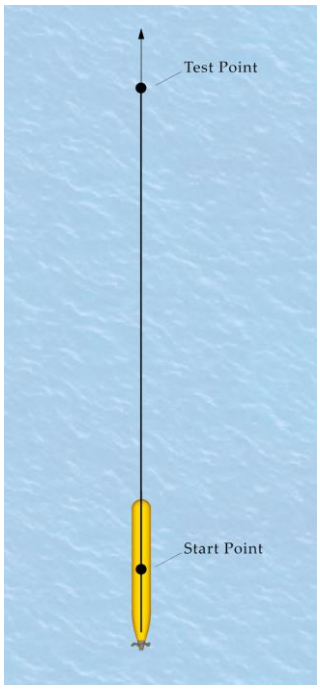

Figure 6.4. Acceleration Test.

6.3.2 Stopping Test

Stopping is the manoeuvre of interest primarily from the point of view of avoiding collisions, rammings, and groundings (Lewis, 1988). The most common manoeuvre in stopping test is the crash-stop from full ahead speed (Bertram, 2012) . For the vehicle equipped with FPP, the motor is stopped and then reversed at full astern. Additionally, for the AUV with large control surfaces, the stopping characteristics can be improved by fluctuating the control surfaces to increase drag resulted from the hull and the control surfaces themselves. The AUV equipped with CCPP configuration can perform the stopping manoeuvre by two methods. In the first method, similar to the conventional FPP configuration, the propeller direction is reversed to obtain a crashback condition. In the second method, the collective pitch angles are changed to the negative setting and the motor speed remains constant. This feature is unique to the CCPP or the controllable pitch propeller in general. In these two methods, the latter method has the better performance since it takes more time for the CCPP to slow to zero and then reverse the rotation direction to reach a new speed in the first method. Moreover, the second method is selected for the simulation study due to the availability of experimental data conducted in previous chapters.

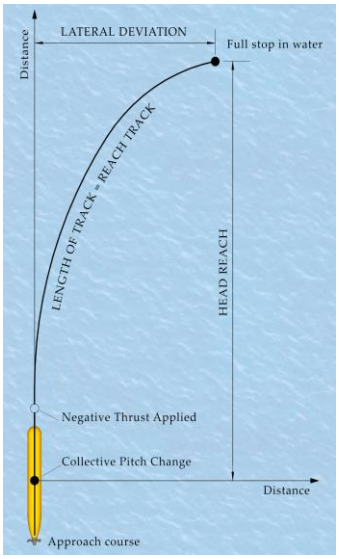

Figure 6.5. Stopping Test.

6.3.3 Turning Circle Manoeuvre

The turning circle manoeuvre is a measure of the ability to turn the underwater vehicle in a certain setting of the propulsion system. The turning circle manoeuvre is to be perform to both starboard and port with the maximum design rudder angle or maximum cyclic pitch setting for CCPP permissible at the test speed. The control action is executed following a steady approach with zero yaw rate. The essential information to be obtained from this manoeuvre is tactical diameter, advance, and transfer (IMO, 2002).

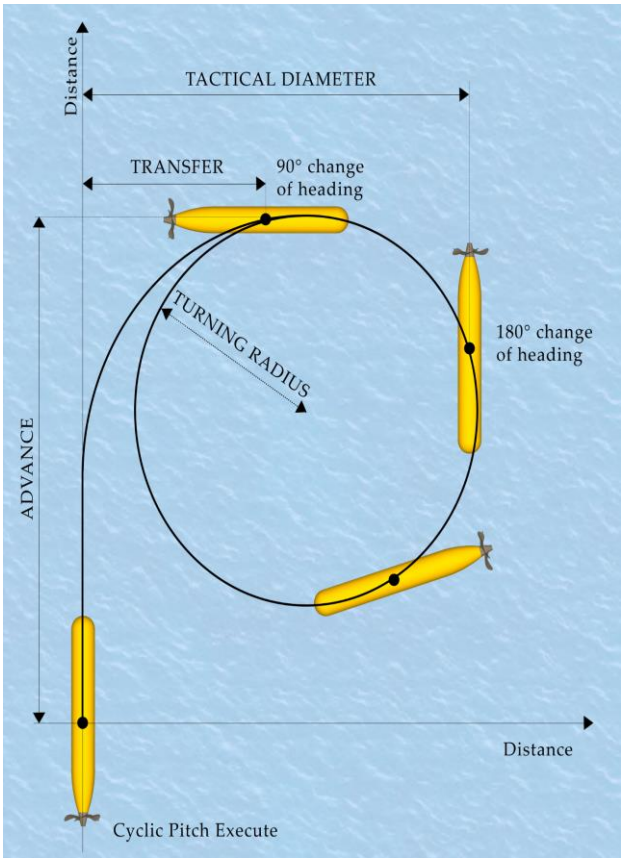

Figure 6.6. Turning Circle Manoeuvre Test.

6.3.4 Static Turning Manoeuvre

The static turning circle manoeuvre is executed as the underwater vehicle accelerating from rest. The static turning manoeuvre is an important manoeuvre in the low speed operation of an AUV. In the static turning, the thrust and manoeuvring forces such as side forces are taken in consideration as the AUV needs to rotate in the case of hovering and turning around or avoiding collision, and receiving the updated control measures.

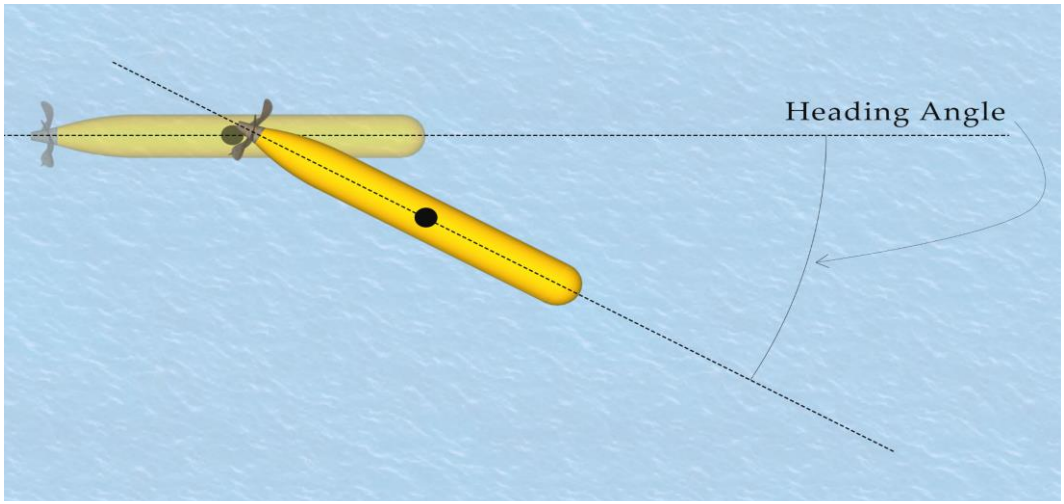

Figure 6.7. Static Turning Manoeuvre Test.

6.3.5 Pull-out Manoeuvre

The pull-out manoeuvre is used as a test to indicate the underwater vehicle's yaw stability. After a turning circle with steady rate of turn, the manoeuvring forces are disabled. If the vehicle is yaw stable, the rate of turn will decay to zero for turns both port and starboard. If the vehicle is yaw unstable, the rate of turn will reduce to some residual rate of turn (Bertram, 2012).

6.3.6 Zig-Zag Manoeuvre

The zig-zag manoeuvre is conducted to indicate the course-changing (horizontal plane) ability of the marine vehicle. For a zig-zag test in the horizontal plane, the rudder is deflected to a

constant angle, δ_0, as quickly and smoothly as possible and maintained at this angle until the change in the heading becomes ψ_0. The rudder is then deflected to $-\delta_0$ and held steady until the vehicle's heading has changed to $-\psi_0$. For a zig-zag in the vertical plane the stern planes are deflected instead of the rudder, and a specified change in pitch is used instead of change in heading (Renilson, 2015). For the underwater vehicle equipped with CCPP, the manoeuvring forces to perform the zig-zag test are obtained from the CCPP cyclic pitch setting instead of the control surfaces in the conventional propulsion. The CCPP is adjusted to a constant cyclic angle δ_{cyc} similar to δ_0.

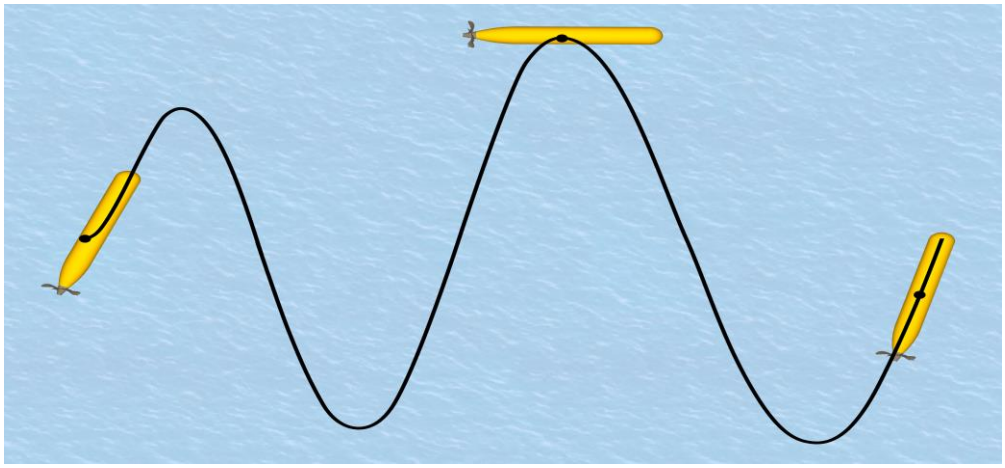

Figure 6.8. Zig-Zag Manoeuvre Test.

6.3.7 Depth-changing manoeuvre

It is important to perform the depth-changing test for the underwater vehicle to examine its diving ability. This manoeuvre is particular to the underwater vehicle and is conducted by changing the control surface angles and the cyclic pitch angle so that the vehicle is able to reach a certain depth in the vertical plane. This manoeuvre is used to represent the combined thrust and side force effects that the configuration has on the ability to rapidly change depth from a certain depth to a different depth from which the AUV will conduct other operations.

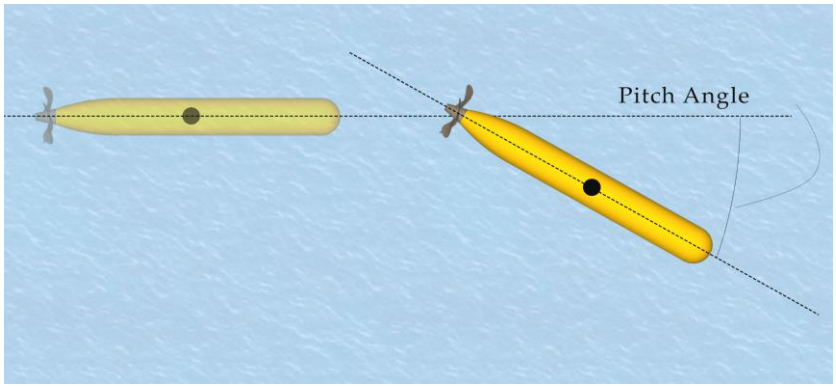

Figure 6.9. Depth-Changing Manoeuvre Test.

6.3.8 Meander Manoeuvre

The meander manoeuvre is similar to the zig-zag manoeuvre in the vertical plane, with the difference that once the execute pitch angle is reached, the manoeuvring control forces are brought to zero (and not reversed as in the zig-zag test) (Renilson, 2015). The objective of this test is to examine the ability of the underwater vehicle to return to a stable state after a disturbance to the pitch angle in the vertical plane.

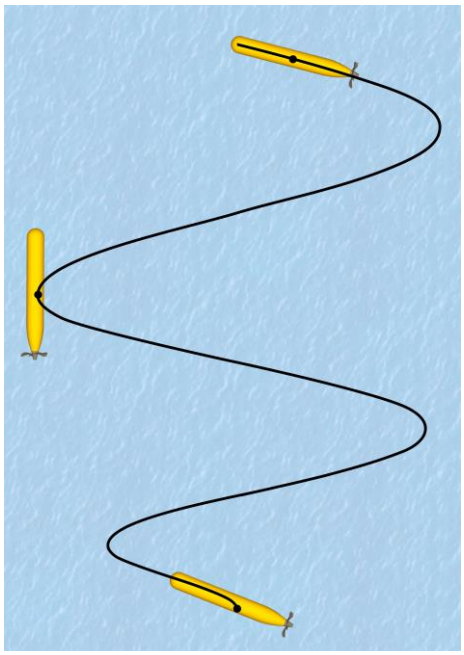

Figure 6.10. Meander manoeuvre test.

6.3.9 Spiral Manoeuvre or Helix Manoeuvre

The spiral manoeuvre is considered a complex manoeuvre, which combines the heading and diving manoeuvre. For the underwater vehicle actuated by the conventional propulsion system, the rudder and stern plane are deflected to specific angles at the same time. For the vehicle equipped with CCPP, both the vertical and horizontal cyclic pitch settings are enabled. The spiral manoeuvre is not a standard manoeuvre but is designed to excite all 6 DOF (Issac et al., 2007) and also to examine the combination of all control actuators.

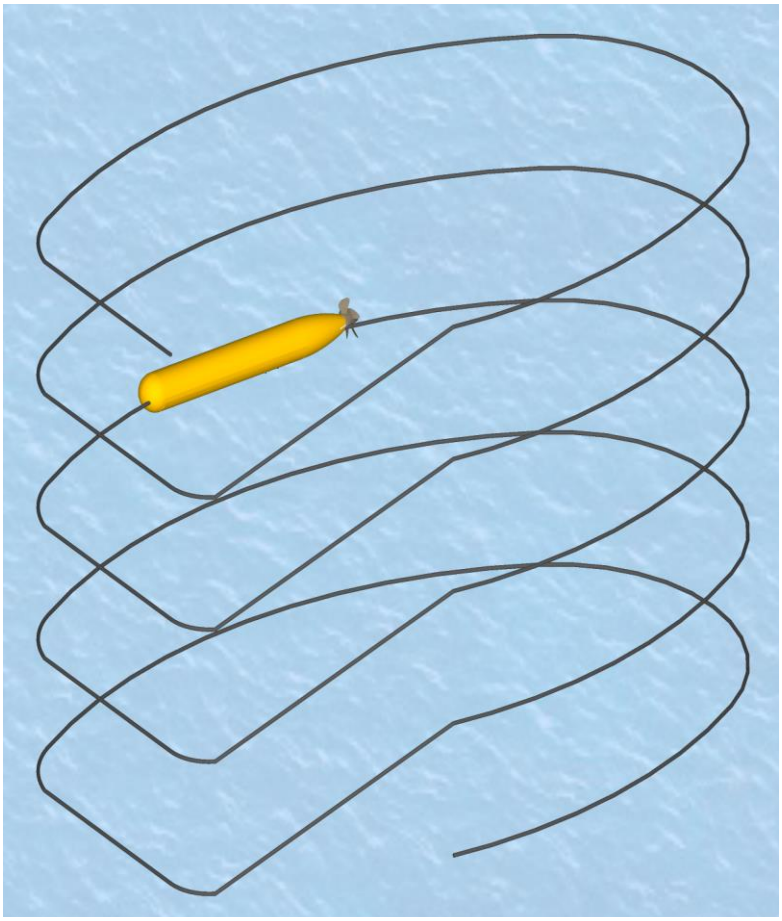

Figure 6.11. Spiral Manoeuvre Test.

6.3.10 Reverse Spiral

The rudder angle required to achieve a given yaw rate is determined. This is then repeated for a range of different yaw angles (Renilson, 2015).

6.4 Results and Discussion

In this section, the numerical simulation results for important manoeuvres are presented for both the conventional FPP and the CCPP propulsion system applied to the Gavia AUV platform. The analysis aims to investigate various manoeuvrability qualities of the two propulsion configurations and their impacts on the AUV manoeuvring. The manoeuvring performance is evaluated based on the typical parameters traditionally adopted in marine vehicle manoeuvring.

All the simulations were assumed to be conducted at a certain depth in which the effects of the free surface were rather small and could be neglected. The maximum collective pitch angle were selected for the most of the simulated scenario to stress the best performance characteristic. Nevertheless, in practical operation when the power consumption problem is of interest, the optimization process is needed to balance the manoeuvring capability and power efficiency. The lower collective pitch angle setting in the range of 50% to 75% would be more appropriate.

The selected manoeuvres for the simulation study are the most common manoeuvres to highlight the differences in performance between the two systems. The comparison is addressed and discussed thoroughly in the following section.

6.4.1 Acceleration Manoeuvre Test

In the acceleration test, the vessel starts with initial velocities $u_0 = v_0 = w_0 = 0$ and the commanded constant propeller revolution speed. The AUV simulation model was set with the commanded input propeller speeds of 500 RPM, 700 RPM and 900 RPM. The simulation time was about 50 seconds for each case.

Figure 6.12 and Figure 6.13 show the travel distance and forward speed of an AUV with FPP in the acceleration test. As can be seen in Figure 6.12, the maximum steady forward speeds are 1.2 m/s, 1.6 m/s and 2 m/s for the cases of 500 RPM, 700 RPM and 900 RPM respectively. The time taken to approach these maximum speeds is approximately 35 seconds as shown in Figure 6.13.

Figure 6.14 and Figure 6.15 show the travel distance and forward speed of an AUV with CCPP at 50% collective pitch setting in the acceleration simulation test. It can be seen in Figure 6.14, the maximum steady forward speeds are about 0.6 m/s, 0.82 m/s and 1.1 m/s for the cases of 500 RPM, 700 RPM and 900 RPM respectively. The time taken to approach these maximum speeds is approximately 25 seconds as shown in Figure 6.15.

Figure 6.16 and Figure 6.17 show the travel distance and forward speed of an AUV with CCPP at 100% collective pitch setting in the acceleration simulation test. In 100% collective pitch setting case, the CCPP generates the maximum thrust. It can be seen in Figure 6.16, the maximum steady forward speeds are about 1.05 m/s, 1.42 m/s and 1.9 m/s for the cases of 500 RPM, 700 RPM and 900 RPM respectively. The time taken to approach these maximum speeds is approximately 15 seconds as shown in Figure 6.17.

The AUV with CCPP has the lower acceleration time or faster response compared to the AUV with conventional FPP. At 900 RPM, the AUV with CCPP at 100% collective pitch angle achieves 1.9 m/s in 20 seconds. On the other hand, the AUV with FPP reaches 2 m/s distance within 30 seconds. Generally, the CCPP with its maximum collective pitch setting has a slightly higher obtained forward speed compared to the FPP at a given propeller rotational speed. However, the CCPP has a faster speed response as the control input signal is applied which suggests that the AUV with CCPP has a better acceleration capability. This feature is critical to the underwater vehicle operating in a confined environment at low speed condition.

The simulation data also show a linear increase in distance as the propeller rotational speed increases. During the acceleration manoeuvre, the AUV pitch and roll angle are in the limited regions. The Gavia AUV seems to have appropriate vertical stability in the tests with no tendency to increase the overshoot in both propulsion configurations. The travelling altitude is relatively constant. The heave velocity reaches to 0.2 m/s as the AUV starts to move and then drops to nearly 0 m/s as the AUV attains a steady state surge velocity.

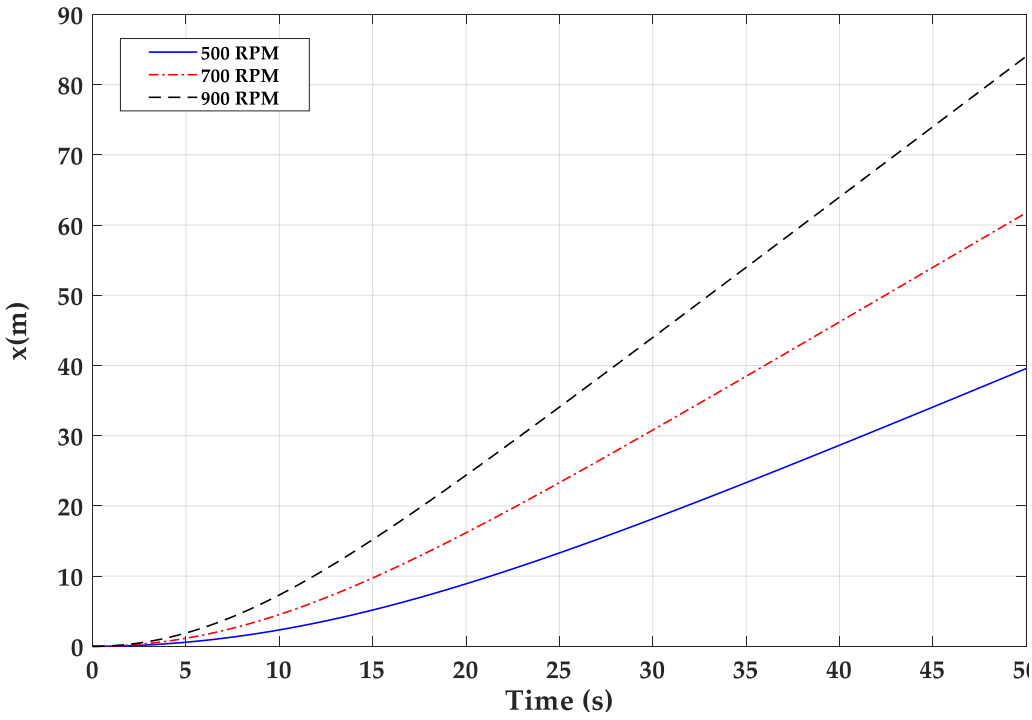

Figure 6.12. The travel distance of an AUV with FPP in the acceleration simulation test.

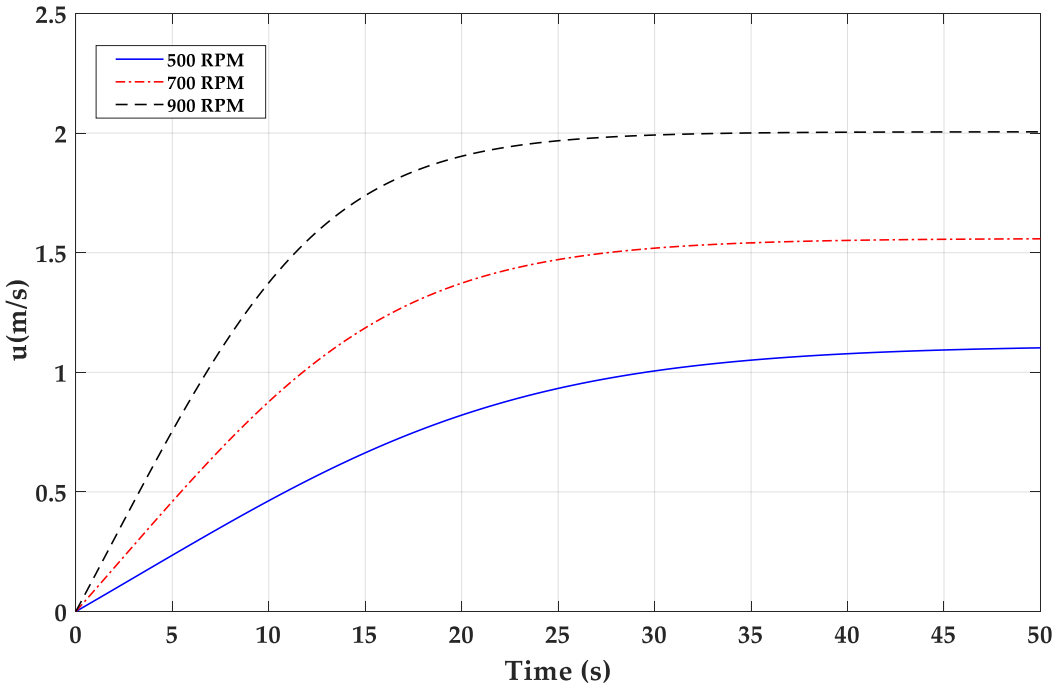

Figure 6.13. The forward speed of an AUV with FPP in the acceleration simulation test.

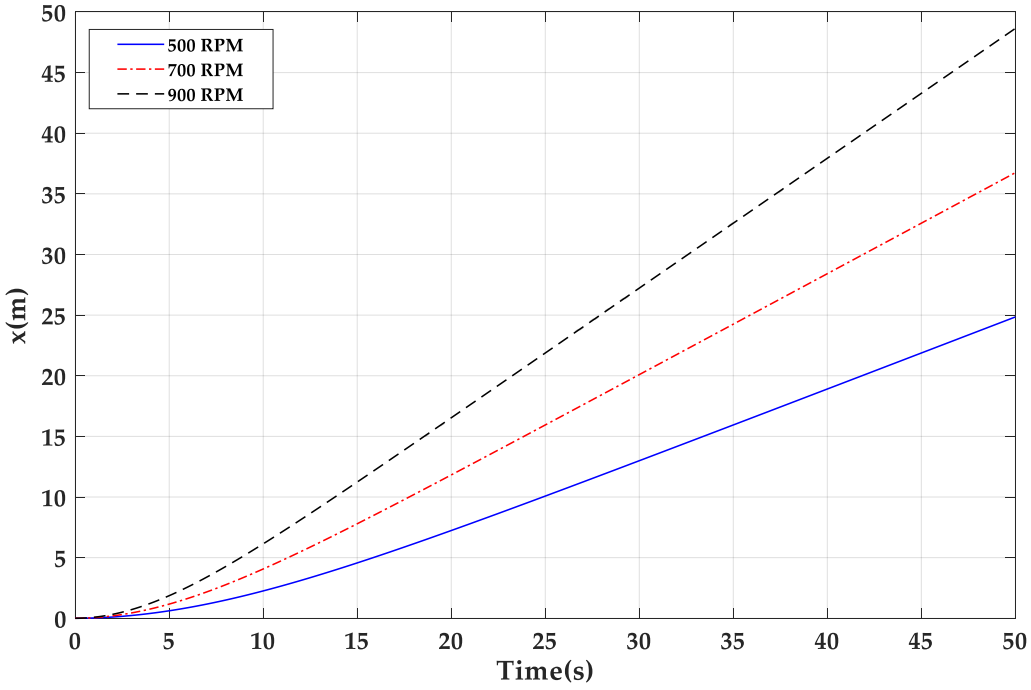

Figure 6.14. The travel distance of an AUV with CCPP at 50% collective pitch setting in the acceleration simulation test.

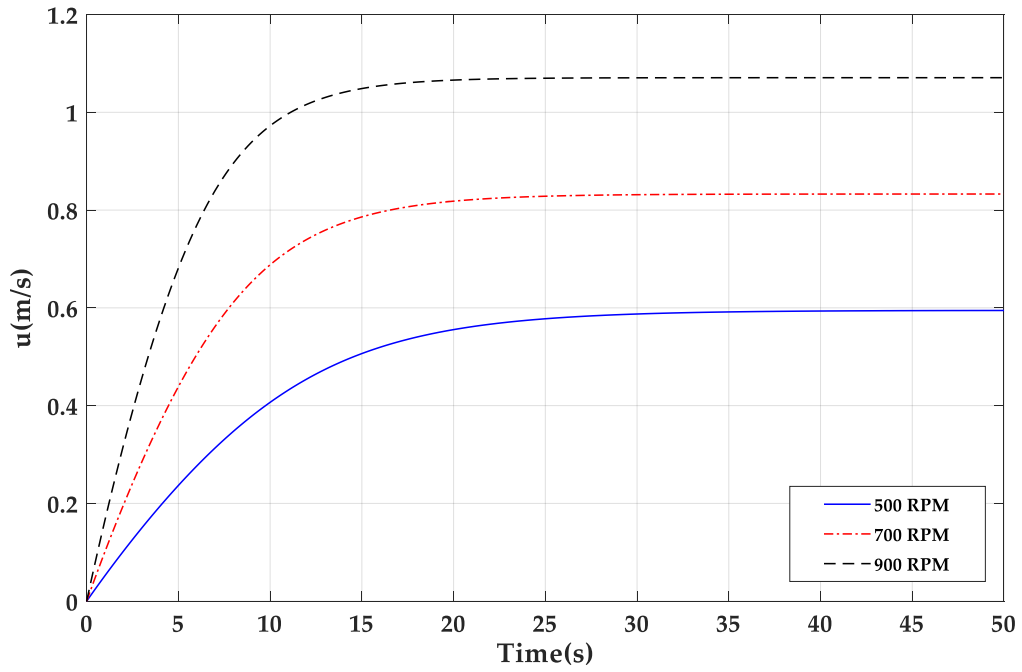

Figure 6.15. The forward speed of an AUV with CCPP at 50% collective pitch setting in the acceleration simulation test.

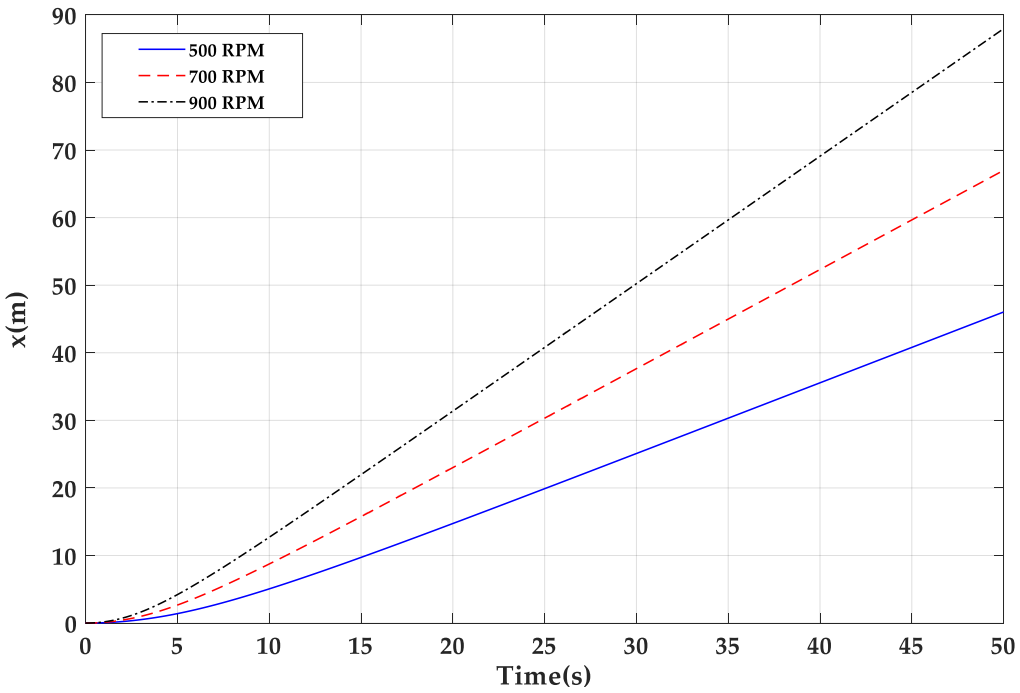

Figure 6.16. The travel distance of an AUV with CCPP at 100% collective pitch setting in the acceleration simulation test.

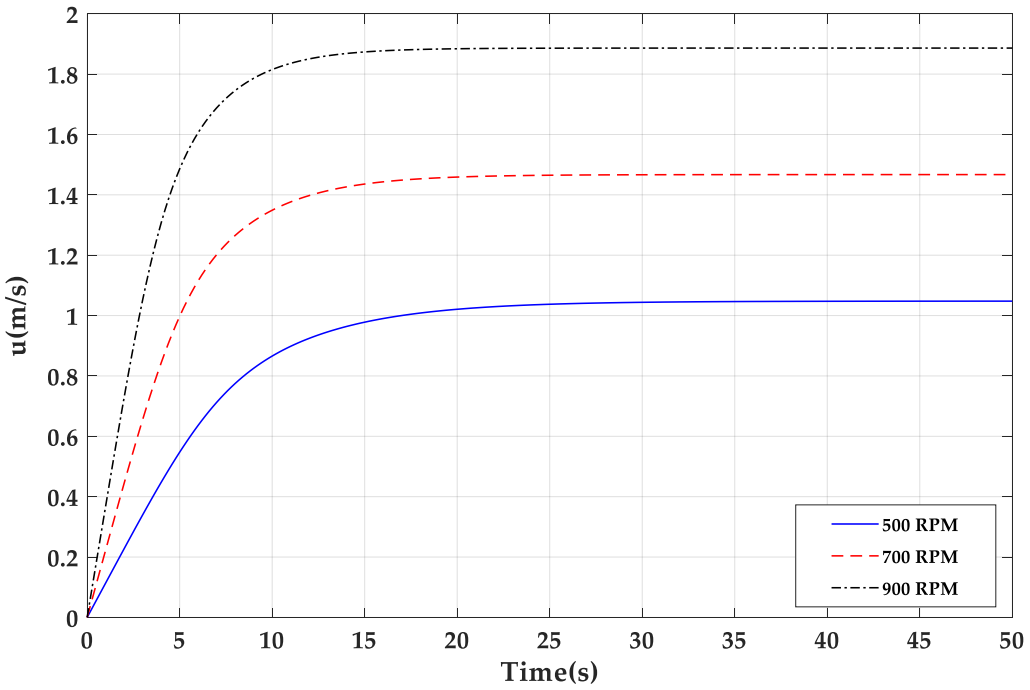

Figure 6.17. The forward speed of an AUV with CCPP at 50% collective pitch setting in the acceleration simulation test.

6.4.2 Stopping Manoeuvre Test

In stopping test simulation, the AUV was forced to stop from the steady forward velocity of 1.5 m/s. The simulation time was about 50 seconds for each case. The results of the deceleration and stopping of Gavia AUV with conventional FPP and CCPP propulsion system follow an expected pattern in the simulation.

To decelerate and stop an underwater vehicle with the conventional FPP propulsion, a crashback on the FPP was applied. In the crashback manoeuvre, the FPP rotational speed is reversed to negative value as the AUV is moving forward and the control surfaces are at neutral position. The stopping distance and stopping time versus propeller rotational speed RPM for the AUV with FPP in the stopping simulation test are shown in Figure 6.18 and Figure 6.19, respectively. It can be seen in Figure 6.18, the stopping distance values are about 18 m, 22 m, and 27 m for the cases of -500 RPM, -300 RPM, and -100 RPM, respectively. The corresponding stopping time

values shown in Figure 6.19 are 15 seconds, 20 seconds, and 23 seconds. The results show that the distance and time to stop is highly depend on the propeller negative rotational speeds.

Figure 6.20 and Figure 6.21 show stopping distance and stopping time versus cyclic pitch angle for the AUV with CCPP in the stopping simulation test. As can be seen in Figure 6.20, at CCPP rotational speed 300 RPM, the stopping distance values are about 13 m, 21 m, and 22 m for the cases of -100%, -50%, and -25%, respectively. At rotational speed 500 RPM, the stopping distance values are about 7 m, 11 m, and 12 m for the cases of -100%, -50%, and -25%, respectively. The distance and time to stop are depend on not only the propeller rotational speeds but also the cyclic pitch angle.

The minimum time to stop for the CCPP as shown in Figure 6.21 is 8 seconds. In this case, it takes approximately three vehicle's lengths to stop. The CCPP's minimum stopping time value is just haft of the FPP's value. The shorter stopping distance and time are due to the faster deceleration rate. The CCPP has a higher deceleration rate as the reversed thrust from CCPP rapidly increases by changing the collective pitch angle. For the FPP, the motor has to stop and the thrust in reverse direction gradually increases as the rotational speed increases.

The stopping manoeuvre for both propulsion configuration could also be conducted by simply switching off the propeller speed. During this time, the AUV decelerates and stops mainly due to the hull frictional resistance. The simulation also shows that the vehicle was able to hold a consistent depth during the stopping manoeuvre. The simulated depth values were around the initial depth since the buoyancy force was adjusted to be equal the weight and the ability to keep balance of the vehicle. This feature is important for the intervention task in which the vehicle is required to approach the exact location in a working area or to stop at the exact recovery position.

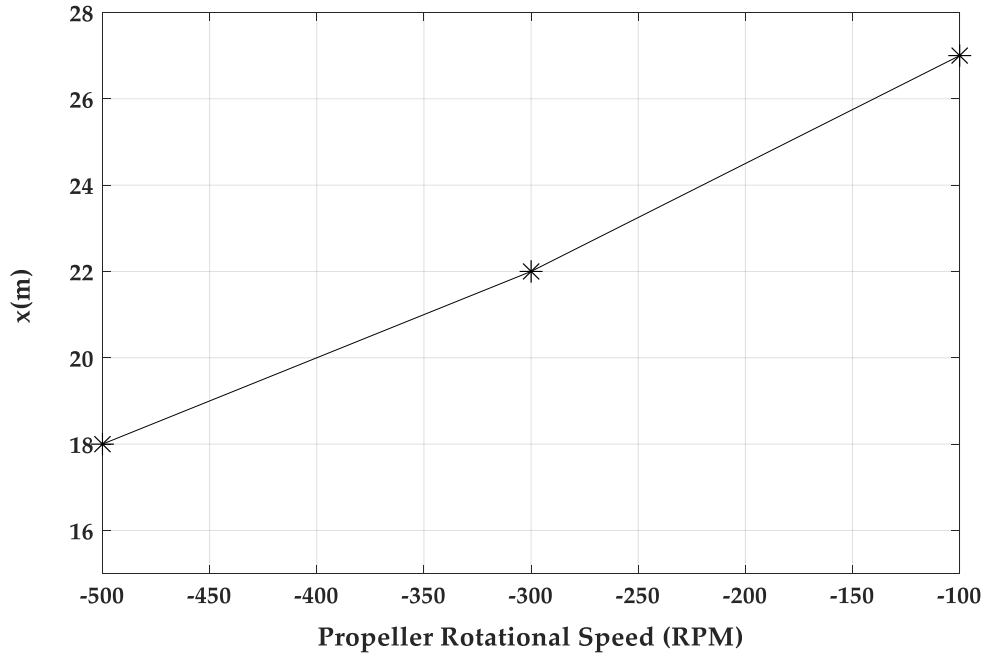

Figure 6.18. The stopping distance versus propeller RPM for the AUV with FPP in the stopping simulation test.

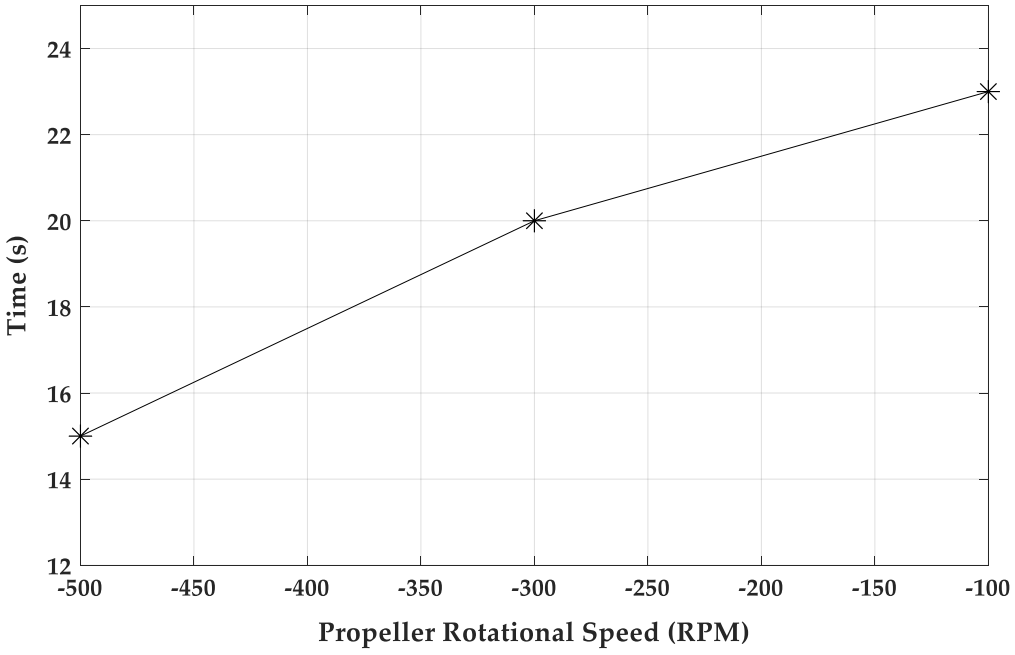

Figure 6.19. The stopping time versus propeller RPM for the AUV with FPP in the stopping simulation test.

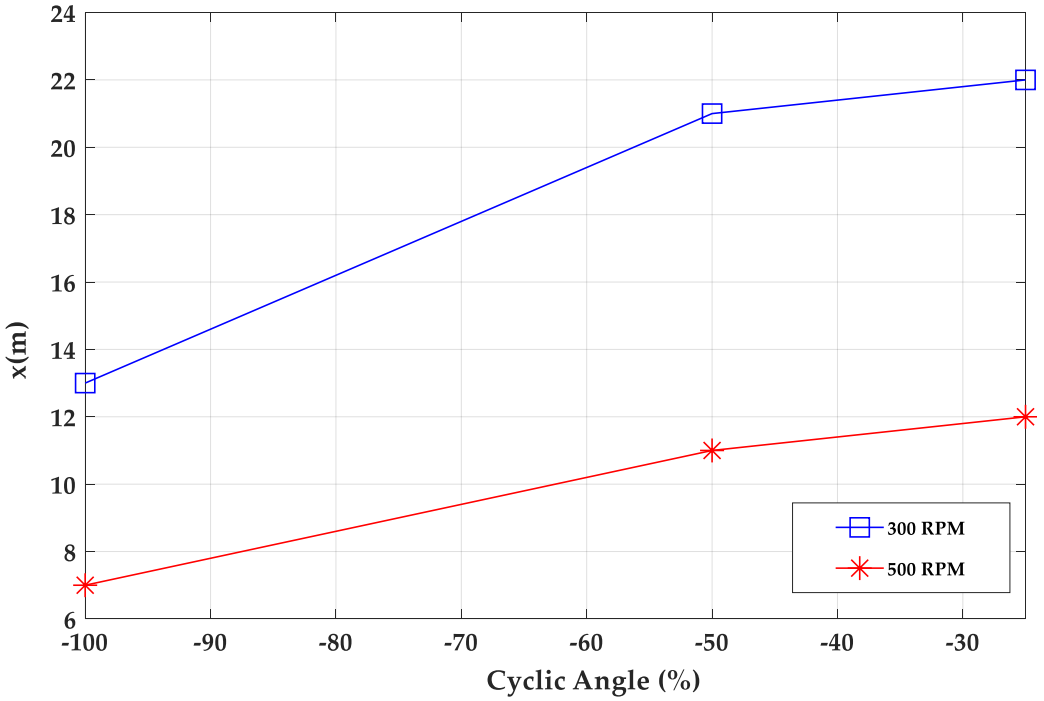

Figure 6.20. The stopping distance versus cyclic angle for the AUV with CCPP in the stopping simulation test.

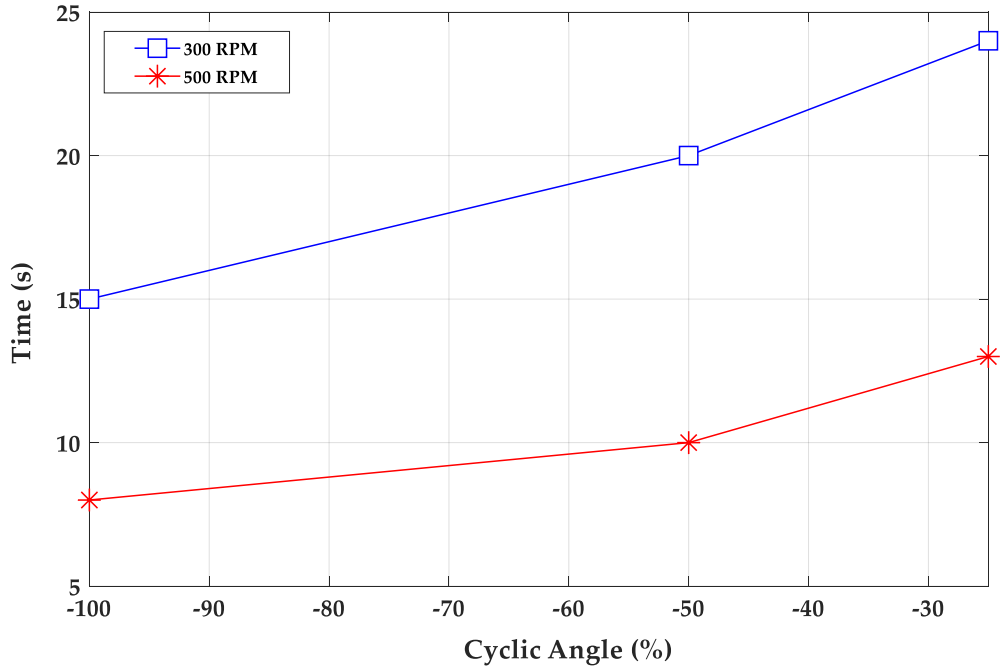

Figure 6.21. The stopping time versus cyclic angle for the AUV with CCPP in the stopping simulation test.

6.4.3 Static Turning Manoeuvre

The turning characteristics of an AUV at low speed are characterised based on the static turning manoeuvre. The standard parameter measured was the steady turning diameter d. In this section, a series of runs was conducted to characterise the turning performance of the AUV equipped with FPP and CCPP.

The AUV starts the static turning manoeuvre at a constant depth by maintaining a constant control surface angle or a steady cyclic pitch angle in the case of the CCPP from the stationary condition.

The results for the turning diameter of the Gavia AUV equipped with conventional FPP propulsion system are shown in Figure 6.22. In this plot, the variation of the turning diameter is plotted versus the average control surface deflection angles at different propeller rotation speeds. In the simulation, the average control surface deflection angle were applied to all four planes, which are 5°, 10°, 15°, and 20°.

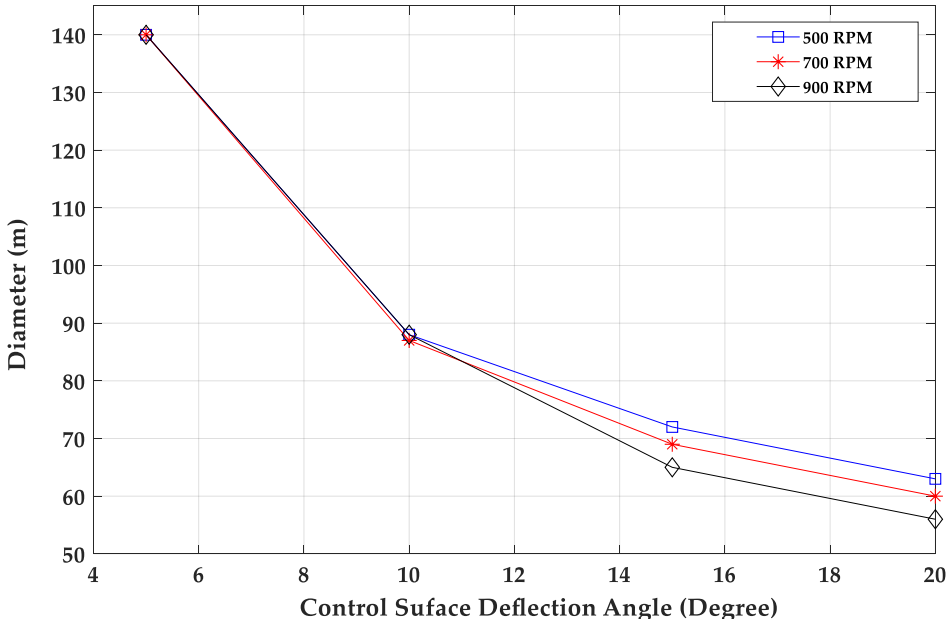

Figure 6.22. The turning diameter versus deflection angle for the AUV with FPP.

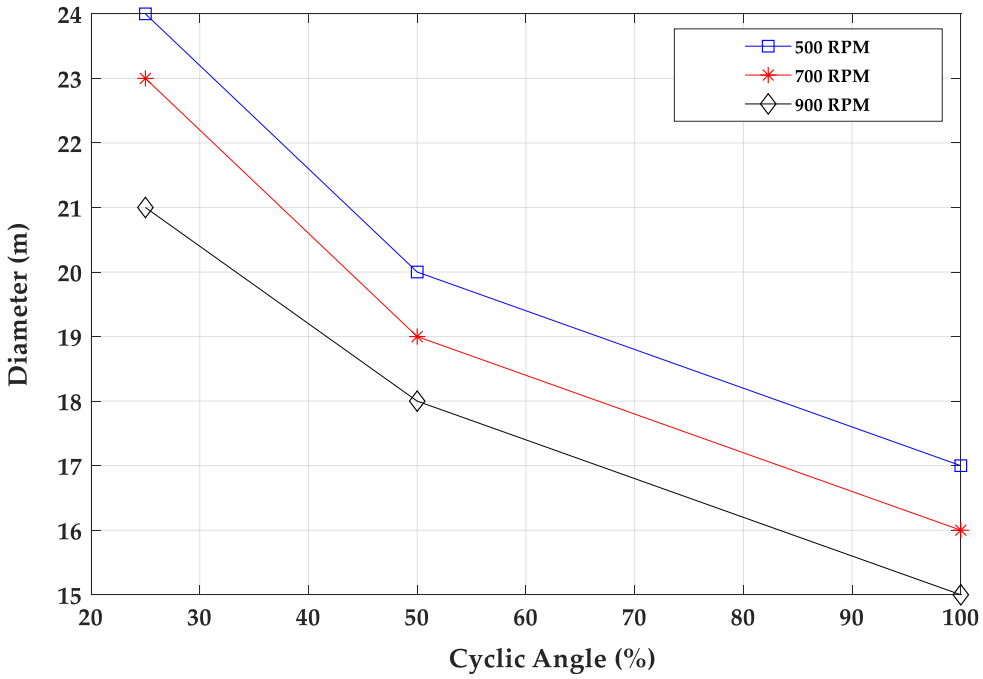

Figure 6.23. The turning diameter versus cyclic angle for the AUV with CCPP.

It can be seen from Figure 6.22 that the turning diameter becomes smaller for the larger control surface deflection angle. The maximum turning diameter is about 140 m at 5^0 deflection for all four speeds and the minimum turning diameter is 55 m at 20^0 deflection angle and 900 RPM. It is also be noted that the turning diameter does not depend notably on the propeller rotation speed or the surge. For the small deflection angles, the examined diameters are identical. For the larger deflection angle, the turning diameter increases as the rotation speed increases. Hence, for the AUV equipped with conventional FPP propulsion system, the deflection angle has a significant impact on the turning characteristics of the AUV compared to the vehicle speed. In addition, there is the speed loss as the turn progresses. In practice, this speed loss is expected and due to the combined effects of the added drag on the hull due to cross flow as well as the added drag due to the rudder deflection (Heberley, 2011).

The results for the turning diameter of the Gavia AUV equipped with CCPP propulsion system are shown in Figure 6.23. In this plot, the variation of the turning diameter is plotted versus the

cyclic pitch angle at different propeller rotation speeds. In the simulation, three cyclic pitch angles were investigated, which are at 25%, 59%, and 100%. The collective pitch angle was kept constant at 100%.

Similar to the FPP, it can be seen from Figure 6.23 that the turning diameter becomes smaller for the larger cyclic pitch angle. The maximum turning diameter is about 23 m at 25% cyclic pitch angle and 500 RPM. The minimum turning diameter is 15 m at 100% cyclic pitch angle and 900 RPM. For the AUV equipped with CCPP propulsion system, both the cyclic pitch angle and the CCPP rotation speed have a significant impact on the turning characteristics of the AUV. The turning diameter increases as the CCPP rotation speed increases.

It can be seen from Figure 6.22 and Figure 6.23 that the AUV with CCPP has a greater turning characteristic in the static turning manoeuvre. The minimum turning diameter for the AUV with CCPP is 15 m, which is significantly smaller than that of the AUV with FPP. The turning quality of the CCPP configuration is superior with respect to the FPP since the side force from CCPP is generated instantly as the CCPP is rotating. On the other hand, the side force from the conventional FPP propulsion system is gradually generated as the AUV speed increases from the start.

For the verification of simulated results in this section, the non-dimensional turning coefficient is used. The non-dimensional turning coefficient d' is defined as

$$d' = \frac{d}{l}$$

where l is the total length of the AUV and d is the turning diameter.

The ISiMI AUV has the minimum $d' = \frac{12}{1.2} = 10$ (Jun et al., 2009). The MUN AUV has $d' = \frac{23}{1.5} = 15.3$ (Issac et al., 2007). In our study, the Gavia AUV with FPP has the minimum $d' = \frac{55}{2.5} = 22$, the Gavia AUV with CCPP has the minimum $d' = \frac{15}{2.5} = 6.$

6.4.4 Zigzag Manoeuvre

The simulation results for the zigzag manoeuvre test are presented in this section. Zigzag manoeuvres are an indicative of the controllability of the vehicle (Issac et al., 2007). The main interest of this manoeuvre test is to evaluate the performance of the propulsion system in generating the continuous side forces used for heading control.

The zigzag tests are conducted with the 20-degree variation in heading angle and at a defined constant propeller rotational speed. The manoeuvre test is called the 20/20 horizontal zigzag test. For the AUV with FPP, the control surfaces were controlled to oscillate between the average deflection angles of -20 degree and 20 degree. All four control surfaces rotate simultaneously. For the CCPP, the blades are controlled in the horizontal cyclic pitch setting in the range of -20% to 20%. Once the vehicle reaches a steady surge, the control surfaces and cyclic pitch setting are enabled to generate the horizontal side forces. The estimation results of trajectory for the Gavia AUV equipped with FPP and CCPP in the zigzag test are plotted in Figure 6.24.

The simulation results show that the overshoot angles for both configurations are in the range of 3 to 6 degree. It can be seen from Figure 6.24 that the heading angle of the AUV with CCPP has a smaller overshoot angle when compared to the AUV with conventional FPP.

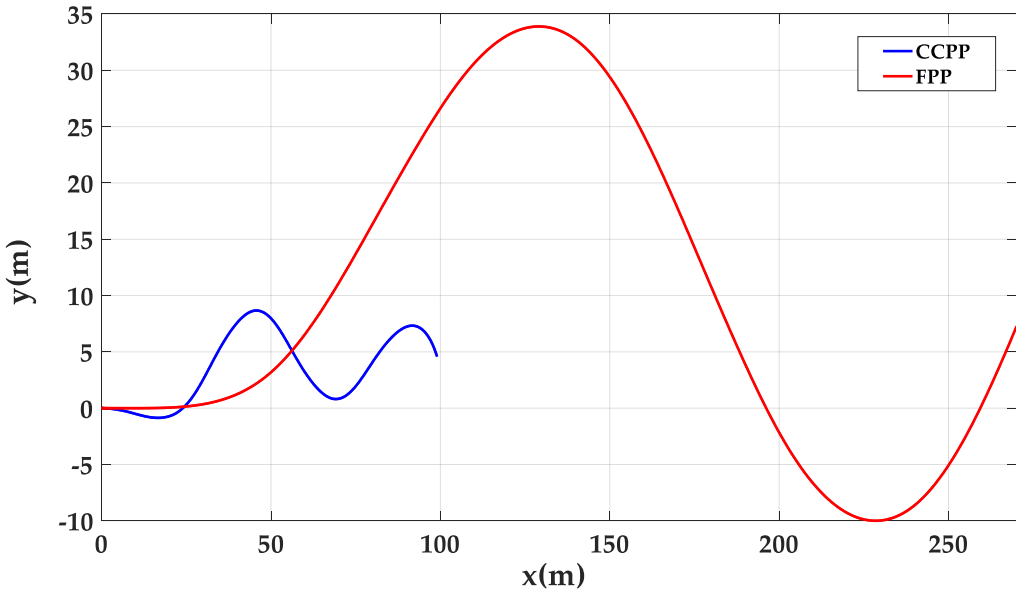

Figure 6.24. Zigzag test of AUV equipped with FPP and CCPP.

In addition, for the FPP, the commanded amplitude and cycle-length for the zigzag are about 34 m and 60 m respectively. For the CCPP, the commanded amplitude and cycle-length are approximately 10 m and 30 m. The smaller cycle-length and smaller overshoot mean that the CCPP has the better manoeuvring capability by combining continuous thrust and side forces in heading control. The reason is the effect of the side force magnitude of the CCPP is higher and especially the faster response of the side force from CCPP compared to FPP. It is also noted that in the AUV with CCPP configuration, the vehicle's state variables in heave direction were not significantly influenced as the zigzag manoeuvre was conducted. Moreover, in the zigzag manoeuvre test the forward velocity of the AUV decreases from the cruising velocity to an unsteady velocity during the turning. This reduction in speed is expected due to the increasing of drag in such a manoeuvre.

The zigzag test simulation for the AUV equipped with CCPP at low propeller rotational speed 100 RPM and small collective pitch setting of 20% was conducted. It was found that the AUV has the lower cycle-length of 45% compared to the previous case with maximum collective pitch

setting and high RPM. Hence, it is proved that the CCPP is capable of providing low enough continuous thrust to enable the low speeds desirable for precision manoeuvring and inspection tasks.

6.4.5 Depth-Changing Manoeuvre

For the comparison of the depth changing abilities between the AUV equipped with FPP and with CCPP, the following manoeuvre is conducted. To address the comparison between the two configurations, the depth variation in time series under the input control signal was simulated and analysed.

In the depth-changing manoeuvre simulation, the AUV's pitch angle was limited to 20 degree. The AUV was initially set to travel a straight course while the control surface and cyclic angle were executed to cause the vehicle to descend at the 25 second. After 10 seconds, the actuators were set back to the neutral position. The simulation was set to about 75 seconds.

The time history of depth for the Gavia AUV with FPP propulsion system are shown in Figure 6.25. The depth variable is presented as the function of the propeller rotational speed and control surface deflection angle. It can be seen from Figure 6.25 that the larger depth are obtained for the higher rotational speed and deflection angle.

Figure 6.26 shows the variation of depth change for the Gavia AUV with CCPP propulsion system. The depth variable is presented as the function of the propeller rotational speed and the vertical cyclic pitch angle. In this manoeuvre, the collective pitch angle was controlled to 100% setting for the maximum thrust generation at a given CCPP rotational speed. As can be seen on the Figure 6.26, after the first execution of the cyclic setting, the AUV starts to descend after a time delay of approximately 4 seconds. It can be seen from Figure 6.26 that the larger depth are obtained for the higher rotational speed and cyclic pitch angle.

It is obvious that the magnitude of obtained depths are much higher for the CCPP configuration than for the FPP configuration with a given propeller rotational speed in a specific time. For example, the CCPP configuration with 100% cyclic pitch setting and rotational speed of 700 RPM is able to reach the 20 meter depth in 18 seconds. On the other hand, the FPP configuration with 20 degree deflection angle and similar rotational speed attains 20 meter depth in approximately 40 seconds. The fundamental difference between two configurations is the quicker response of the CCPP as the control signal is executed. In both configurations, the pitch angle oscillates at the beginning of simulation, but get stable and fluctuate narrowly around neutral position. The AUV with CCPP is capable of achieving the pitch faster than the FPP from the start. Nevertheless, the CCPP with maximum collective pitch setting generates slightly lower thrust compared to the FPP at a given propeller rotational speed in the diving manoeuvre.

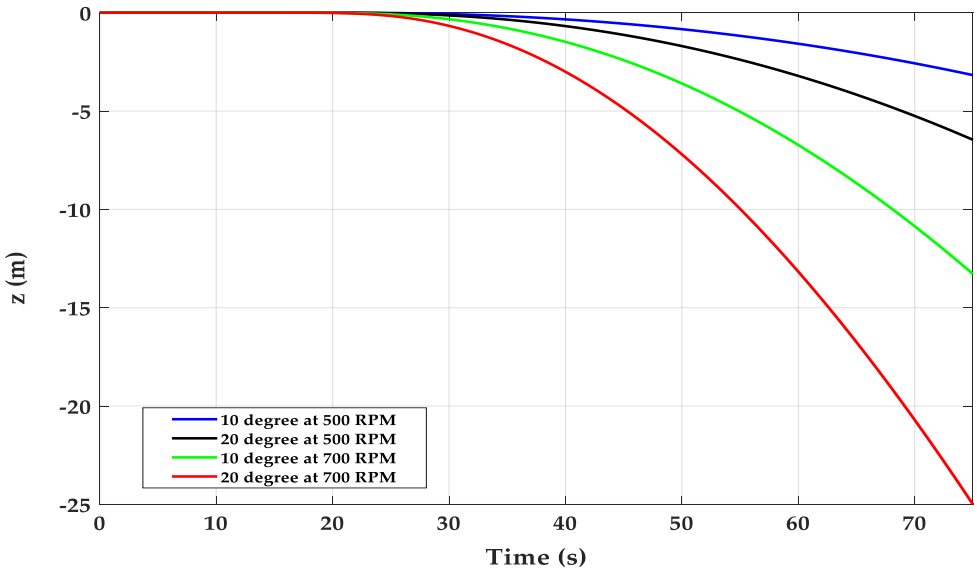

Figure 6.25. The depth change simulation data for the AUV with FPP.

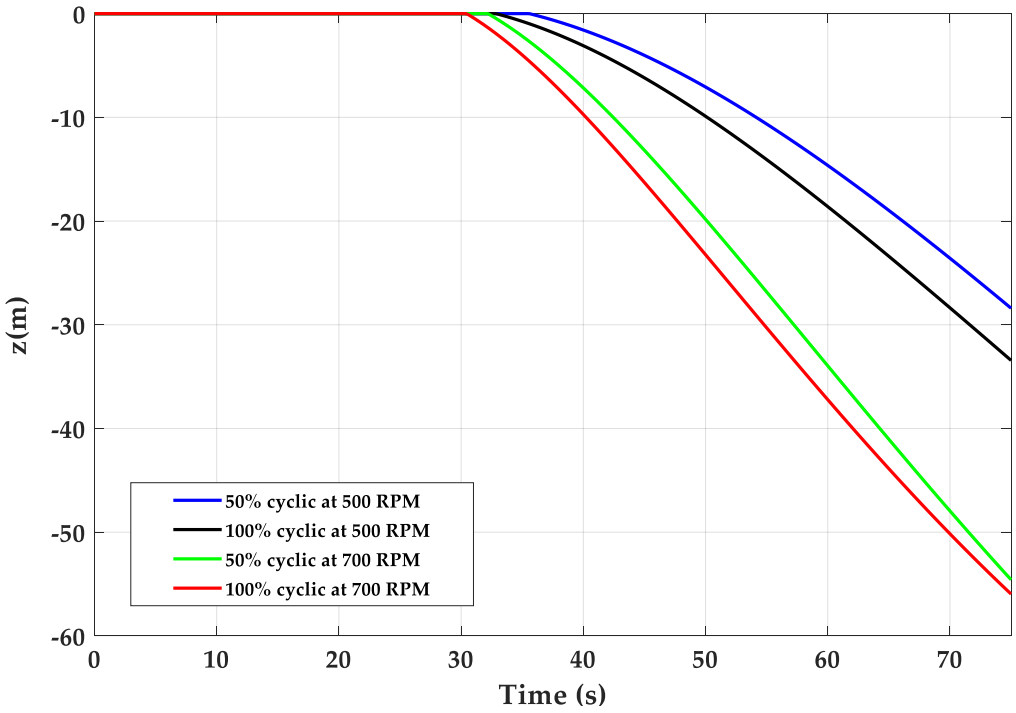

Figure 6.26. The depth change simulation data for the AUV with CCPP.

6.5 Summary

In this chapter, the simulation results of the manoeuvring performance of the Gavia AUV equipped with CCPP propulsion system were compared against the Gavia AUV equipped with conventional FPP propulsion system. The main objective of this exercise was to find an answer to the research question, which propulsion system is more efficient for propelling a AUV in different manoeuvring tests.

A simulator for an underwater vehicle named AUVSIPRO was constructed in MATLAB/Simulink™ environment. This program is developed with the emphasis on the performance prediction of an underwater vehicles equipped with different propulsion systems in the early design stage. The AUVSIPRO could also be extended to adapt to a variety of underwater vehicles and propulsion systems for the simulation study.

The simulation results indicated that the AUV equipped with CCPP provided better manoeuvrability in comparison to the AUV equipped with conventional FPP propulsion system. In the considered manoeuvring tests, the CCPP outperformed the FPP in most of the examined parameters and variables. Five separate fundamental manoeuvring tests were presented to demonstrate the performance differences between the two configurations. A preliminary analysis was conducted based on the obtained results from simulation study. In the acceleration test, the results indicated that the CCPP propulsion had an advantage for high acceleration rate; meanwhile the conventional FPP propulsion was beneficial better steady forward speed. In the static turning manoeuvre and zigzag test, there was a clear advantage with respect to the CCPP configuration in terms of heading changing ability. The shorter stopping distance and time were due to the faster deceleration rate in the stopping test showed the better stopping performance of CCPP. The simulation results revealed that the CCPP had the superior diving characteristic in the vertical plane.

CHAPTER 7

CONTROL APPLICATION

The final objective of the thesis is to execute the AUV equipped with CCPP in autonomous missions, thus the control application is considered in this chapter. While there exist numerous works on the control of AUV, there are a few works existing for the control of an AUV with the configuration similar to CCPP. The complex, inherently unstable and nonlinear nature of AUVs poses significant challenges for design and implementation of a controller. The nonlinear system obtained from previous chapters is linearized to provide an approximation to the system dynamics that is more approachable for control synthesis. Since the linear model of Gavia AUV is of interest, it is more accurate to obtain the validated model directly from the experimental data using SI compared to the first principle modelling approach discussed in Chapter 3. This approach is a relevant technique to determine the practical AUV model for designing controllers. Chapter 7 includes the system identification (SI) of the Gavia AUV platform and the controller design for an AUV equipped with CCPP.

To design a successful controller, it is essential to capture the AUV dynamics as accurate as possible. In the first section, the two-stage identification of mathematical models governing dynamics in both vertical and horizontal planes for an axisymmetric torpedo shaped AUV are presented. The experimental data used for the system identification study are acquired from the

AUV on-board sensors during the field trails. The general equations for six degrees of freedom motions are decoupled into non-interacting longitudinal and lateral subsystems in the form of linear state space models with unknown parameters. Rather than roughly identifying the model parameters during a certain period of time in one stage computation, the identified model is optimised subsequently based on least squares algorithm in this study. The objective of the two-stage system identification is to estimate simulator's coefficients for reasonably predicting the vehicle performance over time from a given initial condition. The accuracy of the identified model was verified by simulation in time domain, using a set of different trial data.

The second section of this chapter aims to design an optimal state feedback controller using the Linear Quadratic Regulator for an AUV equipped with CCPP. The development of the control algorithms has a certain challenge due to the multivariable character of the problem. The non-interacting longitudinal and lateral subsystems in the form of linear state space models obtained from SI section are utilised. The propulsor dynamic models are linearised from the empirical models in chapter 4 and 5. The control objectives are to maintain the autonomous underwater vehicle at desired depth and heading with the CCPP. The performance of the controller is demonstrated by simulation using MATLAB/Simulink™.

Part of this chapter has been published in "*Proceedings of the 3rd Vietnam Conference on Control and Automation*" and in "*Proceeding of the 2017 Asian Control Conference in Gold Coast, Australia*". The citations for the conference journals are:

Minh Tran, Supun A.T. Randeni, Hung D. Nguyen, Jonathan Binns, Shuhong Chai and Alex Forrest, Least Squares Optimisation Algorithm Based System Identification of an Autonomous Underwater Vehicle, *Proceedings of the 3rd Vietnam Conference on Control and Automation*, Vietnam, 2015.

Tran M, Binns J, Chai S, et al. (2017). Optimal control of an autonomous underwater vehicle equipped with the collective and cyclic pitch propeller. *Control Conference (ASCC), 2017 11th Asian.* IEEE, 354-359.

7.1 System Identification

7.1.1 Introduction

With the objective of assessing the high-fidelity simulation of AUV with different propulsion configurations, this section develops a two-stage system identification (SI) algorithm in order to accurately and rapidly identify the hydrodynamic coefficients of the AUV mathematical linear model. A precise dynamic model of an underwater vehicle is also essential for accurate autopilot control and navigation system design.

Obtaining accurate model of an underwater vehicle is considerably complicated. There are four fundamental methods to determine a mathematical model of an underwater vehicle. The first method is an analytical approach to calculate the hydrodynamic coefficients by using empirical equations and component build-up method (Prestero, 2001a). This method is a class of the first principle approach discussed in chapter 3. The second is using Experimental Fluid Dynamic (EFD) methods such captive model experiments (Ridao et al., 2001). The third method is conducting Computational Fluid Dynamic (CFD) simulations to replicate the EFD testings (Phillips et al., 2007; P. et al., 2015) and the final one is SI which is employed in this chapter. In the SI method, the hydrodynamic coefficients that characterise the vehicle dynamics of an AUV could be estimated using data acquired by on-board sensors from free running field trials (Avila et al., 2013). The analytical and CFD approaches are generally used in the preliminary design stage to estimate hydrodynamic coefficients of AUV based on the empirical equations and the vehicle geometry. The use of EFD such as the experiment in the towing tank or model test basin requires extensive time and high cost for the setup and testing. On the other hand, SI method can be effectively used to determine the parameters of a fully developed vehicle. This approach provides the dynamic model with the high degree of fidelity since the experimental data utilised

for modelling are acquired under real operational conditions. Also, the variation of the hydrodynamic coefficients due to changes in the external configuration of a modular underwater vehicle in a specific mission (for example, in a case of adding an extra payload module to the base vehicle configuration of the vehicle) can be rapidly determined using SI. For that reason, the SI approach is versatile and cost effective. However, there are some practical concerns associated with performing system identification on AUVs. The first is that the experimental data were collected in the presence of noise and turbulence. Despite relatively calm wind and water conditions at test site, there are external influences to a certain degree. The noise could result in an increased variance in the least squares parameter estimation. Therefore the SI approach requires the physical system to be sufficiently instrumented in order to accurately measure the necessary state variables with minimum noise effects. The second issue is the estimation of mathematical model relied on the data collected from close-loop feedback control system which may cause the immeasurable noise to be correlated with the input (Ljung, 1998).

In the literature, there have been a wide range of SI algorithms developed for the underwater vehicle, including Least Squares (LS), Extended Kalman filter (Kim et al., 2002; Sabet et al., 2014), Maximum Likelihood and Neural Network (Badillo and Ceron; Shafiei and Binazadeh, 2015) for both offline and online applications. These methods generally minimises the errors between vehicle state variables predicted by the dynamic model and actual measured state variables. A compromise between complication and accuracy was considered to determine an appropriate method for the study. Since the underwater vehicle nonlinear dynamic equations of motion can be expressed in state space models linearized in the range of the cruising conditions, the LS algorithm is prevalent and effective for the practical system identification. It is able to be derived in the offline condition, the Ordinary or Weighted Least Squares, and in the online condition, the Recursive Least Squares. While there has been a significant amount of published works on LS technique for open frame ROVs (Avila et al., 2013; Martin and Whitcomb, 2014; Weiss and

Du Toit, 2013; Xu et al., 2015; Avila et al., 2008), studies for torpedo-shaped AUVs are limited, which are carried out in horizontal plane for steering subsystem (Hegrenaes et al., 2007; Eng et al., 2016) and vertical plane for diving subsystem respectively (Petrich et al., 2007) .

This thesis utilises the offline LS algorithm to derive an experimentally validated state space model that is able to describe the manoeuvring characteristics of a torpedo shaped AUV for both steering and diving subsystems. The experimental data used for the system identification study are acquired from the on-board sensors during the field trails. The proposed SI approach consists of two stages, which are comprehensively described in the next sections. Instead of estimating the hydrodynamic coefficients and predicting the system response based on the state variables in a given time period, the simulator with optimised hydrodynamic coefficients resulted from the proposed procedure is able to simulate system response from specific initial conditions in the time domain to meet the desired requirements. This approach is slightly different from previous studies on system identification of underwater vehicle and it is the main contribution of this section.

7.1.2 Linear Mathematical Model

There is a large number of linear as well as nonlinear hydrodynamic derivatives presented in the 6-DOF mathematical model of the AUV. Therefore, the identification of the complete set of coefficients is rather complex task. That is the reason why the assumptions should be made to simplify it. A widely used approximation can be achieved if it is assumed that the hydrodynamic force function $f(\boldsymbol{\nu},\boldsymbol{\theta},\mathrm{t})$ consists of the linear drag forces only, the hydrostatic force function $g(\boldsymbol{\nu},\boldsymbol{\theta},\mathrm{t})$ consists of the buoyancy forces only and if the inertia matrix including the added mass is time-space invariant and diagonal (Tiano et al., 2007).

The complete 6-DOF can be decomposed into three essentially non-interacting subsystems constituted by (a) the lateral subsystem, (b) the longitudinal subsystem and (c) the speed subsystem. These subsystems combined will provide an overall picture of the hydrodynamics of the AUV. This traditional approach is applicable in practice for streamlined torpedo-shaped AUVs when the coupling between subsystems is weak and may be reasonably neglected without serious loss of information (Hong et al., 2013; Caccia et al., 2000). In this work, the lateral subsystem and longitudinal subsystem are of specific interest.

The additional assumptions in the horizontal plane (x-y plane) and the vertical plane (x-z plane) for decoupled subsystems respectively are given in Table 7.1 as follows (Hong et al., 2013; Jalving, 1994):

Table 7.1. Assumptions in horizontal and vertical planes.

Horizontal plane (Lateral subsystem)	**Vertical plane (Diving subsystem)**
Heave velocity $w = 0$	Sway velocity $v = 0$
Roll angle $\phi = 0$	Roll angle $\phi = 0$
Pitch angle $\theta = \text{constant}$, $\dot{\theta} = 0$	Yaw angle $\psi = \text{constant}$, $\dot{\psi} = 0$
For small roll and pitch angles, $\dot{\psi} = \frac{\sin\theta}{\cos\theta} q + \frac{\cos\phi}{\cos\theta} r \approx r$	For small pitch angle, $\dot{\theta} = q$

Finally, under the assumption of constant forward speed $u \approx U_0$, a corresponding set of linearized time-invariant models are derived in horizontal plane and vertical plane respectively are presented as follows:

The lateral subsystem:

$$\begin{bmatrix} I_{zz}-N_{\dot{r}} & 0 \\ 0 & 1 \end{bmatrix}\begin{bmatrix} \dot{r} \\ \dot{\psi} \end{bmatrix}+\begin{bmatrix} -N_r & 0 \\ -1 & 0 \end{bmatrix}\begin{bmatrix} r \\ \psi \end{bmatrix}=\begin{bmatrix} N_{\delta 1} \\ 0 \end{bmatrix}\delta_1+\begin{bmatrix} N_{\delta 2} \\ 0 \end{bmatrix}\delta_2+\begin{bmatrix} N_{\delta 3} \\ 0 \end{bmatrix}\delta_3+\begin{bmatrix} N_{\delta 4} \\ 0 \end{bmatrix}\delta_4 \tag{7.1}$$

The longitudinal subsystem:

$$\begin{bmatrix} I_{yy}-M_{\dot{q}} & 0 & 0 \\ 0 & 1 & 0 \\ 0 & 0 & 1 \end{bmatrix}\begin{bmatrix} \dot{q} \\ \dot{\theta} \\ \dot{z} \end{bmatrix}+\begin{bmatrix} -M_q & \overline{BG_z}W & 0 \\ -1 & 0 & 0 \\ 0 & U_0 & 0 \end{bmatrix}\begin{bmatrix} q \\ \theta \\ z \end{bmatrix}=\begin{bmatrix} M_{\delta 1} & M_{\delta 2} & M_{\delta 3} & M_{\delta 4} \\ 0 & 0 & 0 & 0 \\ 0 & 0 & 0 & 0 \end{bmatrix}\begin{bmatrix} \delta_1 \\ \delta_2 \\ \delta_3 \\ \delta_4 \end{bmatrix} \tag{7.2}$$

where I_{yy}, I_{zz} are the moment of inertia, $\overline{BG_z}$ is the distance between the centre of gravity and the centre of buoyancy; $N_{\dot{r}}, N_r, N_{\delta i}, M_{\dot{q}}, M_q, M_{\delta_i}$ are the hydrodynamic derivatives. They are the partial derivatives of the forces and moments with respect to the corresponding accelerations, velocities or control surface deflection, e.g. $N_r := \frac{\partial N}{\partial r}$

Equation (7.1) and (7.2) are presented in state space model for computational convenience below:

$$\begin{bmatrix} \dot{r} \\ \dot{\psi} \end{bmatrix}=\begin{bmatrix} a_1 & 0 \\ 1 & 0 \end{bmatrix}\begin{bmatrix} r \\ \psi \end{bmatrix}+\begin{bmatrix} b_1 & b_2 & b_3 & b_4 \\ 0 & 0 & 0 & 0 \end{bmatrix}\begin{bmatrix} \delta_1 \\ \delta_2 \\ \delta_3 \\ \delta_4 \end{bmatrix} \tag{7.3}$$

where $a_1 = \frac{N_r}{I_{zz}-N_r}$

$$\begin{bmatrix} \dot{q} \\ \dot{\theta} \\ \dot{z} \end{bmatrix}=\begin{bmatrix} c_1 & c_2 & 0 \\ 1 & 0 & 0 \\ 0 & -U_0 & 0 \end{bmatrix}\begin{bmatrix} q \\ \theta \\ z \end{bmatrix}+\begin{bmatrix} d_1 & d_2 & d_3 & d_4 \\ 0 & 0 & 0 & 0 \\ 0 & 0 & 0 & 0 \end{bmatrix}\begin{bmatrix} \delta_1 \\ \delta_2 \\ \delta_3 \\ \delta_4 \end{bmatrix} \tag{7.4}$$

where $c_1 = \frac{M_q}{I_{yy}-M_{\dot{q}}}$, $c_2 = -\frac{\overline{BG_z}W}{I_{yy}-M_{\dot{q}}}$, $d_i = \frac{M_{\delta i}}{I_{yy}-M_{\dot{q}}}$

Rewriting equation (7.3) and (7.4) with the focus on equations which include parameters to be estimated:

$$\dot{r} = \begin{bmatrix} r & \delta_1 & \delta_2 & \delta_3 & \delta_4 \end{bmatrix} \begin{bmatrix} a_1 \\ b_1 \\ b_2 \\ b_3 \\ b_4 \end{bmatrix} \tag{7.5}$$

$$\dot{q} = \begin{bmatrix} q & \theta & \delta_1 & \delta_2 & \delta_3 & \delta_4 \end{bmatrix} \begin{bmatrix} c_1 \\ c_2 \\ d_1 \\ d_2 \\ d_3 \\ d_4 \end{bmatrix} \tag{7.6}$$

Due to Gavia's unique control surface configuration, input signals consist of four independent values δ_i in degree respectively. In previous works (Hong et al., 2013; Petrich et al., 2007) , there was only one input signal for each subsystem; i.e., elevator input signal for diving subsystem and rudder input signal for steering subsystem. In the state space equations in both steering and diving subsystems, a_i, b_i, c_i, d_i are the model parameters, which consist of physical parameters and hydrodynamic coefficients sufficiently describing the system characteristics. It is important to note that the hydrodynamic coefficients are not determined specifically but this does not affect the applicability of identified model. The following section describes the identification procedure and least squares algorithm implemented to identify a_i, b_i, c_i, d_i.

7.1.3 Identification Procedure and Least Squares Method

7.1.3.1 Proposed identification procedure

Figure 7.1 outlines the proposed system identification procedure based on reference (Klein and Morelli, 2006).

Within the previous section, the mathematical model of the AUV was developed using *prior* model postulation about hydrodynamic characteristics of underwater vehicles. Field experiments were then carried out with the AUV and the collected data were analysed for parameter estimation. In the stage one of the two-stage identification process, the least squares algorithm was utilised to identify the estimated parameters for the previously developed mathematical model.

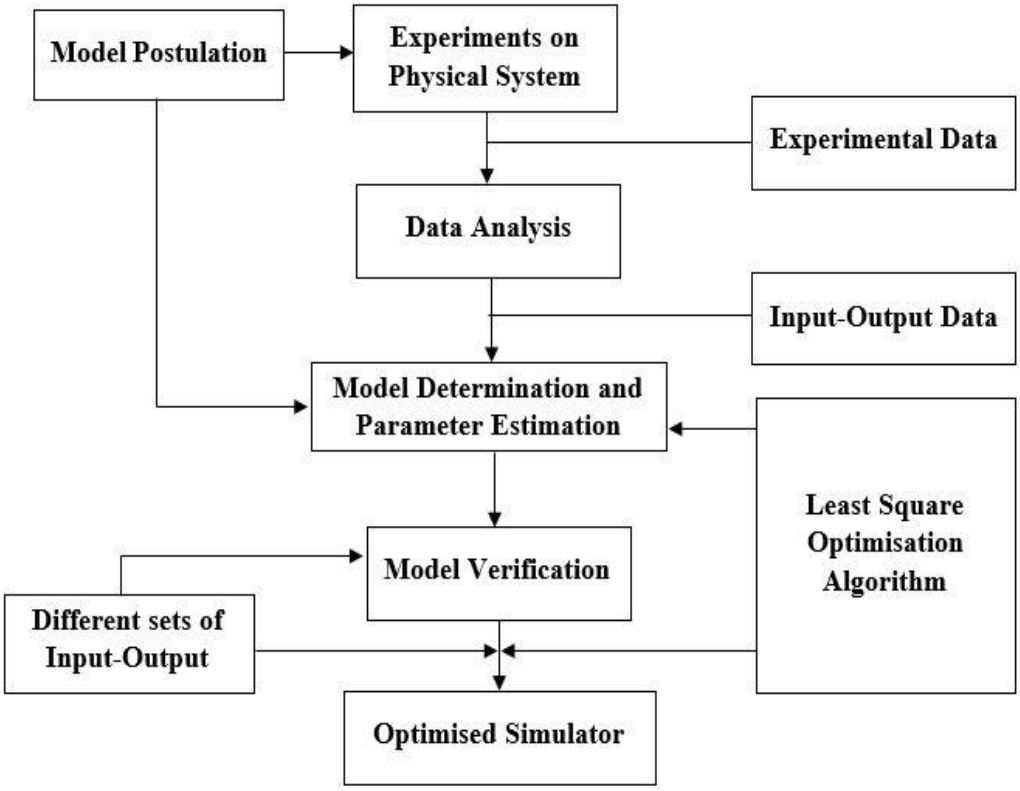

Figure 7.1. Summary of the proposed identification procedure.

The goal was to find a set of parameter $\boldsymbol{\theta}_i$ that minimises the average residual error (Chirarattananon and Wood, 2013):

$$r_i = \frac{d}{dt}\boldsymbol{X}_i\Big|_{\text{measurement}} - \frac{d}{dt}\boldsymbol{X}_i\Big|_{\text{prediction}} \tag{7.7}$$

where $\boldsymbol{X}_1 = r$, $\boldsymbol{\theta}_1 = \begin{bmatrix} a_1 & b_1 & b_2 & b_3 & b_4 \end{bmatrix}^T$ in equation (7.5)

$\boldsymbol{X}_2 = q$, $\boldsymbol{\theta}_2 = \begin{bmatrix} c_1 & c_2 & d_1 & d_2 & d_3 & d_4 \end{bmatrix}^T$ in equation (7.6)

Model verification was also executed for different sets of data to verify the identified model. At this stage, the identified model was only able to predict the system response $(\dot{r}, \dot{q})$ from given current measured states (r, q, θ) for a certain period of time. The principal goal of the study was to develop the desired simulator which could capture the accurate response of vehicle for a long term behaviour from a given initial condition. Motivated by these references in the unmanned aerial vehicle field (Hoburg and Tedrake, 2009; Chirarattananon and Wood, 2013), the next optimisation process was considered in stage two to determine an updated set of parameter $\boldsymbol{\theta}_i$ that minimise the error e_i between the measured output signal and simulated output signal computed by simulating the identified model from specified initial condition with similar control input signals:

$$e_i = \boldsymbol{X}_i\big|_{\text{measurement}} - \boldsymbol{X}_i\big|_{\text{simulation}} \tag{7.8}$$

where $\boldsymbol{X}_i\big|_{\text{simulation}}$ is obtained by simulating equation (7.5) and (7.6) with initial set of parameter $\boldsymbol{\theta}_i$.

The final results were the updated values of parameter $\boldsymbol{\theta}_i$. Both minimisation processes for equation (7.7) and (7.8) were based on the least squares algorithm which is presented in the following section.

7.1.3.2 Least Squares Optimisation algorithm

Using the matrix notations, the dynamic equations (7.5) and (7.6) can be written in the form of equation (7.9)

$$\boldsymbol{y} = \boldsymbol{H\theta} \tag{7.9}$$

where $\boldsymbol{H}$ is the measured state and control input vector

$\boldsymbol{y}$ is the estimated output vector

The measured output vector z of $\boldsymbol{y}$ is defined

$$z = \boldsymbol{H\theta} + \boldsymbol{\varepsilon} \tag{7.10}$$

where $\boldsymbol{\varepsilon}$ is the vector of random measurement errors and assumed to be zero mean and uncorrelated with constant variance.

The Ordinary Least Square (OLS) identification method is based on the Equation Error Method. According to this, the identification of parameter vector θ is equivalent to the minimization of a scalar cost function (Klein and Morelli, 2006; Ljung, 1998):

$$J(\theta) = \frac{1}{2}\sum \varepsilon^2 = \frac{1}{2}\sum \left(z - \boldsymbol{H\theta}\right)^2 \tag{7.11}$$

Solving equation $\frac{\partial J}{\partial \boldsymbol{\theta}} = 0$ for the unknown parameter vector $\boldsymbol{\theta}$ gives the formula for the OLS estimator,

$$\hat{\boldsymbol{\theta}} = \left(\boldsymbol{H}^T\boldsymbol{H}\right)^{-1}\boldsymbol{H}^T z \tag{7.12}$$

In practical cases, the assumptions of uncorrelated measurement errors and homogeneous variance are not valid (Klein and Morelli, 2006). The noise covariance matrix $\boldsymbol{V}$ is introduced and the formula for Weighted Least Squares (WLS) estimator,

$$\hat{\boldsymbol{\theta}} = \left(\boldsymbol{H}^T \boldsymbol{V}^{-1} \boldsymbol{H}\right)^{-1} \boldsymbol{H}^T \boldsymbol{V}^{-1} \boldsymbol{z} \tag{7.13}$$

To validate the result of estimator, the Mean Squares Error (MSE) σ^2 can be estimated (Klein and Morelli, 2006):

$$\hat{\sigma}^2 = \frac{1}{N} \sum_{i=1}^{N} \left[z(i) - \hat{z}(i) \right]^2 \tag{7.14}$$

7.1.4 Experimental Setup and Data Processing

A series of trials with Gavia AUV were conducted in May 2015 at Trevallyn Lake, Tasmania, Australia as shown in Figure 7.2. The tests were conducted in relatively calm wind and current conditions. In order to identifying the hydrodynamic coefficients of the two subsystems, the free running tests in both longitudinal and lateral subsystem were performed separately to fully excite the dynamic models of AUV system. It is important to design the missions that covers the total operational range.

During the experiments, the vehicle was controlled to cruise in certain design manoeuvre. For experiments in vertical plane, the AUV was continuously changing depth in the range of 0 – 5 m while maintaining constant heading. On the other hand, for experiments in horizontal plane, it was controlled to perform turning manoeuvers while keeping constant depth. The control surface angles varied from -20 to 20 degree. During all experiments, the AUV was commanded to track predefined waypoints with a constant forward speed at 1.6 m/s.

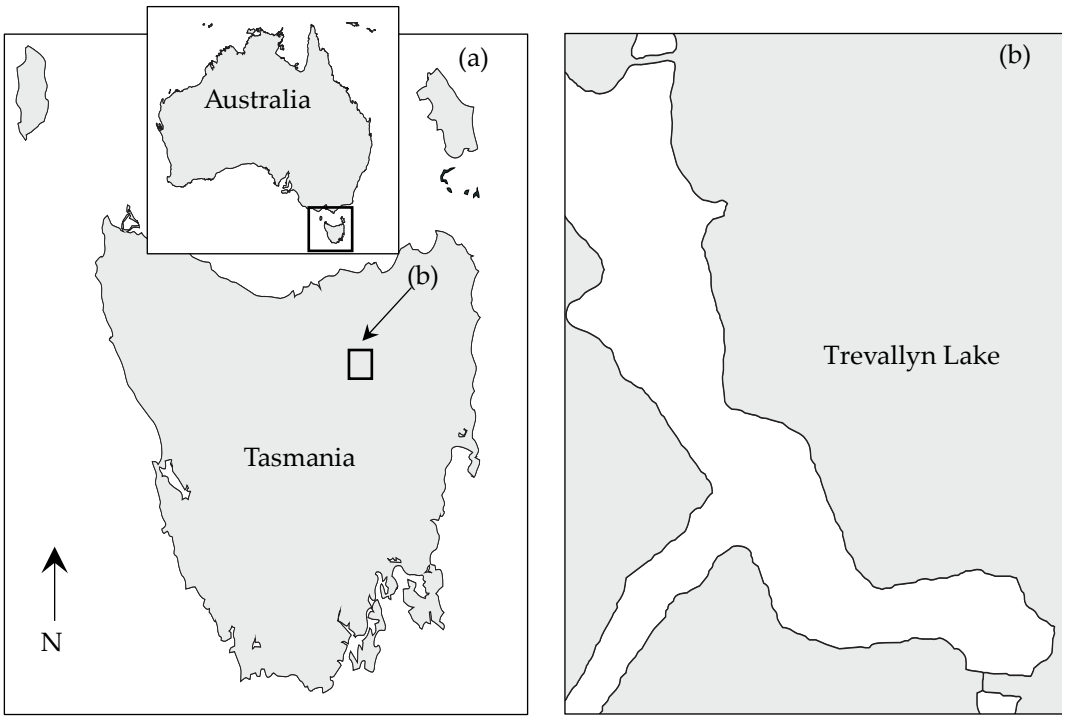

Figure 7.2. Experimental location (Tran et al., 2015a).

Figure 7.3. Gavia AUV performing designed manoeuvrability.

The Gavia AUV was instrumented to measure the necessary state variables. It used the Kearfott T-24 integrated seaborne navigation system combined with a Kalman filter. The INS provided accurate linear and angular accelerations, the Doppler Velocity Log (DVL) provided velocity

(Hiller et al., 2011). The acceleration data were obtained and used as input to the SI process by numerical differentiation of gyro data in the case that the efficient acceleration sensors were not available (Hong et al., 2013; Petrich et al., 2007). 3DM-GX1 Gyro Enhanced Orientation Sensor supplied additional information about the angular velocity and orientation. Since there are no integrated sensors to measure the actual control surface angles, the commanded angles sent by the autopilot system were used. The measured trial dynamic data obtained by the on-board sensors. Prior to applying SI procedure, these data from were resampled to form an integrated set of data since the sensors had different sampling rates.

7.1.5 Results and Discussion

7.1.5.1 Stage one – Identifying the model

After pre-processing data from system files, previously described methods were applied to identify the parameters for both lateral and longitudinal subsystems of the *Gavia* AUV dynamic model. In the stage one, the initial goal was to fit the experimental measured angular acceleration data to the predicted data. Four segments of experimental data were utilised in these stages for lateral and longitudinal subsystem identification respectively.

The comparison between the measured data and the predicted results of the angular acceleration calculated in stage one is illustrated in Figure 7.4 and Figure 7.5. As can be seen, the data from predicted models are generally in good fit with the measured data as expected. The mean square errors are $\hat{\sigma}_1^{\,2} = 1.92 \times 10^{-4}$ for $\dot{r}$ (rrate) data and $\hat{\sigma}_2^2 = 1.94 \times 10^{-4}$ for $\dot{q}$ (qrate) data. There are overshoots and undershoots at some points. This might be a consequence of fast response of physical system in which angular velocity and acceleration could not be captured accurately by sensors. In addition, angular velocity and acceleration data were recorded by two sensors separately (Gyro and INS).

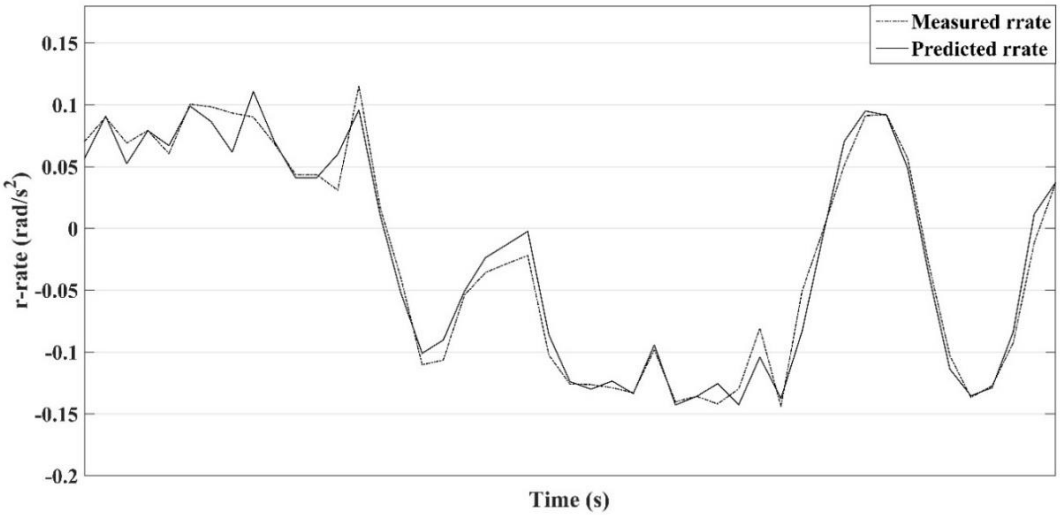

Figure 7.4. Comparison between the predicted (solid line) and measured (dash lines) angular accelerations for lateral subsystem.

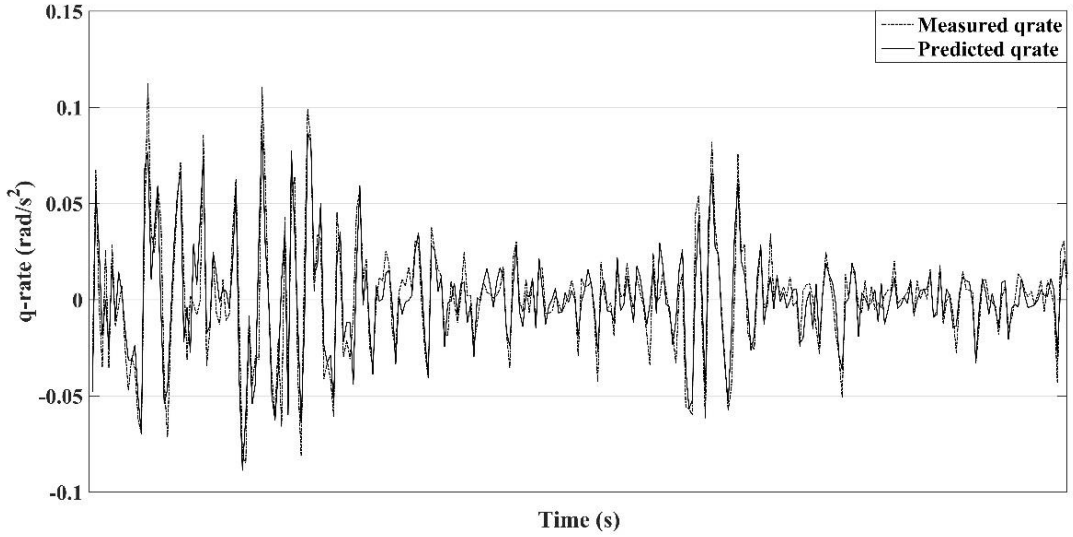

Figure 7.5. Comparison between the predicted (solid lines) and measured (dash lines) angular accelerations for longitudinal subsystem.

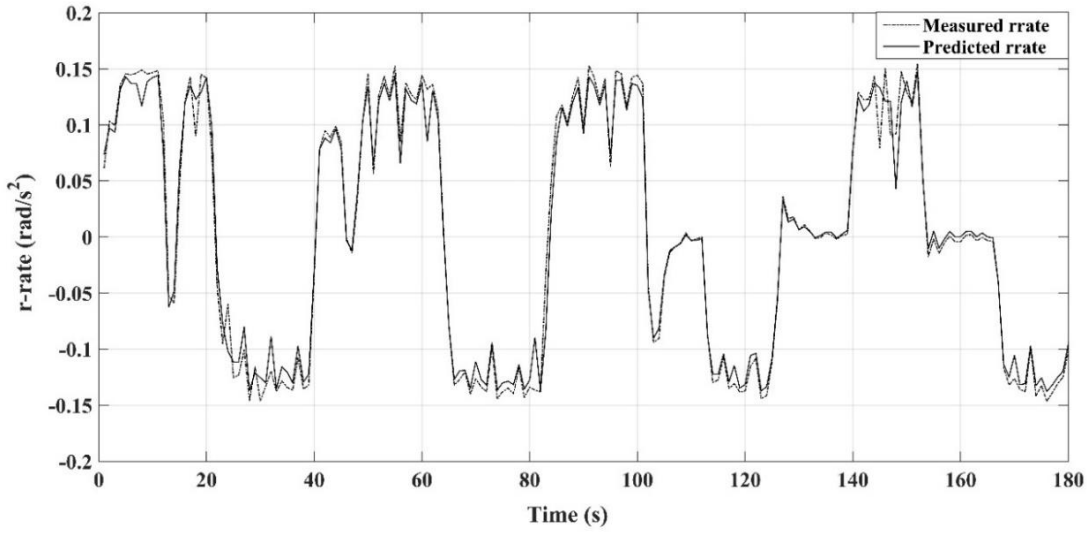

Figure 7.6. Comparison between the predicted (solid lines) and measured (dash lines) yaw angular acceleration for the lateral subsystem.

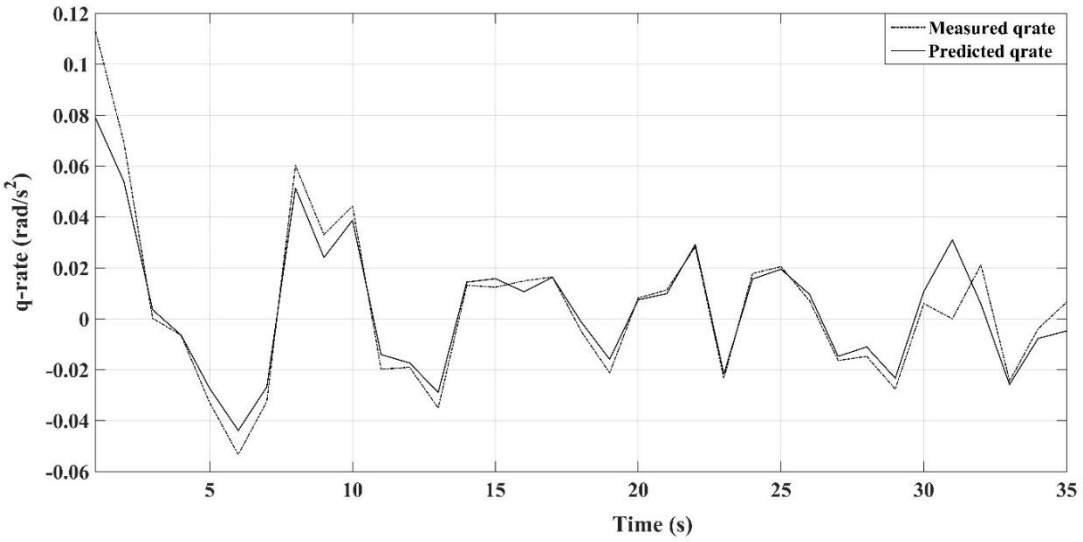

Figure 7.7. Comparison between the predicted (solid lines) and measured (dash lines) pitch angular accelerations for the longitudinal subsystem.

A new set of experimental data, different from the data used in the previous stage, was applied to verify the fidelity of estimated parameter. This validation process is essential in SI to check whether or not the model identified from a particular experimental data is applicable under different operational conditions.

In the comparison shown in Figure 7.6 and Figure 7.7 it can be seen that the predicted angular acceleration responses fit closely to the measured data in both lateral and longitudinal subsystems. Their magnitudes and trends over time are mostly coincidental. From the results obtained in the stage one of the SI and in the validation process, it can be concluded that the identified model are able to accurately predict the system response from given vehicle state's values.

7.1.5.2 Stage two – Optimising the model

The obtained identified model was sufficiently effective in predicting the system responses for a certain time period or for a combination of different set of data. It means that the identified model up to this stage only demonstrates the vehicle hydrodynamic characteristics in a specific condition at which the experimental data were collected. However, in order to develop a robust simulator to accurately predicting the response in a long term behaviour from a given initial condition, in the stage two the identified model was optimised by fitting the experimental data to the simulated data generating from numerical simulator in the stage one. The initial condition was selected equally to the first state value in the set of experimental data used as inputs for simulation validation. Numerical simulations in the time domain were performed based on the optimised model by using the Fourth Order Runge-Kutta ODE integration algorithm.

In Figure 7.8 and Figure 7.9, the numerical simulation results of optimised model for angular acceleration are compared to the actual measured results for a set of experimental data in the lateral and longitudinal systems.

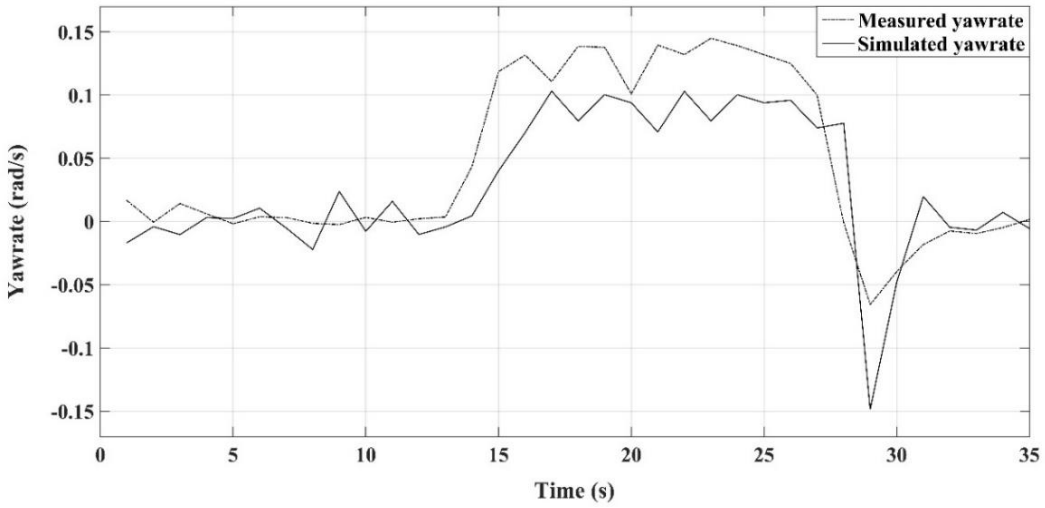

Figure 7.8. Comparison between the simulated (solid lines) and measured (dash lines) angular velocity yawrate for lateral subsystem.

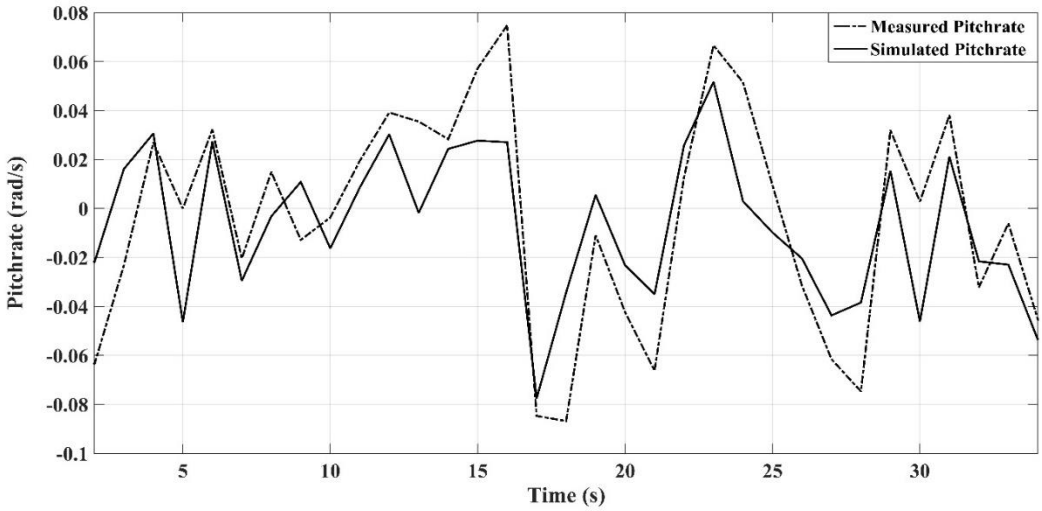

Figure 7.9. Comparison between the simulated (solid lines) and measured (dash lines) angular velocity pitchrate for the longitudinal subsystem

In the lateral subsystem, it is noted in Figure 7.8 that the optimised model is able to represent appropriate tendency and frequency response compared to the measured response for the yawrate. Nevertheless, the comparison shows that there is a small offset and oscillation between the simulated and measured data, their amplitudes are not consistent. This is probably due to the variation in the forward speed of the vehicle during manoeuvres since the controller continuously changes the propeller rotational speed to compensate for the thrust loss during the turning manoeuvre in horizontal plane. The assumption of constant forward speed is valid in the simulation, whereas there is a slight difference in practice.

It is seen from Figure 7.9 that in the longitudinal system, the pitchrate response from the simulation program demonstrates a good agreement with the measured data. However, there are some overshoots during pitch motion that the simulated data do not fit closely with the experimental data. The differences in their responses at the peaks are mainly due to the control surface saturation in practice during the manoeuvres in which the vehicle performs the continuous pitching and diving motion. Additionally, the minor environmental disturbances occurring in the field trials might result in the variation between the simulated and measured data in both model. In essence, two optimised models for lateral and longitudinal subsystems derived following the two-stage SI procedure are able to reasonably predict the responses of the torpedo shaped underwater vehicle in a given initial condition. The parameters obtained from the LS optimised model are summarised in Table 7.2.

Furthermore, based on these parameters, the analysis could be performed to evaluate the stability of the vehicle. The negative value of a_1 and c_1 shows that the yaw dynamics and pitch dynamics are stable (Hong et al., 2013). It is worth noting that the absolute values of four control surface hydrodynamic parameters b_i and d_i are identical in each subsystem. The sign difference is resulted from the definition of rotational direction for each control surface.

Table 7.2. Identified parameters for longitudinal and diving subsystems

Lateral Subsystem		**Longitudinal Subsystem**	
Parameter	**Value**	**Parameter**	**Value**
a_1	-0.9497	c_1	-0.9093
b_1	0.00062	c_2	-0.0094
b_2	-0.00062	d_1	-0.006
b_3	0.00062	d_2	0.006
b_4	-0.00062	d_3	0.006
		d_4	-0.006

In addition, the eigenvalues of equations of motion are also utilised to determine the stability and response of the system. From the obtained values of the parameters a_1, c_1, c_2, the stability of yaw and pitch dynamics are able to be analysed based on the stability conditions of linear state space model.

From equation (5) the eigenvalues of the matrix $A = \begin{bmatrix} a_1 & 0 \\ 1 & 0 \end{bmatrix} = \begin{bmatrix} -0.9497 & 0 \\ 1 & 0 \end{bmatrix}$ are $\lambda_{A1} = -0.9497$ and $\lambda_{A2} = 0$. Since $\lambda_{A1} \le 0$ and $\lambda_{A2} \le 0$ the yaw dynamic of AUV is stable.

From equation (6) the eigenvalues of matrix $B = \begin{bmatrix} c_1 & c_2 & 0 \\ 1 & 0 & 0 \\ 0 & -U_0 & 0 \end{bmatrix} = \begin{bmatrix} -0.9093 & -0.0094 & 0 \\ 1 & 0 & 0 \\ 0 & -1.6 & 0 \end{bmatrix}$ are $\lambda_{B1} = 0$, $\lambda_{B2} = -0.0105$ and $\lambda_{B3} = -0.8988$. Since $\lambda_{B1}, \lambda_{B2}, \lambda_{B3} \le 0$ the pitch dynamic of AUV is stable.

7.1.6 Summary

In this section, the two-stage system identification based on least squares algorithm is developed to estimate reasonably the underwater vehicle linear mathematical model. The experimental data used for the system identification study were acquired from the on-board sensors during the field trails. The model parameters are identified and optimised. The obtained results have proved the effectiveness of the proposed two-stage SI in determining the linear hydrodynamic coefficients of a torpedo-shaped underwater vehicle. In the next section, the linear control design based on the developed linear mathematical model is presented.

7.2 Control Application

7.2.1 Introduction

The optimal control design presented in this section is a part of the research project to examine the control of an AUV equipped with CCPP at both cruising speed and low speed in a typical surveying mission.

The system modelling and control design for underwater vehicle are challenging and complicated in practice due to the nonlinear behaviour of underwater vehicles and the external disturbance of operating environments. The wide range of applications and AUV configuration has resulted in the development of control system with various control strategies. There are three typical types of controller for marine robotics including the classical feedback control, the modern feedback control and the advanced nonlinear control. A number of commonly used control algorithms for AUV are the Proportional Integral Derivative controller (PID) (Taubert et al., 2014), H-infinity controller (Wang et al., 2015), neural network (van de Ven et al., 2005), sliding mode control (SMC) (Londhe et al., 2016), fuzzy logic (Ishaque et al., 2011), adaptive control technique (Hassanein et al., 2016) and the linear quadratic regulator (LQR). After considering

the control strategy of various AUVs, the optimal LQR algorithm is considered in this study due to its reliability, computationally inexpensive, and ease of implementation in the primary design stage. LQR is a commonly used controller and has been applied successfully in various autonomous systems such as unmanned aerial vehicles (Bouabdallah et al., 2004), and unmanned surface vessel (Naeem et al., 2008). In addition, as compared to the classic control method such as PID, the modern control method LQR has several advantages such as stability and non-sensitivity to the dynamic model. The LQR controller could handle the model uncertainty, sensor noise and environmental disturbance better than the PID controller could.

The design of LQR for AUV equipped with CCPP is based on the assumption that the vehicle dynamics can be decoupled to the linear longitudinal and lateral subsystem. In this study, two separate LQR controllers for the depth and heading control are presented.

The following sections describe the optimal LQR algorithm; derive the control objective for the study; and perform the simulation of proposed LQR for depth and heading control.

7.2.2 Control Algorithm

Much of the controller design for AUV system in practical operation uses linear control methods, based on either the simplified linear models, or the linearisations of the nonlinear model. The effectiveness of the linear controller such as optimal control method on the AUV with CCPP is yet to be demonstrated in literature. In this section, the closed-loop optimal control for AUV is addressed.

7.2.2.1 Linear Quadratic Regulator

The general 6 DOF model of an AUV involves highly nonlinear and coupled equations that results in the high complexity in the model based controller. Therefore, in the common practice of

control design, the general motion equations can be decomposed into three subsystems to describe the hydrodynamics of an AUV: the lateral subsystem, the longitudinal subsystem, and the speed subsystem. In this study, the focus is on the longitudinal and lateral subsystems. This traditional approach is applicable in practice for streamlined torpedo-shaped AUVs to reduce the complexity when the coupling between subsystems is weak (Eng et al., 2016).

In addition, the nonlinear dynamic model of the AUV was linearized at certain equilibrium conditions in order to apply the linear LQR controller. The equilibrium conditions were investigated at which the AUV cruising speed was 1.5 m/s and the other translational velocities are zero. The state space models for lateral and longitudinal subsystems are presented as (Tran et al., 2015a):

$$\begin{bmatrix} \dot{r} \\ \dot{\psi} \end{bmatrix} = \begin{bmatrix} a_1 & 0 \\ 1 & 0 \end{bmatrix} \begin{bmatrix} r \\ \psi \end{bmatrix} + \begin{bmatrix} \alpha \\ 0 \end{bmatrix} \delta_{cyc} \tag{7.15}$$

$$\begin{bmatrix} \dot{q} \\ \dot{\theta} \\ \dot{z} \end{bmatrix} = \begin{bmatrix} b_1 & b_2 & 0 \\ 1 & 0 & 0 \\ 0 & -U_0 & 0 \end{bmatrix} \begin{bmatrix} q \\ \theta \\ z \end{bmatrix} + \begin{bmatrix} \beta \\ 0 \\ 0 \end{bmatrix} \delta_{cyc} \tag{7.16}$$

where a_1, b_1, b_2 are the model hydrodynamic coefficients derived by using the system identification method (Tran et al., 2015a) and verified by the analytical method. α, β are the propulsion model coefficients estimated from previous sections.

This section presents the optimal state feedback controller using LQR technique. The LQR technique is a class of modern feedback control method. The controller is used to control the horizontal and vertical movements separately at equilibrium conditions. Equation (7.15) and equation (7.16) can be expressed in the general state space form:

$$\begin{aligned} \dot{\boldsymbol{x}} &= \boldsymbol{A}\boldsymbol{x} + \boldsymbol{B}\boldsymbol{u} \\ \boldsymbol{y} &= \boldsymbol{C}\boldsymbol{x} + \boldsymbol{D}\boldsymbol{u} \end{aligned} \tag{7.13}$$

The LQR design problem is to calculate the state feedback controller K such that the objective quadratic function J is minimised (Antsaklis and Michel, 2007):

$$J = \int_0^\infty \left(\boldsymbol{x}^T \boldsymbol{Q} \boldsymbol{x} + \boldsymbol{u}^T \boldsymbol{R} \boldsymbol{u} \right) dt \tag{7.14}$$

Where Q and R are the state and control penalty matrices. They are defined and selected to ensure accurate dynamics of the system.

The applied control law is given as:

$$\boldsymbol{u} = -\boldsymbol{K} \cdot \boldsymbol{x} \tag{7.15}$$

where x is the error in the outputs that are controlled and u is the control signals.

The constant K is obtained:

$$\boldsymbol{K} = \boldsymbol{R}^{-1} \boldsymbol{B}^T \boldsymbol{P} \tag{7.16}$$

P is determined by solving the Riccatti equation (Lewis et al., 2012):

$$\boldsymbol{A}^T \boldsymbol{P} + \boldsymbol{P}\boldsymbol{A} - \boldsymbol{P}\boldsymbol{B}\boldsymbol{R}^{-1}\boldsymbol{B}^T \boldsymbol{P} + \boldsymbol{Q} = \boldsymbol{0} \tag{7.17}$$

7.2.2.2 Control Objective

One of the typical missions of surveying style AUV is conducting a survey with the lawn mower pattern while maintaining a desired depth over the bottom. This mission is practically conducted in several applications including oceanographic research, biological sampling, and mine-sweeping. The surveying mission is selected as the case study for the controller design of the AUV equipped with CCPP in which the heading and depth control are considered. These two control tasks are one of the most popular control modes in the control study of an unmanned underwater vehicle. The simulation is conducted to demonstrate the feasibility of the design control law.

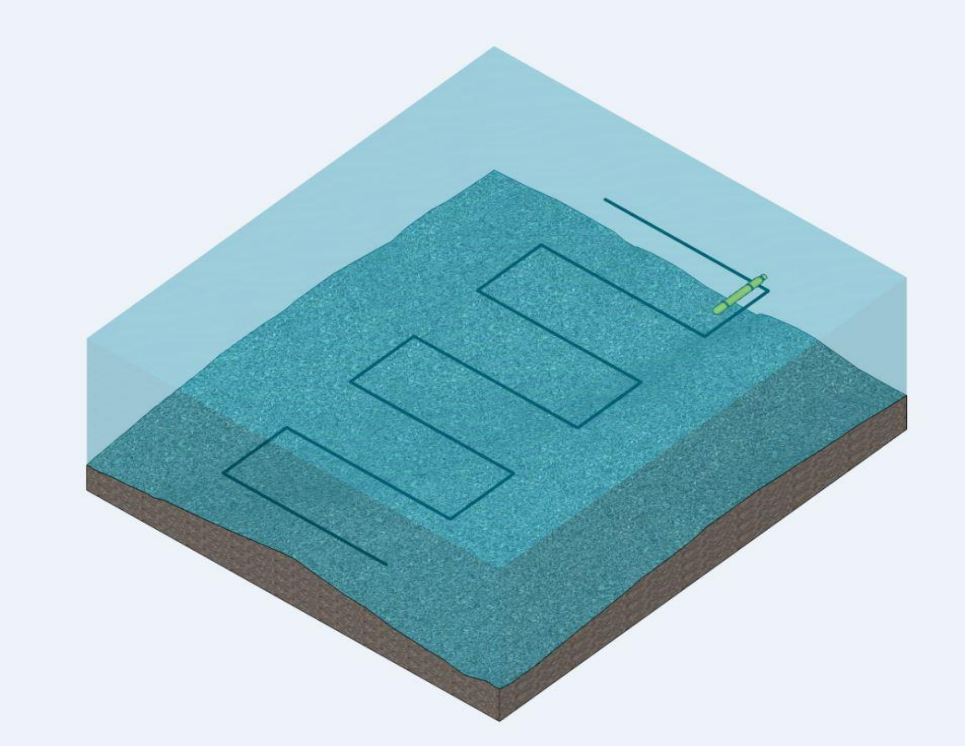

Figure 7.10. The lawn mower pattern.

During this mission, the control objective was to control the AUV at desired depth and heading values by adjusting the input cyclic angle δ_{cyc}. δ_{cyc} was limited to 20 degree for the control design. It was also assumed that the AUV forward speed is constant in these operating conditions and the state initial values were zero. The performance requirement for the system under control was minor oscillation about the reference input signals.

7.2.3 Simulation Results

The AUV dynamic model and LQR controller are implemented in the simulator using MATLAB/Simulink™. The Runge-Kutta fourth order solver are utilised. The simulation aims to demonstrate the performance of the AUV equipped with CCPP in the time domain. The full state feedback is assumed for the controller. The AUV depth and heading control problem are conducted and examined separately.

7.2.3.1 Depth Control

In the proposed manoeuvre for the depth control problem, the AUV was controlled to maintain the desired depth of 18 m and then 3 m after 80 s. The simulation time was 125 s.

Figure 7.11, Figure 7.12, and Figure 7.13 show the depth, pitch angle and control input signal as the function of time respectively. As can be seen, the depth variable is successfully controlled with minor overshoot. After a short period, the depth value converges to the first reference input value. The setting time is approximately 22 s. This value is reasonable considering that the AUV is in the low speed operation. The simulation also shows a decrease in depth as the controller acquire a second reference input. The AUV is therefore able to track the continuous reference input signals.

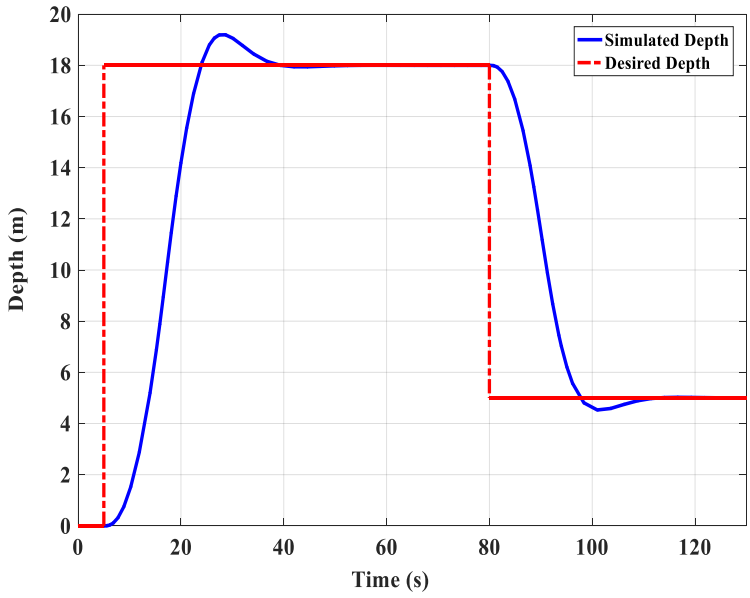

Figure 7.11. Depth control using the LQR.

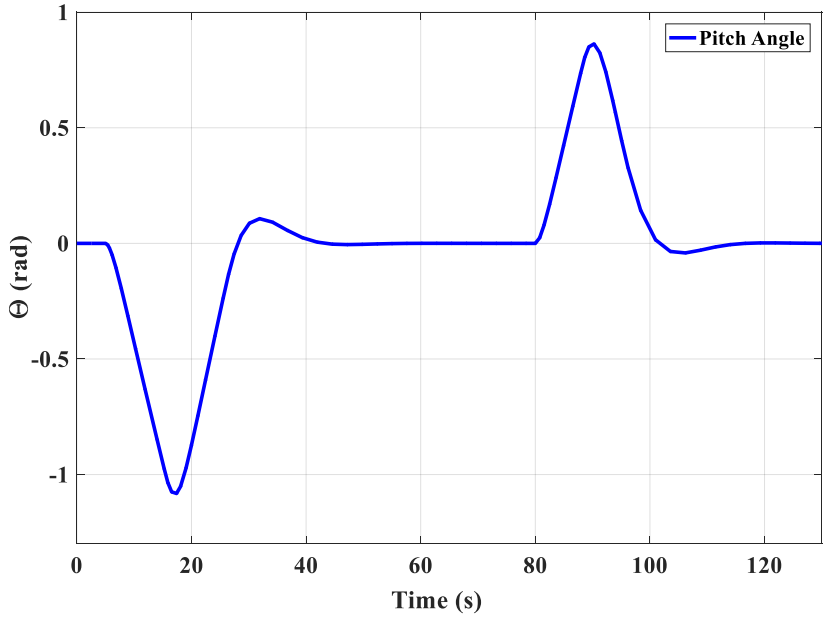

Figure 7.12. Pitch angle variation in the depth control.

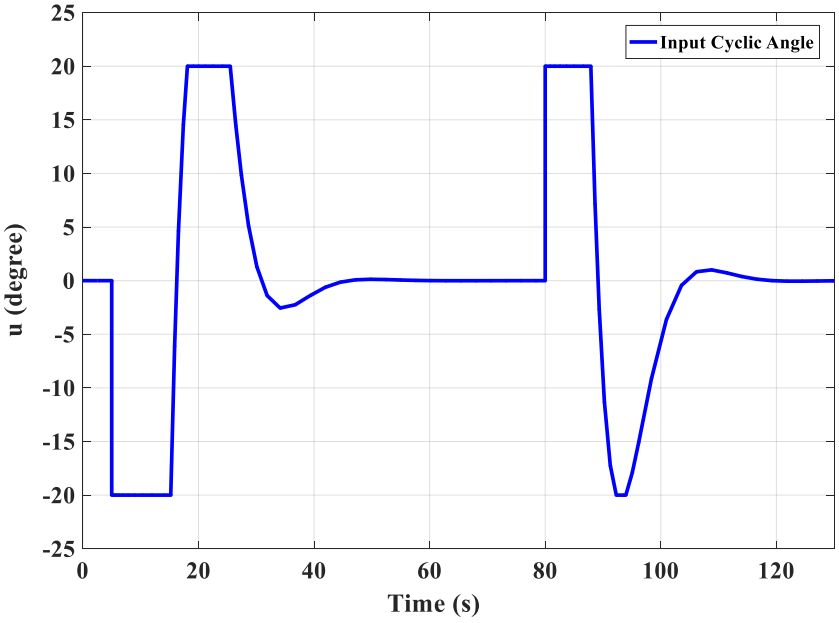

Figure 7.13. Input cyclic angle of the CCPP.

7.2.3.2 Heading Control

Similarly, the performance of the heading control system using LQR is presented. The simulated scenario for the heading control was that the AUV needs to change the yaw angle to 0.8 rad and then to -0.3 rad after 30 s. The total simulation time was 60 s.

Figure 7.14 shows the response of yaw angle in the lateral plane and Figure 7.15 shows the corresponding control signal as the function of time. It can be seen from the simulation that the AUV is able to maintain the desired heading with no overshoot and the CCPP works effectively. The cyclic angle is adjusted to its maximum value and then gradually to its initial position.

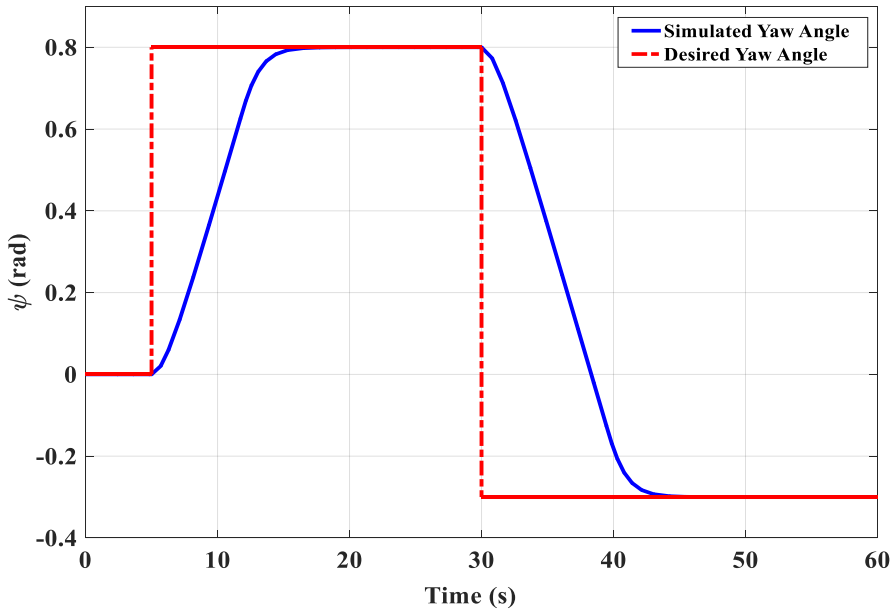

Figure 7.14. Heading control using the LQR.

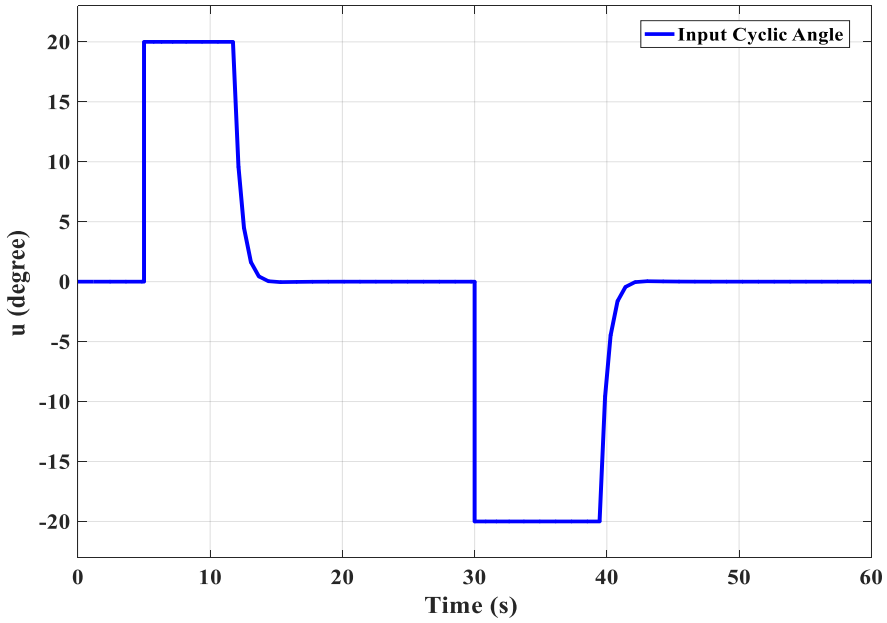

Figure 7.15. Input cyclic angle of the CCPP.

7.3 Summary

The goal of this chapter was to accurately control the depth and heading of an AUV equipped with CCPP. In the study, the Gavia AUV was used as the research platform to implement the designed controller. In the first section, the two-stage system identification based on least squares algorithm was developed to estimate reasonably the underwater vehicle linear mathematical model. The experimental data used for the system identification study were acquired from the on-board sensors during the field trails. The time-domain validation test showed that the proposed two-stage SI approach delivered a high-fidelity dynamic model. In the second section, the LQR algorithm was implemented for the control design of an AUV equipped with CCPP. Two separate LQR controllers were designed for the longitudinal and lateral subsystems. The effectiveness of the proposed controllers was analysed by using the numerical simulation approach. As could be seen on the simulation results, the heading control behaved as good as the depth control. The AUV performance with CCPP under LQR controller demonstrated that

the linearised dynamic model was suitable for the application of the optimal control. The steady state response of the system such as overshoot and settling time met the performance requirements.

CHAPTER 8

CONCLUSIONS AND FUTURE WORK

This thesis focused on the analysis of the CCPP propulsion system in order to improve the underwater vehicle performance and manoeuvrability with respect to the conventional FPP system. The experimental and simulation studies presented in the previous chapters gave valuable insights into the performance characteristics of the CCPP propulsion system and the AUV equipped with CCPP. In the final chapter, the results of the research project are summarised, including the completed works, main findings, conclusions, and the significance of the research project. The potential avenues for future work are also illustrated.

8.1 Summary of the Completed Works

The use of CCPP as the propulsion system for a torpedo-shaped AUV represents a novel and challenging problem and is the main motivation for the research project. This thesis presents the performance analysis of the innovative CCPP propulsion and a comparison study of two propulsion systems named FPP and CCPP as applied to the Gavia AUV. A considerable amount of significant tasks was conducted during the course of the research project and are summarised in this section.

For the purpose of improving the manoeuvrability of AUVs at low speeds, the need for an innovative propulsion system was addressed. A variety of state of the art propulsion systems for an underwater vehicle were described and analysed. A comprehensive literature study was mentioned to describe the relevant propulsion systems with different configurations as alternative propulsion system to the conventional one. A brief description and performance analysis of these propulsion systems were conducted, discussing the advantages and disadvantages of using these systems.

The process of developing the AUV's equations of motion that can effectively model the vehicle's behaviour and performance characteristics was illustrated. The derivation of the six DOF nonlinear equations for an AUV was considered. The six degree of freedom equations of motion for underwater vehicle simulation are general sufficient to simulate the trajectories and responses of the submarine resulting from normal manoeuvres as well as for extreme manoeuvres (Gertler and Hagen, 1967). The hydrodynamic coefficients are the sensitive parameters to the AUV performance in the simulation. In this stage, the experimental study of Gavia AUV in the Towing Tank has not been conducted to determine its hydrodynamic coefficients. Therefore, in the scope of this project, the hydrodynamic coefficients were mainly estimated based on the

analytical approaches that represent a reasonable trade-off in terms of accuracy and ease of implementation. The asymmetric shape of Gavia AUV helps to reduce the hydrodynamic complexity in the modelling process. These coefficients were validated and verified to minimise the uncertainty in the calculations. The obtained results were adjusted considering the data from the previous studies in the literature.

There has been extensive experimental work conducted to increase the knowledge of the principles and characteristics of the conventional FPP propulsion and CCPP propulsion system. The propulsion systems have the high level of effects on the AUV behaviour and the study on their performance is critical. The new modelling of the FPP and CCPP propulsion system characteristics was developed using the experimental approach. The accurate modelling of the propulsion system paves the way for development of the simulation and control study. The fundamental objective of these two chapters was to measure the thrust and manoeuvring forces generates from these two propulsion systems. The sensitivity analysis based on the obtained test data provided the validity of the experimental results. The experimental procedure and data analysis were mainly based on the ITTC standard for marine propulsion testing. The experimental data were then applied to derive the propulsion system empirical model incorporated in the numerical simulation program.

A simulator for an underwater vehicle named AUVSIPRO was constructed in MATLAB/Simulink™ platform. AUVSIPRO was a part of a research project to examine the applicability of the FPP and CCPP to an AUV. This program was developed with the emphasis on the performance prediction of an underwater vehicles equipped with different propulsion systems in the early design stage. The AUVSIPRO could also be extended to adapt to a variety of underwater vehicles and propulsion systems, for example the Mullaya AUV and Explorer class AUV at AMC-UTAS. A model predicting the manoeuvring forces generated by the FPP and

CCPP propulsion system was applied to AUSIPRO. The forces and moments generated by the propulsion systems were mapped to the dynamics of the AUV to form the complete model. This method provided advantages of comprehensive formulation and rapid computation.

The controller design for an AUV equipped with CCPP was developed to guarantee the system robustness against external disturbances in operation. The two-stage identification method to define the linear model of Gavia AUV and the optimal control development were analysed. The depth and heading control was conducted to validate the controller. The performance of the proposed controller was demonstrated and verified by simulation. This controller was computationally inexpensive and effective in application.

8.2 Main Findings and Conclusions

The experiment of an FPP for Gavia AUV was tested at the towing tank in all four quadrants of operation. The conventional open water performance in the first quadrant and the performance characteristic in four-quadrant operation are presented in this study. An analysis of using polynomial and Fourier series regression model in representing the experimental data sets is examined. It is concluded that the four-term and three-term Fourier series regression models are considered the most appropriate models in representing the thrust and torque coefficient curves respectively in the specified condition of this study. These two models form the four-quadrant underwater propeller model. They are able to produce a reasonable approximation of thrust and torque coefficients with a small number of parameters.

Although the initial experiments of CCPP prototype were conducted in previous studies, this investigation has provided a systematic experimental data on the CCPP performance. The improvements were made to the experimental system and data collection. A series of comprehensive bollard pull and captive model tests were designed and conducted on the innovative propulsor CCPP to evaluate its performance. The effects of the collective and cyclic pitch settings

on the CCPP performance have been examined and discussed. According to the obtained results, it was shown that the CCPP was capable of generating effective manoeuvring forces in both bollard pull and captive model conditions. The results also provide an insight into the relationship between these manoeuvring forces and controlled parameters that enable the simulation and control study of the underwater vehicle equipped with CCPP. The dynamic modelling of the propulsion systems using the experimental approach is reliable and integrated in the entire AUV dynamic model to create a realistic simulation.

The proposed simulation program proved to be quite effective and feasible in describing the manoeuvring capabilities of an AUV equipped with these two examined propulsion system. The standard manoeuvring tests for marine vehicles were presented for the investigation about the influences of conventional FPP and CCPP propulsion on the Gavia AUV. The simulation results indicate that the AUV equipped with CCPP provides better manoeuvrability in comparison to the AUV equipped with conventional FPP propulsion system. In the considered manoeuvring tests, the CCPP outperforms the FPP in most of the examined parameters and variables. Five separate fundamental manoeuvring tests are presented to demonstrate the performance differences between the two configurations. The simulation program presented the obtained results, which were consistent with the expected behaviours of the two propulsion configurations. In the acceleration test, the results indicated that the CCPP propulsion has an advantage for high acceleration rate; meanwhile the conventional FPP propulsion is beneficial better steady forward speed. In the static turning manoeuvre and zigzag test, there is a clear advantage with respect to the CCPP configuration in terms of heading changing ability. The shorter stopping distance and time are due to the faster deceleration rate in the stopping test show the better stopping performance of CCPP. The simulation results also reveal that the CCPP has the superior diving characteristic in the vertical plane. In conclusion, with respect to the primary manoeuvres rep-

resenting the operation of an AUV, the CCPP propulsion system has better performance characteristic, which allows for precise surveying tasks. Furthermore, it is proved that the CCPP is capable of providing low enough continuous thrust to enable the low speeds desirable for accurate manoeuvring and inspection tasks. It could be concluded that the CCPP provides the manoeuvrability to a greater degree and this is the most important aspect considered in this thesis. This type of propulsion system is feasible and it is one of the viable alternatives to the conventional FPP configuration in an AUV, especially in the low speed operation. It also be noted that the CCPP selection does not represent the best trade-off in every situation.

The other important feature concerning the application of a newly developed propulsion system for an AUV is its accurate operation under the controller. The CCPP is able to provide control authorities independent of the relative flow as compared to the conventional FPP with control surfaces. The new two-stage system identification based on least squares algorithm was developed with the goal of estimating reasonably the Gavia AUV linear mathematical model. The experimental data used for the system identification study were acquired from the on-board sensors during the field trials. This methodology is considered as a general tool that could be reused for design and evaluation of different systems. The LQR algorithm was implemented for the control design of an AUV equipped with CCPP. Two separate LQR controllers were designed for the longitudinal and lateral subsystems. The effectiveness of the proposed controllers was analysed by using the numerical simulation approach. The integrated simulation and design framework facilitate the development and testing of the controllers. From the simulation results, the heading control behaved as good as the depth control. The optimal controller provided the desired accuracy in both heading and depth control in which there were smooth transitions between different operating conditions in low speed performance. The AUV performance with CCPP under LQR controller has demonstrated that the developed dynamic model is suitable for the application of the optimal control. The obtained results enable a good basis

for the future controller design as the proposed control strategy is applied to the realistic vehicle to enhance its autonomy.

8.3 Significance of the Research

The new applications of marine science and engineering require the underwater vehicle with high autonomy, excellent performance characteristic, and precise manoeuvrability. These aspects are highly subject to the propulsion system. The primary content of this thesis is about the performance characteristic of an underwater vehicle equipped with the novel CCPP propulsion system and its manoeuvring comparison to the conventional FPP propulsion. The ultimate objective of the thesis is to investigate the feasibility of the CCPP as the propulsion system of choice for a torpedo shaped underwater vehicle instead of the conventional FPP with control surfaces. This research effort has provided the contributions to the field of underwater robotics.

The research and development of a new AUV is both complex and expensive, especially for the AUV equipped with a new propulsion system. The greatest difficulty lays in characterizing its system performance. In current research, the analytical approach, experimental method and numerical simulation are utilised to validate the performance of an AUV in the preliminary development stage. The proposed methods and procedures are presented in a systematic process and they are applicable to any changes of the system design, as well as to other systems of similar characteristics. Time and money can be saved by using a systematic approach when the new designs are frequently updated. The unified simulation model based on the experimental data provides researchers with the ability to test new designs or any modifications to existing ones in a simulation environment. The developed AUVSIPRO simulator could be easily extended to different propulsion system and to various underwater vehicle configurations. It provides a useful means to verify the system and the software design before implementing on the hardware platform.

In conclusion, the main finding highlights and proves the superior manoeuvrability and reliability of the CCPP propulsion system with respect to the conventional FPP configuration. The considerable advantages of CCPP propulsion in performance are confirmed in the study using experimental and simulation approach. The successful implementation of the optimal control strategy on the AUV with the CCPP propulsion system is also considered as a significant aspect of the overall contribution. The analysis presented in this thesis can serve as a proof-of-concept for the research of underwater propulsion system. It is concluded that the CCPP propulsion system is an excellent alternative propulsion to the conventional FPP for an AUV, especially in the operations that require the combination of both high-speed surveying and low-speed manoeuvrability.

8.4 Future Research

In the course of this thesis, although a considerable number of tasks has been accomplished some works could not be completely conducted in the given timeframe. This section will highlight some of the works, which require additional thorough research and investigation for the more accurate results. Moreover, the suggestions and recommendations for the future study are also presented.

In the context of this project, the interactions between the CCPP propulsion system and the AUV hull have not been examined in term of hydrodynamics. It is assumed that this interaction has the minor contribution to the total forces. However, the knowledge about this issue would pave way for the optimisation of the CCPP blade design and the improvement of the manoeuvring performance simulation. Additionally, the simulations have taken into consideration the interaction effects between the collective and cyclic pitch settings by using the empirical model from the tests. The hydrodynamic investigation on their performance characteristic has not been considered in the experimental approach. These issues have been addressed with the use of CFD

approach in the works of other PhD student at AMC. The stabilisation analysis of the CCPP could be conducted from the study of this interaction.

Since the CCPP propulsion is characterised by a high manoeuvrability at low speed, the cavitation would be an interesting issue to examine. The study of cavitation will demonstrate the limitation in the operational range of an AUV with CCPP. Hence, the cavitation should be considered in the future study to gain a better insight into the CCPP hydrodynamics. Further developments will take advantage of the experimental setup and control software designed from this research study to analyse the cavitation phenomenon in the CCPP.

As mentioned in the previous sections, the CCPP system has its own drawback on the mechanical design. In the scope of this study, the modification of its internal mechanism has not been considered. The disadvantage is its electro-mechanical complexity in that many linkages are required to transfer the forces from rotating shaft to the propeller blades. Moreover, the movement of these components is not as fast as expected. These facts mean that the CCPP would have lower operational and propulsive efficiency compared to the conventional FPP propulsion in their current design. It is recommended that the number of actuators could be reduced to two and their movement direction should be changed so that their generated forces exerting directly on the swashplate. The modification into a simpler mechanical model would help the system achieve higher efficiency and faster response in manoeuvring performance.

Constraints of time and budget means the second version of the CCPP prototype has not been constructed with reference to existing design. For this reason, it was decided that the experimental procedure and simulation framework should be developed in detail for the further research. The next research stage in this project would be able to reuse the current foundation to design a more efficient propulsion system. The obtained results from this study would be applied for the optimisation to create a smaller and simpler CCPP propulsion that physically fits

into the Gavia AUV platform. The free-running model would definitely give the green light to the exact evaluation of the proposed system. The results of the free-running trails could be used to validate the simulation results in this study.

The linear controller is used as the primary control algorithm due to its easy of application in the development stage. However, application of this controller on the physical prototype system would not be without difficulty. The analysis of limitations of such controller should be carried out to determine the boundaries beyond which the CCPP can no longer be under control. An observer and a navigation system should also be developed and integrated into the control system. Moreover, in an attempt to increase the robustness and accuracy of the optimal controller, the dynamic model of Gavia AUV could be refined in term of the linear and nonlinear hydrodynamic coefficients. A better estimation of these parameters using could provide a more accurate controller performance. In addition, different types of control algorithm could also be examined based on the same platform to verify the obtained results.

The innovative Collective and Cyclic Pitch Propeller offers a promising alternative to the traditional propulsion system. Its superior capability in term of manoeuvrability is validated by various experiments and simulations in this research project. A great deal of effort has been made during the development process by scientists and engineers in order to ensure that the innovative CCPP propulsion could be applied to the new generation of marine underwater vehicles.

Research Team at the Australian Maritime College, University of Tasmania

Launceston, Tasmania, Australia 2017

References

Abraham I and Yi J. (2015) Model predictive control of buoyancy propelled autonomous underwater glider. *American Control Conference (ACC), 2015.* IEEE, 1181-1186.

Alam K, Ray T and Anavatti SG. (2014) A brief taxonomy of autonomous underwater vehicle design literature. *Ocean Engineering* 88: 627-630.

Allotta B, Pugi L, Bartolini F, et al. (2015) Preliminary design and fast prototyping of an autonomous underwater vehicle propulsion system. *Proceedings of the Institution of Mechanical Engineers, Part M: Journal of Engineering for the Maritime Environment* 229: 248-272.

Alvarez A, Caffaz A, Caiti A, et al. (2009) Folaga: A low-cost autonomous underwater vehicle combining glider and AUV capabilities. *Ocean Engineering* 36: 24-38.

Antonelli G. (2013) *Underwater robots*: Springer.

Antsaklis PJ and Michel AN. (2007) *A linear systems primer*: Birkhäuser Boston.

Avila JP, Donha DC and Adamowski JC. (2013) Experimental model identification of open-frame underwater vehicles. *Ocean Engineering* 60: 81-94.

Avila JPJ, Maruyama N and Adamowski JC. (2008) Hydrodynamic parameter estimation of an open frame unmanned underwater vehicle. *17th IFAC World Congress, IFAC.*

Bachmayer R, Whitcomb LL and Grosenbaugh MA. (2000) An accurate four-quadrant nonlinear dynamical model for marine thrusters: Theory and experimental validation. *Oceanic Engineering, IEEE Journal of* 25: 146-159.

Badillo AGG and Ceron IFC. Development of Autonomous Underwater Vehicles; A brief overview.

Bellingham JG. (2016) Autonomous Underwater Vehicle Docking. *Springer Handbook of Ocean Engineering*. Springer, 387-406.

Bertram V. (2012) *Practical ship hydrodynamics*: Elsevier.

Blevins R. (1979) Formulas for natural frequency and mode shape. *Kreiger Publ. Comp., New York*.

Bose N. (2008) *Marine powering prediction and propulsors,* New York: SNAME publication.

Bouabdallah S, Noth A and Siegwart R. (2004) PID vs LQ control techniques applied to an indoor micro quadrotor. *Intelligent Robots and Systems, 2004.(IROS 2004). Proceedings. 2004 IEEE/RSJ International Conference on.* IEEE, 2451-2456.

Briggs R, McCarter B, Neu WL, et al. (2010) Design elements of a prototype self-mooring AUV. *OCEANS 2010.* IEEE, 1-8.

Brown JP. (1993) Four quadrant dynamic model of the AUV II thruster. DTIC Document.

Caccia M, Indiveri G and Veruggio G. (2000) Modeling and identification of open-frame variable configuration unmanned underwater vehicles. *Oceanic Engineering, IEEE Journal of* 25: 227-240.

Carlton J. (2012) *Marine propellers and propulsion*: Butterworth-Heinemann.

Chakrabarti R, Gelze J, Lehr H, et al. (2014) Maneuverability and handling of the penguin-shaped autonomous underwater vehicle (AUV) PreToS, analytical and experimental results. *OCEANS 2014-TAIPEI.* IEEE, 1-6.

Chakrabarti SK. (1994) *Offshore structure modeling*: World Scientific.

Chirarattananon P and Wood RJ. (2013) Identification of flight aerodynamics for flapping-wing microrobots. *Robotics and Automation (ICRA), 2013 IEEE International Conference on.* IEEE, 1389-1396.

Colgate JE and Lynch KM. (2004) Mechanics and control of swimming: A review. *IEEE Journal of Oceanic Engineering* 29: 660-673.

Cruz N and Matos AC. (2008) The MARES AUV, a modular autonomous robot for environment sampling. *OCEANS 2008*. IEEE, 1-6.

Dang J, Brouwer J, Bosman R, et al. (2012) Quasi-Steady Two-Quadrant Open Water Tests for the Wageningen Propeller C-and D-Series. *Proceedings of the Twenty-Ninth Symposium on Naval Hydrodynamics, Gothenburg, Sweden*.

De Barros E, Pascoal A and De Sa E. (2008) Investigation of a method for predicting AUV derivatives. *Ocean Engineering* 35: 1627-1636.

Delefortrie G and Vantorre M. (2009) Modelling propeller and rudder induced forces acting on deep drafted vessels in muddy navigation areas. *Journal of marine science and technology* 14: 171-184.

Dubbioso G, Broglia R and Zaghi S. (2017) CFD analysis of turning abilities of a submarine model. *Ocean Engineering* 129: 459-479.

Eng YH, Teo KM, Chitre M, et al. (2016) Online System Identification of an Autonomous Underwater Vehicle Via In-Field Experiments. *IEEE Journal of Oceanic Engineering* 41: 5-17.

Eskesen J, Owens D, Soroka M, et al. (2009) Design and performance of Odyssey IV: a deep ocean hover-capable AUV. Massachusetts Institute of Technology. Sea Grant College Program.

Farnsworth J, Amitay M, Huyer S, et al. (2010) Preswirl Maneuvering Propulsor: Part 2 Experiments. *Paper No. AIAA-2010-4959, 28th Applied Aerodynamics Conference, Chicago, IL*.

Feldman J. (1979) Dtnsrdc revised standarrd submarine equations of motion. DAVID W TAYLOR NAVAL SHIP RESEARCH AND DEVELOPMENT CENTER BETHESDA MD SHIP PERFORMANCE DEPT.

Fossen TI. (2011) *Handbook of marine craft hydrodynamics and motion control*: John Wiley & Sons.

Fossen TI and Blanke M. (2000) Nonlinear output feedback control of underwater vehicle propellers using feedback form estimated axial flow velocity. *Oceanic Engineering, IEEE Journal of* 25: 241-255.

Furlong ME, McPhail SD and Stevenson P. (2007) A concept design for an ultra-long-range survey class AUV. *OCEANS 2007-Europe.* IEEE, 1-6.

Gertler M and Hagen GR. (1967) Standard equations of motion for submarine simulation. DAVID W TAYLOR NAVAL SHIP RESEARCH AND DEVELOPMENT CENTER BETHESDA MD.

Gomáriz S, Masmitjà I, González J, et al. (2015) GUANAY-II: an autonomous underwater vehicle for vertical/horizontal sampling. *Journal of marine science and technology* 20: 81-93.

Hagen PE, Storkersen N, Vestgard K, et al. (2003) The HUGIN 1000 autonomous underwater vehicle for military applications. *OCEANS 2003. Proceedings.* IEEE, 1141-1145.

Hajosy MF. (1994) Six degree of freedom vehicle controller design for the operation of an unmanned underwater vehicle in a shallow water environment. Massachusetts Institute of Technology and Woods Hole Oceanographic Institution.

Hassanein O, Anavatti SG, Shim H, et al. (2016) Model-based adaptive control system for autonomous underwater vehicles. *Ocean Engineering* 127: 58-69.

Heberley BD. (2011) Analysis of the operational impacts of alternative propulsion configurations on submarine maneuverability. Massachusetts Institute of Technology.

Hegrenaes O, Hallingstad O and Jalving B. (2007) Comparison of mathematical models for the HUGIN 4500 AUV based on experimental data. *2007 Symposium on Underwater Technology and Workshop on Scientific Use of Submarine Cables and Related Technologies.* IEEE, 558-567.

Helgason B. (2012) Low speed modeling and simulation of Gavia AUV. *School of Science and Engineering.* Reykjavik University.

Hiller T, Reed T and Steingrimsson A. (2011) Producing Chart Data from Interferometric Sonars on Small AUVs. *The International Hydrographic Review*.

Hiller T, Steingrimsson A and Melvin R. (2012) Expanding the small auv mission envelope; longer, deeper & more accurate. *Autonomous Underwater Vehicles (AUV), 2012 IEEE/OES.* IEEE, 1-4.

Hobson BW, Bellingham JG, Kieft B, et al. (2012) Tethys-class long range AUVs-extending the endurance of propeller-driven cruising AUVs from days to weeks. *Autonomous Underwater Vehicles (AUV), 2012 IEEE/OES.* IEEE, 1-8.

Hoburg W and Tedrake R. (2009) System identification of post stall aerodynamics for UAV perching. *Proceedings of the AIAA Infotech@ Aerospace Conference.* 1-9.

Hong EY and Chitre M. (2015) Roll control of an autonomous underwater vehicle using an internal rolling mass. *Field and Service Robotics.* Springer, 229-242.

Hong EY, Meng TK and Chitre M. (2013) Online system identification of the dynamics of an Autonomous Underwater vehicle. *Underwater Technology Symposium (UT), 2013 IEEE International.* IEEE, 1-10.

Hubbard JJ, Fleming M, Palmre V, et al. (2014) Monolithic IPMC fins for propulsion and maneuvering in bioinspired underwater robotics. *IEEE Journal of Oceanic Engineering* 39: 540-551.

Humphrey TC. (2005) Design and Fabrication of a Collective and Cyclic Pitch Propeller. Memorial University of Newfoundland.

Huyer S, Dropkin A, Beal D, et al. (2010) Pre-swirl Maneuvering Propulsor: Part 1 Computations. *Paper No. AIAA-2010-4958, 28th Applied Aerodynamics Conference, Chicago, IL June.*

Huyer S, Dropkin A, Beal DN, et al. (2012) Preswirl Maneuvering Propulsor. *Oceanic Engineering, IEEE Journal of* 37: 122-138.

IMO. (2002) Explanatory notes to the standards for ship manoeuvrability. IMO Circular MSC/Circ. 1053.

Ishaque K, Abdullah SS, Ayob SM, et al. (2011) A simplified approach to design fuzzy logic controller for an underwater vehicle. *Ocean Engineering* 38: 271-284.

Issac MT, Adams S, He M, et al. (2007) Manoeuvring experiments using the MUN Explorer AUV. *2007 Symposium on Underwater Technology and Workshop on Scientific Use of Submarine Cables and Related Technologies.* IEEE, 256-262.

ITTC. (2002) ITTC - Recommended Procedures: Propulsion, Propulsor Uncertainty Analysis, No. 7.5-02-03-02.2.

ITTC. (2008a) ITTC - Recommended Procedures and Guidelines: Testing and Extrapolation Methods - Propulsion, Propulsor Open Water Test, No. 7.5-02-03-02.1.

ITTC. (2008b) Recommended Procedures and Guidelines for Uncertainty Analysis: Instrumentation Calibration, ITTC, No. 7.5-01-03-01.

ITTC. (2011a) Recommended Procedures and Guidelines, Propulsion/Bollard Pull Test. *International Towing Tank Conference* 7.5-02-03-01.1, Revision 04.

ITTC. (2011b) Recommended Procedures and Guidelines, Resistance Test. *International Towing Tank Conference* 7.5-02-02-01, Revision 03.

ITTC. (2014) Recommended Procedures, Captive Model Test Procedure. *International Towing Tank Conference* 7.5-02-06-02, Revision 04.

Jalving B. (1994) The NDRE-AUV flight control system. *Oceanic Engineering, IEEE Journal of* 19: 497-501.

Jenkins SA and D'Spain G. (2016) Autonomous Underwater Gliders. *Springer Handbook of Ocean Engineering.* Springer, 301-322.

Jun B-H, Park J-Y, Lee F-Y, et al. (2009) Development of the AUV 'ISiMI'and a free running test in an Ocean Engineering Basin. *Ocean Engineering* 36: 2-14.

Jung H-J, Kim MJ, Lee P-Y, et al. (2012) A study on Numerical Analysis of Controllable Pitch Propeller (CPP) using tunnel inspection AUV. *OCEANS, 2012-Yeosu.* IEEE, 1-4.

Khaled N and Chalhoub N. (2011) A dynamic model and a robust controller for a fully-actuated marine surface vessel. *Journal of Vibration and Control* 17: 801-812.

Kim J, Kim K, Choi HS, et al. (2002) Estimation of hydrodynamic coefficients for an AUV using nonlinear observers. *IEEE Journal of Oceanic Engineering* 27: 830-840.

Kim TW, Marani G and Yuh J. (2016) Underwater vehicle manipulators. *Springer Handbook of Ocean Engineering.* Springer, 407-422.

Klein V and Morelli EA. (2006) *Aircraft system identification: theory and practice*: American Institute of Aeronautics and Astronautics Reston, Va, USA.

Korde UA. (2004) Study of a jet-propulsion method for an underwater vehicle. *Ocean Engineering* 31: 1205-1218.

Korkmaz D, Akpolat ZH, Soygüder S, et al. (2015) Dynamic simulation model of a biomimetic robotic fish with multi-joint propulsion mechanism. *Transactions of the Institute of Measurement and Control* 37: 684-695.

Korotkin AI. (2008) *Added masses of ship structures*: Springer Science & Business Media.

Kuiper G. (1992) The Wageningen propeller series.

Lewis EV. (1988) Principles of Naval Architecture. Second Revision. Volume III. Motions in Waves and Controllability. *Published by The Society of Naval Architects and Marine Engineers* 601.

Lewis FL, Vrabie D and Syrmos VL. (2012) *Optimal control*: John Wiley & Sons.

Liu P, Bose N, Frost R, et al. (2015) Model testing and performance comparison of plastic and metal tidal turbine rotors. *Applied Ocean Research* 53: 116-124.

Liu P, Bose N, Frost R, et al. (2014) Model testing of a series of bi-directional tidal turbine rotors. *Energy* 67: 397-410.

Ljung L. (1998) *System identification*: Springer.

Londhe P, Dhadekar DD, Patre B, et al. (2016) Uncertainty and disturbance estimator based sliding mode control of an autonomous underwater vehicle. *International Journal of Dynamics and Control*: 1-17.

Lucieer VL and Forrest AL. (2016) Emerging Mapping Techniques for Autonomous Underwater Vehicles (AUVs). *Seafloor Mapping along Continental Shelves.* Springer, 53-67.

Ludvigsen M and Sørensen AJ. (2016) Towards integrated autonomous underwater operations for ocean mapping and monitoring. *Annual Reviews in Control* 42: 145-157.

Martin SC and Whitcomb LL. (2014) Experimental identification of six-degree-of-freedom coupled dynamic plant models for underwater robot vehicles. *Oceanic Engineering, IEEE Journal of* 39: 662-671.

Mazlan A and Naddi A. (2015) A fully actuated tail propulsion system for a biomimetic autonomous underwater vehicle. University of Glasgow.

McPhail S. (2009) Autosub6000: A deep diving long range AUV. *Journal of Bionic Engineering* 6: 55-62.

Mohseni K. (2006) Pulsatile vortex generators for low-speed maneuvering of small underwater vehicles. *Ocean Engineering* 33: 2209-2223.

Naeem W, Xu T, Sutton R, et al. (2008) The design of a navigation, guidance, and control system for an unmanned surface vehicle for environmental monitoring. *Proceedings of the Institution of Mechanical Engineers, Part M: Journal of Engineering for the Maritime Environment* 222: 67-79.

Nagashima Y, Taguchi N and Ishimatsu T. (2006) Development of a compact hybrid underwater vehicle using variable vector propeller. *Proc. of 23rd International Symposium on Automation and Robotics in Construction (ISARC2006).* Citeseer, 66-71.

Nicholson J and Healey A. (2008) The present state of autonomous underwater vehicle (AUV) applications and technologies. *Marine Technology Society Journal* 42: 44-51.

Niyomka P. (2014) Performance and Control of a Collective and Cyclic Pitch Propeller for an Underwater Vehicle. University of Tasmania.

Oosterveld MWC. (1970) Wake adapted ducted propellers. TU Delft, Delft University of Technology.

Oosurveld M and Van Oossanen P. (1975) Further computer-analyzed data of the Wageningen B-screw series.

P. SATR, Leong ZQ, Ranmuthugala D, et al. (2015) Numerical investigation of the hydrodynamic interaction between two underwater bodies in relative motion. *Applied Ocean Research* 51: 14-24.

Palmer AR. (2009) Analysis of the propulsion and manoeuvring characteristics of survey-style AUVs and the development of a multi-purpose AUV. University of Southampton.

Petrich J, Neu WL and Stilwell DJ. (2007) Identification of a simplified AUV pitch axis model for control design: Theory and experiments. *OCEANS 2007.* IEEE, 1-7.

Philips A, Steenson L, Rogers E, et al. (2013) Delphin2: An over actuated autonomous underwater vehicle for manoeuvring research. *Transactions of the Royal Institution of Naval Architects, Part A–International Journal of Maritime Engineering* 155: 171-180.

Phillips A, Furlong M and Turnock SR. (2007) The use of computational fluid dynamics to assess the hull resistance of concept autonomous underwater vehicles. *OCEANS 2007-Europe.* IEEE, 1-6.

Pivano L, Fossen TI and Johansen TA. (2006) Nonlinear model identification of a marine propeller over four-quadrant operations. *14th IFAC Symposium on System Identification, SYSID. Newcastle, Australia.*

Pivano L, Johansen TA and Smogeli ON. (2009) A four-quadrant thrust estimation scheme for marine propellers: Theory and experiments. *Control Systems Technology, IEEE Transactions on* 17: 215-226.

Polidoro V. (2003) Flapping foil propulsion for cruising and hovering autonomous underwater vehicles. Massachusetts Institute of Technology.

Polsenberg Thomas A. (2007) Exploration into the feasibility of underwater synthetic jet propulsion. California Institute of Technology.

Porgilsson H. (2006) Control of a small unmanned underwater vehicle using zero optimised PID controllers. *Faculty of Engineering.* University of Iceland.

Prestero T. (2001a) Development of a six-degree of freedom simulation model for the REMUS autonomous underwater vehicle. *OCEANS, 2001. MTS/IEEE Conference and Exhibition.* IEEE, 450-455.

Prestero TTJ. (2001b) Verification of a six-degree of freedom simulation model for the REMUS autonomous underwater vehicle. Massachusetts institute of technology.

Read DA. (2001) Oscillating foils for propulsion and maneuvering of ships and underwater vehicles. Massachusetts Institute of Technology.

Renilson M. (2015) *Submarine hydrodynamics*: Springer.

Ridao P, Batlle J and Carreras M. (2001) Model identification of a low-speed UUV. *IFAC Conference Control Applications in Marine Systems, Glasgow, Scotland.* Citeseer.

Riggs PR. (2010) The use of flexible biomimetic fins in propulsion. University of Bath.

Roberts GN and Sutton R. (2006) *Advances in unmanned marine vehicles*: Iet.

Roberts GN and Sutton R. (2012) *Further advances in unmanned marine vehicles*: IET.

Roddy RF, Hess DE and Faller WE. (2007) A tool to predict the four-quadrant performance of the Wageningen B-screw series for ship performance simulations. *Ship Technology Research* 54: 103-113.

Roper D, Sharma S, Sutton R, et al. (2011) A review of developments towards biologically inspired propulsion systems for autonomous underwater vehicles. *Proceedings of the Institution of Mechanical Engineers, Part M: Journal of Engineering for the Maritime Environment* 225: 77-96.

Russell G and Bellec P. (1981) The Investigation of Submersible Maneuverability by Simulation. *OCEANS 81.* IEEE, 137-141.

Sabet MT, Sarhadi P and Zarini M. (2014) Extended and Unscented Kalman filters for parameter estimation of an autonomous underwater vehicle. *Ocean Engineering* 91: 329-339.

Sanz PJ, Ridao P, Oliver G, et al. (2012) TRIDENT: Recent improvements about autonomous underwater intervention missions. *IFAC Proceedings Volumes* 45: 355-360.

Saunders A and Nahon M. (2002) The effect of forward vehicle velocity on through-body AUV tunnel thruster performance. *OCEANS'02 MTS/IEEE.* IEEE, 250-259.

Seddon JM and Newman S. (2011) *Basic helicopter aerodynamics*: John Wiley & Sons.

Shafiei M and Binazadeh T. (2015) Application of neural network and genetic algorithm in identification of a model of a variable mass underwater vehicle. *Ocean Engineering* 96: 173-180.

Smogeli ØN. (2006) Control of marine propellers: From normal to extreme conditions.

SNAME T. (1950) Nomenclature for treating the motion of a submerged body through a fluid. *The Society of Naval Architects and Marine Engineers, Technical and Research Bulletin No.*: 1-5.

Steele JH, Thorpe SA and Turekian KK. (2009) *Elements of physical oceanography: a derivative of the encyclopedia of ocean sciences*: Academic Press.

Stettler JW. (2004) Steady and unsteady dynamics of an azimuthing podded propulsor related to vehicle maneuvering. Massachusetts Institute of Technology.

Stokey RP, Roup A, von Alt C, et al. (2005) Development of the REMUS 600 autonomous underwater vehicle. *OCEANS, 2005. Proceedings of MTS/IEEE.* IEEE, 1301-1304.

Sutulo S, Moreira L and Soares CG. (2002) Mathematical models for ship path prediction in manoeuvring simulation systems. *Ocean Engineering* 29: 1-19.

Tannuri EA, Rateiro F, Fucatu CH, et al. (2014) Modular mathematical model for a low-speed maneuvering simulator. *ASME 2014 33rd International Conference on Ocean, Offshore and Arctic Engineering.* American Society of Mechanical Engineers, V01BT01A036-V001BT001A036.

Tarbiat S, Ghassemi H and Fadavie M. (2014) Numerical Prediction of Hydromechanical Behaviour of Controllable Pitch Propeller. *International Journal of Rotating Machinery* 2014.

Taubert R, Eichhorn M, Ament C, et al. (2014) Model identification and controller parameter optimization for an autopilot design for autonomous underwater vehicles. *OCEANS 2014-TAIPEI.* IEEE, 1-9.

Tiano A, Sutton R, Lozowicki A, et al. (2007) Observer Kalman filter identification of an autonomous underwater vehicle. *Control engineering practice* 15: 727-739.

Tran M, Binns J, Chai S, et al. (2015a) Least Squares Optimisation Algorithm Based System Identification of an Autonomous Underwater Vehicle. *Proceedings of the 3rd Vietnam Conference on Control and Automation, Vietnam*.

Tran N-H, Choi H-S, Bae J-H, et al. (2015b) Design, control, and implementation of a new AUV platform with a mass shifter mechanism. *International Journal of Precision Engineering and Manufacturing* 16: 1599-1608.

Triantafyllou MS, Techet AH and Hover FS. (2004) Review of experimental work in biomimetic foils. *IEEE Journal of Oceanic Engineering* 29: 585-594.

Ullah B, Ovinis M, Baharom MB, et al. (2015) Underwater gliders control strategies: A review. *Control Conference (ASCC), 2015 10th Asian.* IEEE, 1-6.

van de Ven PW, Flanagan C and Toal D. (2005) Neural network control of underwater vehicles. *Engineering Applications of Artificial Intelligence* 18: 533-547.

Van Der Heijden F, Duin R, De Ridder D, et al. (2005) *Classification, parameter estimation and state estimation: an engineering approach using MATLAB*: John Wiley & Sons.

Van Lammeren W, Van Manen J and Oosterveld M. (1969) The Wageningen B-screw series.

von Ellenrieder K and Ackermann L. (2006) Force/flow measurements on a low-speed, vectored-thruster propelled UUV. *OCEANS 2006.* IEEE, 1-6.

Wang L-L, Wang H-J and Pan L-X. (2015) H∞ control for path tracking of autonomous underwater vehicle motion. *Advances in Mechanical Engineering* 7: 1687814015582083.

Watts CM. (2009) A comparison study of biologically inspired propulsion systems for an autonomous underwater vehicle. University of Glasgow.

Weiss JD and Du Toit NE. (2013) Real-time dynamic model learning and adaptation for underwater vehicles. *Oceans-San Diego, 2013.* IEEE, 1-10.

Woodward M, Atlar M and Clarke D. (2005) Comparison of stopping modes for pod-driven ships by simulation based on model testing. *Proceedings of the Institution of Mechanical Engineers, Part M: Journal of Engineering for the Maritime Environment* 219: 47-64.

Xin B, Xiaohui L, Zhaocun S, et al. (2013) A vectored water jet propulsion method for autonomous underwater vehicles. *Ocean Engineering* 74: 133-140.

Xu S, Han D and Ma Q. (2015) Hydrodynamic forces and moments acting on a remotely operate vehicle with an asymmetric shape moving in a vertical plane. *European Journal of Mechanics-B/Fluids* 54: 1-9.

Appendix A

The experimental procedure for the experiment with CCPP system in chapter 5

Bollard Pull Procedure

- Make sure two power generator is on. (10V generator for actuators and 48V generator for BLDC motor).
- Insert the run number in the data sheet and identify experiment condition for the run.
- Zero value (initial state) for the external and internal load cell is recorded before the experiment is conducted.
- Start the LabVIEW control program:

Blade Control Program:

Enable all actuators and set them in auto mode.

Set the desired value for collective and cyclic angle in percentage.

Wait till the “In tol light” flashed for all actuators.

Shaft speed control program:

Enable the motor amplifier.

Set the control program in auto mode.

Set the desired rpm in conjunction with the experiment condition.

Wait until the rotation speed of the shaft stables.

- Start record the data simultaneously for internal and external load cells for 20 seconds.

- Once the data recorded, the rotation of propeller shaft is stopped and the LabVIEW control program is halted.
- Making sure the recorded file is in the correct name.

Captive Test Procedure

- Recognized the experiment condition for the run from the data sheet.
- The carriage speed is set at the desired value and the direction of the carriage is set in forward state.
- Zero value (initial state) for the external and internal load cell is recorded before the experiment is conducted.
- Start the LabVIEW control program:

Blade control program:

Enable all actuators and set them in auto mode.

Set the desired value for collective and cyclic angle in percentage.

Wait till the “In tol light” flashed for all actuators.

Shaft speed control program:

Enable the motor amplifier.

Set the control program in auto mode.

Set the desired rpm in conjunction with the experiment condition.

Wait until the rotation speed of the shaft stables.

- The carriage power supply is started up and initiated the towing carriage at the desired speed.

- The data is recorded once the carriage speed reached the desired speed and both external and internal load cells is recorded simultaneously.
- The data is recorded for 20 seconds and the carriage is stopped.
- The carriage is moved back to its initial state and the next run is waited for at least 5 minutes due to the wave disturbance after being towed.

Equipment Calibration Photos

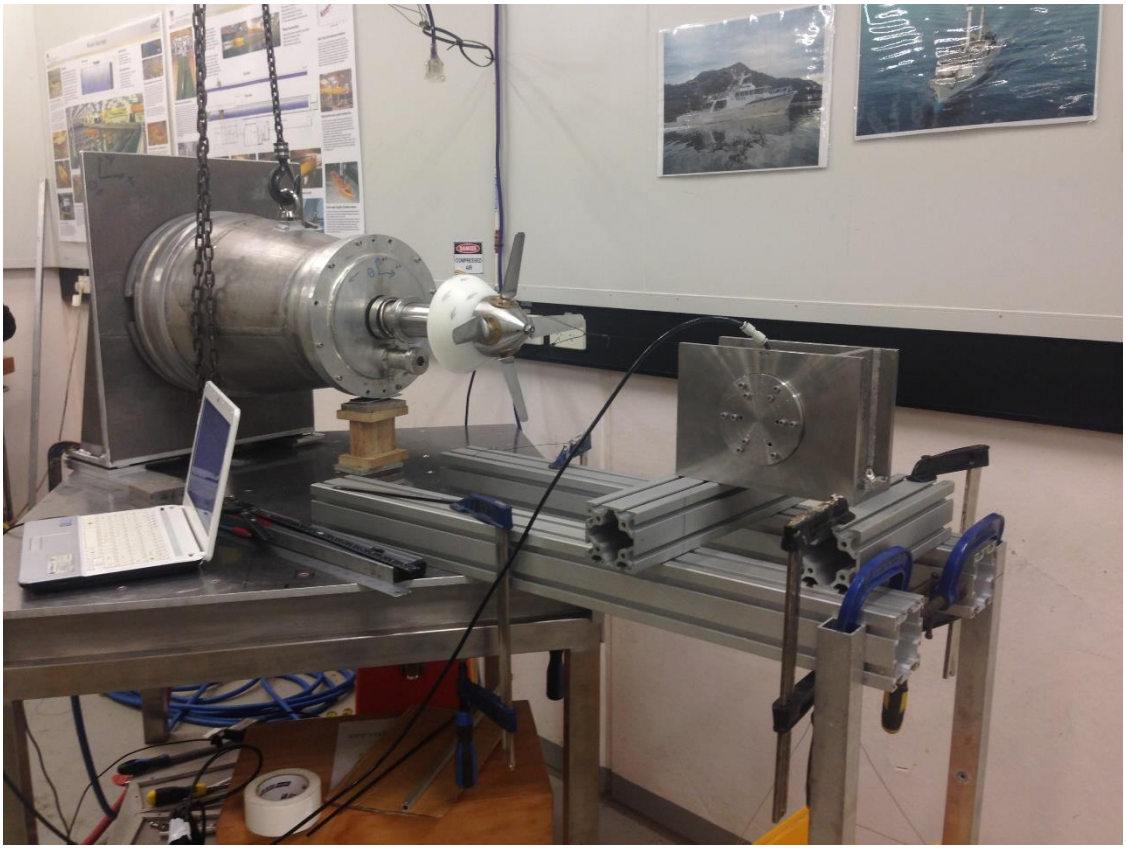

Figure A.1. Internal Balance Calibration Setup.

Figure A.2. External Balance Calibration Setup.

Appendix B

Simulink/Matlab Diagram

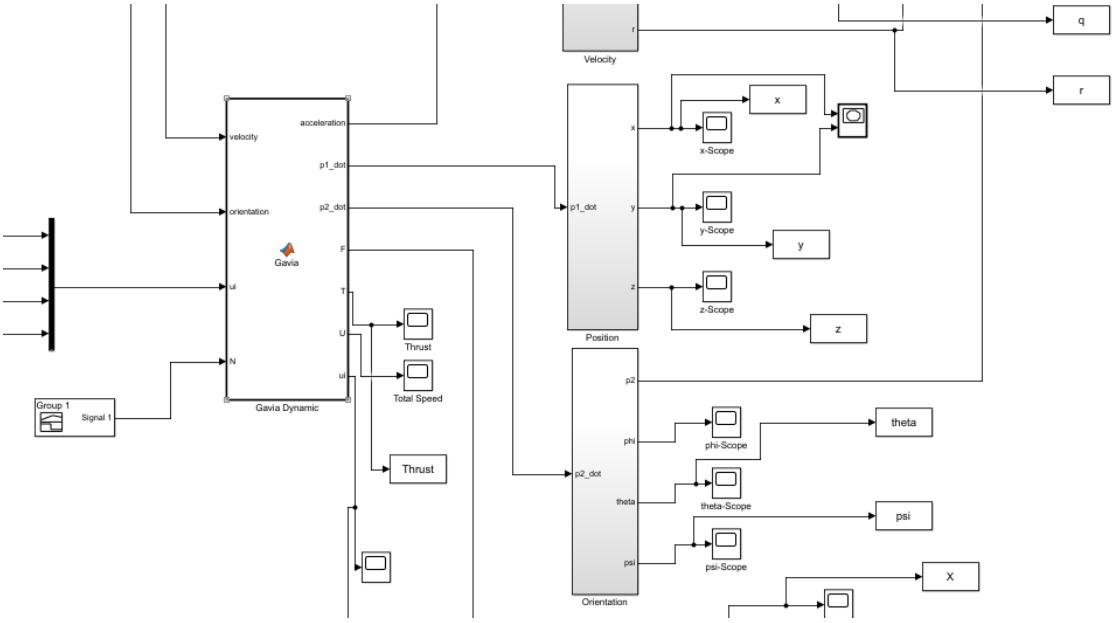

Figure B.1. Simulink Model for the Simulation.

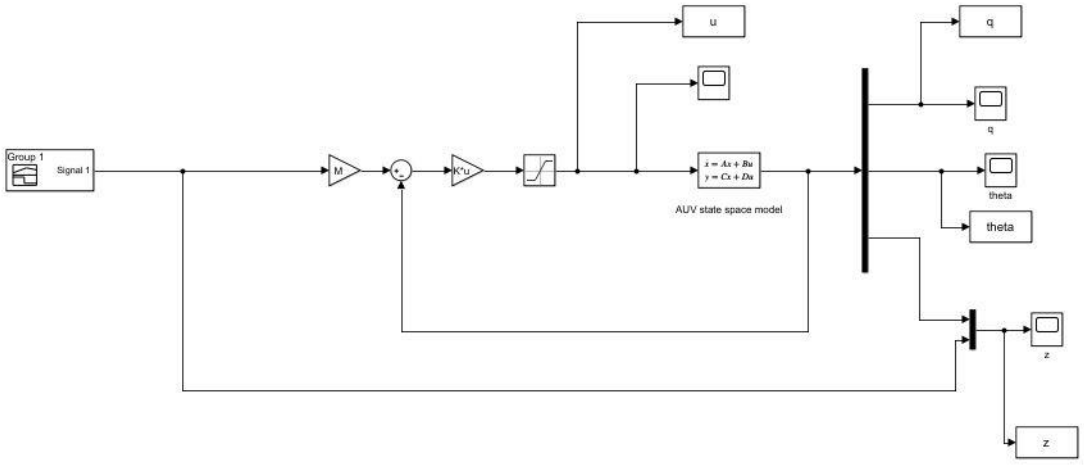

Figure B.2. Simulink Model for the Depth Control.

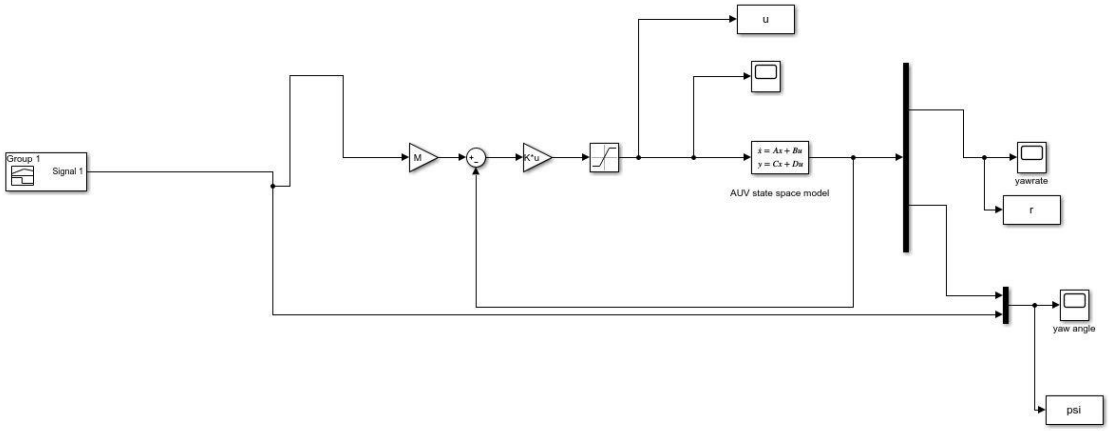

Figure B.3. Simulink Model for the Heading Control.

Hydrodynamic Coefficients for Gavia standard configuration used in Matlab code

```
% Geometric Configuration
% Note to modify as changing the module attached
% L = 2.3           Length (m)
% D = 0.2           Maximum Diameter (m)
% g= 9.81;          %Acceleration due to gravity     (kg/m^2)
% m= 63;            %Total Mass                      (kg)
% W= m*g;           %Total weight                    (N)
% B= (m+0.5)*g;     %Vehicle Buoyancy
% rho= 1000;        %Water density
%
% %Moments of Inertia WRT origin at hafl-length
% I_xx= 1;              %kg*m^2
% I_yy= 28.5;           %kg*m^2
% I_zz= I_yy;           %kg*m^2
% I_yz= 0;
% I_zy=I_yz;

% Added mass Coefficients and Nonlinear Damping Coefficients for the
hull
% % Note that the Added Mass Coefficients have negative values re-
garding to the specified equation of motion in this study.

% X_udot= -6.3;          %Added mass (kg)
% X_uu= -3.13;           %Cross-flow drag (kg/m)
% X_wq= -77.8 ;          %Added mass cross term (kg/rad)
% X_qq= -4.16 ;          %Added mass cross term (kg*m/rad)
% X_vr= 72 ;             %Added mass cross term (kg/rad)
% X_rr= -4.16 ;          %Added mass cross term (kg*m/rad)
%
% Y_vdot= -X_vr;         %Added mass (kg)
% Y_rdot=-X_rr;
% Y_vv= -123.9;         %Cross-flow drag (kg/m)
% Y_rr= -13;            %Cross flow drag (kg*m/rad^2)
% Y_ur=X_udot;          %Added mass cross term and fin lift (kg/rad)
```

```
% Y_wp=-X_wq;            %Added mass cross term
% Y_pq=-X_qq;            %Added mass cross term
% Y_uv= 11.6;            %Reconsider Consider this! Body lift force
and fin lift
%
% Z_wdot= X_wq;          %Added mass (kg)
% Z_qdot= X_qq;          %Added mass (kg*m/rad)
% Z_ww= -285;            %Cross-flow drag (kg/m)
% Z_q= -Y_rr;            %Cross-flow drag (kg*m/rad)
% Z_uq= - 0.884;         %Added mass cross term and fin lift (kg/rad)
% Z_vp= Y_vdot;          %Added mass cross term (kg/rad)
% Z_rp= Y_rdot;          %Added mass cross term (kg/rad)
% Z_uw= Y_uv;            %Body lift force and Fin lift (kg/m)
% Zuu_gamma_s = -2.13 (kgm/rad) %Fin Lift Force Coefficient (Stern
Plane)
%
% K_pdot= -0.0104;         %Added mass (kg*m^2/rad)
% K_pp= -0.13;             %Rolling resistance
%
% M_wdot= Z_qdot;          %Added mass (kg*m)
% M_qdot= -45.2;           %Added mass (kg*m^2/rad)
% M_ww= -8.82;             %Cross-flow drag (kg)
% M_qq= -2810;             %Cross-flow drag (kg*m^2/rad^2)
% M_uw= -0.548;            %Body and Fin Lift and Munk Moment (kg)
% M_uq= -X_qq;             %Added mass cross-term and fin lift
(kg*m/rad)
% M_vp= -M_uq;             %Added mass cross-term (kg*m/rad)
% M_rp= 45.2;              %Added mass cross-term (kg*m^2/rad^2)
% Muu_gamma_r = -14.6 (kg/rad)     %Fin Lift Moment (Rudder)

% N_vdot= Y_rdot;           %Added mass (kg*m)
% N_rdot= M_qdot;
% N_vv= -M_ww;              %Cross-flow drag (kg)
% N_rr=  M_qq;              %Cross-flow drag (kg*m^2/rad^2)
% N_ur=  M_uq;              %Added mass cross-term and fin lift
(kg*m/rad)
% N_uv=  - 0.548;           %Body and Fin lift and Munk moment (kg)
% N_wp=  -N_ur;             %Added mass cross-term (kg*m/rad)
% N_pq=  -M_rp;             %Added mass cross-term (kg*m^2/rad^2)
% Nuu_gamma_s = -14.6 (kg/rad)     %Fin Lift Moment (Stern-Plane)
```